The Effect of Catalyst Composition on the Fundamental Properties of Isotactic Polypropylene

by
Jacob Lourens Kleynhans

Department of Chemistry and Polymer Science

University of Stellenbosch

Thesis presented in fulfilment of the requirements for the degree of Master of Science in Chemistry and Polymer Science in the Faculty of Science at Stellenbosch University

M.Sc (Chemistry and Polymer Science)

Supervisor: Prof A.J. van Reenen

April 2019

Declaration

By submitting this thesis electronically, I declare that the entirety of the work contained therein is my own, original work, that I am the sole author thereof (save to the extent explicitly otherwise stated), that reproduction and publication thereof by Stellenbosch University will not infringe any third party rights and that I have not previously in its entirety or in part submitted it for obtaining any qualification.

Date: December 2018

Acknowledgements

There are several people who played a significant role during this study, whom I would like to mention.

First and foremost thank you to Prof Albert van Reenen for not only enabling me to do a masters degree, but also his guidance and calmness throughout the year. I would not have continued my studies if it wouldn't have been under his leadership.

Thank you also to Sasol for the opportunity to do this project in collaboration with them. A word of appreciation for the visit to the Secunda plant which was a remarkable experience.

To my family - my parents, my brother and my sister - for their unwavering support throughout my entire masters experience.

Carla Sequeira, for everything she meant to me this year, and never failing to be there.

Thank you to the Olefins group in the Polymer Science building for creating an environment conducive to excellent results whilst enjoying the occasional laugh.

Not to forget everyone else in the Polymer Science building who always smiled and greeted and made coming to work a better experience.

Thank you to CAF for using their NMR and SEM instruments.

Thank you to Dr Jaco Brand and Elsa Malherbe for HT-^{13}C NMR analysis.

Thank you to Dr. Anthony Ndiripo and Mawande Sigwinta for CRYSTAF and HT-SEC analysis throughout the year.

Thank you to Megan Matthews for all the solid-state NMR work.

Thank you to Sifiso Magagula for all his guidance throughout the year.

Abstract

Isotactic polypropylene is an important commercial polymer in the world today. Falling under the group of polyolefins, polypropylene serves as the largest commercial polymer worldwide together with polyethylene. Isotactic polypropylene is typically produced by a multi-sited Ziegler-Natta catalyst, the composition of which plays a critical role in the molecular properties of the final sample.

The work in this study was done in order to set up a baseline of results of five different grades of isotactic polypropylene, varying in their final form (reactor powder and extruded pellet forms), as well as the catalyst composition used during polymerisation (Lynx and NHP catalysts). There were four variations possible of each different grade of isotactic polypropylene, which lead to the investigation of twenty different bulk polymer samples. Extensive analysis and characterisation was done on each of these bulk samples, as well as the fractions of each bulk sample which resulted from performing preparative temperature rising elution fractionation (*p*-TREF). The full analytical toolbox was implemented for the characterisation of these samples, which include SEM, DSC, HT-SEC, XRD, SSA, solution- and solid-state ^{13}C NMR spectroscopy. By obtaining and investigating the results it was able to investigate the effect that the catalyst composition has on the fundamental properties of isotactic polypropylene samples, such as percentage isotacticity, crystallinity, molar mass, crystal structure and surface morphology.

This study was performed to serve as a starting point for future projects related to these isotactic polypropylene samples investigated, such as for example the production of heterophasic ethylene propylene copolymers (HECOs). The main theme throughout this study will thus be to set up a baseline of results, for future project based on the same materials.

Table of Contents

List of Figures

List of Tables

Acronyms and Abbreviations

^{13}C	Carbon thirteen, isotope of carbon twelve with mass thirteen
3D	3-Dimensional
ATR-FTIR	Attenuated total reflectance Fourier transform infrared
CPMAS	Cross polarization magic angle spinning
CRYSTAF	Crystallisation analysis by fractionation
DSC	Differential scanning calorimetry
d-TCE	Deuterated tetrachloroethane
HECOs	Heterophasic ethylene propylene copolymers
HT-SEC	High temperature size exclusion chromatography
iPP	Isotactic polypropylene
M_n	Number average molar mass
M_w	Weight average molar mass
NMR	Nuclear magnetic resonance
PDI	Polydispersity index
PE	Polyethylene
SCALLS	Solution crystallisation analysis by laser light scattering
SEM	Scanning electron microscopy
SSA	Successive self-nucleation and annealing
TCB	Trichlorobenzene

T_c	Crystallization temperature
T_m	Melting temperature
TREF	Temperature rising elution fractionation
WAXD	Wide angle X-ray diffraction
wt%	Weight percentage
XRD	X-ray diffraction
ZN	Ziegler-Natta

Chapter 1

Introduction

A short introduction regarding the material studied in this project is provided, as well as an outline of the aims and objectives of the project.

1.1 Introduction

Isotactic polypropylene falls under the polyolefin chemical group and thus forms part of the most important commodity polymers today. Polypropylenes together with polyethylenes are the largest commercial polymers in the world by tonnes used in a year. [1–3] The world-wide capacity of polypropylene was 11 million tonnes back in 1988, of which 60 % was produced in the USA and Europe alone. [4] This number has significantly increased to 55 million tonnes produced in 2013 and it is estimated that more than 300 000 tonnes of polypropylene raw material was consumed in South Africa in 2016. [5] The reason for this is due to the large diversity of structures that can be obtained by producing these polymers. Major uses of polypropylene specifically are in injection moulding, film and sheet applications, and raffia. Worldwide polypropylene markets are topped by the homopolymer due to ease of production setups (single reactor) compared to what is needed for copolymers (multiple reactors) and thus a substantial amount of effort is put into optimizing and understanding the end properties of these homopolymers. This is necessary not only for processing of the homopolymers, but also to gain knowledge of how the homopolymers will react when copolymerized with ethylene to form impact copolymers, which also make up a significant amount of the commercial plastics market.

Propylene homopolymerizations are typically catalysed using transition metal catalysts. The highly advanced transition metal catalysts that are available today, together with newly developed polymerization technologies, have led to the production of polymers ranging from soft elastomers to hard thermoplastics. [1] The exact composition of these catalysts could possibly lead to differences in the fundamental molecular properties of the polypropylene samples, a factor which could possibly have major influence on the end properties of polypropylene materials. The five grades of polymers studied in this project were all obtained from Sasol together with some basic information summarized in Table 1.1.

Table 1.1: Grades of polypropylene investigated during study

Grade	MFI (g/10min)	Tensile modulus (MPa)	Charpy impact strength (KJ/m^2)	Useful for
HKQ 205	3	1400	4.5	Biaxially oriented film
HKR 102	3.5	1600	3.5	Extrusion tapes and fibres (monofilaments), injection moulding
HMR 127	8.5	1550	3	Extrusion film, injection moulding
HNR 100	12	1550	2.8	Injection moulding
HNR 101	12	1550	2.8	Extrusion tapes and fibres (monofilaments)

1.2 Aims

One of the key parameters that influence the molecular properties of commercially produced isotactic polypropylene include the composition of the catalyst used. The aim of this project is to obtain a set of analytical results regarding the properties of isotactic polypropylene samples, utilizing catalysts of different compositions and the same polymerization technology, to serve as a baseline for future studies related to the same materials. This will serve as the main theme throughout the project and can be separated into the components stated below:

- Making use of the full analytical toolbox available to analyse and characterize bulk, and subsequently fractionated polymer samples.
- Identifying key areas of interest and applying further analytical techniques to investigate results more in depth.

1.3 Objectives

A set of five grades of isotactic polypropylene, made with different catalysts and utilizing the same polymerization technology were obtained in both reactor powder and extruded pellet form. These polymer samples will be investigated throughout this study to achieve the broad aim of the project mentioned previously.

The following objectives will be implemented to achieve the desired aims:

1. Fractionation of bulk polymer samples
2. Basic analysis and characterization of bulk and fractionated polymer samples
3. Identification of key areas from basic analysis
4. In depth analysis and characterization of key areas

1.4 Layout of thesis

Chapter 1 - Introduction

A brief introduction to the study is provided, along with an overview of the specific aims. The presented objectives in this study are also discussed.

Chapter 2 - Theoretical background

Chapter 2 serves as a literature study to provide background to the different components of this project. This will include information on the material investigated during this project, the catalysts investigated as well as the complete set of analytical techniques implemented throughout this project.

Chapter 3 - Materials and methodology

Chapter 3 will summarize the specifications of the materials studied in this project. It will also contain detailed experimental procedures followed during the project as well as a detailed example of the sample preparation required for each technique.

Chapter 4 - Analysis and characterization: Bulk samples

Chapter 4 will relay and discuss selected results of the fractionation and analysis of the bulk polymer samples investigated during this project. This chapter will serve as **part 1** of the results of the thesis.

Chapter 5 - Analysis and characterization: Fractionated samples

Chapter 5 will relay and discuss selected results of the analysis of the fractionated polymer samples investigated during this project. This chapter will serve as **part 2** of the results of the thesis.

Chapter 6 - In depth study on selected samples

Chapter 6 will serve as an in-depth investigation into a smaller set of samples, to gain detailed knowledge regarding the fine molecular structure present within the samples. The results obtained from this study will be documented and discussed comprehensively throughout the chapter. This chapter will serve as **part 3** of the results of the thesis.

Chapter 7 - Conclusions and recommendations

Chapter 7 will summarize the observations made from Chapters 4 through 6 and conclude the entire project. Some further recommendations for this study, as well as some suggestions for future work based on this project are mentioned.

Annexure - Graphs and tabulated values

The appendix will contain a summary of all the results that weren't explicitly shown within the bulk content of the thesis. This will include both graphs and tables relating to the results of several analytical techniques employed throughout the study.

1.5 References

1. Viville, P., Daoust, D., Jonas, A.M., Nysten, B., Legras, R., Dupire, M., Michel, J. & Debras, G. Characterization of the molecular structure of two highly isotactic polypropylenes. *Polymer (Guildf)*. **42**, 19531967 (2001).
2. Soares, J. B. P. & Hamielec, A. E. Kinetics of propylene polymn. with a non-supported heterogeneous Z-N catalyst - effect of hydrogen on rate of polymn., stereoregularity and MWD. *Polymer (Guildf)*. **37**, 46074614 (1996).
3. Soares, J. B. P., Kim, J. D. & Rempel, L. G. Analysis and control of the molecular weight and chemical composition distributions of polyolefins made with metallocene and Ziegler-Natta catalysts. *Ind. Eng. Chem. Res.* **36**, 11441150 (1997).
4. Ven, S. van der. Polypropylene and other Polyolefins: Polymerization and Characterization. *Journal of Chemical Information and Modeling* **53**, (1990).
5. Plastics SA. Our Footprint. Plastics SA Our Footprint (2017). Available at: http://www.plasticsinfo.co.za /annual-reports/. (Accessed: 10th July 2018)

Chapter 2

Theoretical background

Chapter 2 serves as a literature study to provide background to the different components of this project. This will include information on the material investigated during this project, the catalysts investigated as well as the complete set of analytical techniques implemented throughout this project.

2.1 Isotactic polypropylene: An overview

Isotactic polypropylene (iPP) is a form of polypropylene in which the majority of methyl groups (CH_3) are oriented in the same direction, as can be seen in the repeat unit structure of the polymer in Figure 2.2 (left). The polymeric form is obtained by polymerizing propylene gas with a homogeneous (metallocene) or heterogeneous transition metal catalyst as can be seen in the scheme presented in Figure 2.1. iPP has received an increasing amount of attention in recent decades due to its physical, mechanical, thermomechanical, and other properties which make it optimal for use in industry, [1] and is also seen as one of the most important synthetic polymers. [2] Polypropylene can be present in three different tactic forms, namely the highly crystalline isotactic form (Figure 2.2), the less crystalline syndiotactic form (Figure 2.2), and finally the amorphous atactic form (Figure 2.3). [2] From Figures 2.2-2.3 we can see that isotactic polypropylene has a consistent methyl orientation to one side, syndiotactic polypropylene has a consistent alternating methyl orientation and atactic polypropylene has a random orientation of the methyl group.

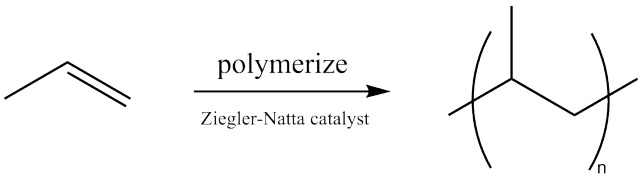

Figure 2.1: Basic scheme for polypropylene polymerization

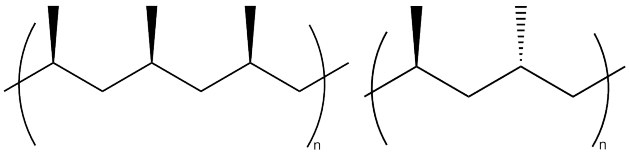

Figure 2.2: Basic structure for isotactic polypropylene (left) and syndiotactic polypropylene (right)

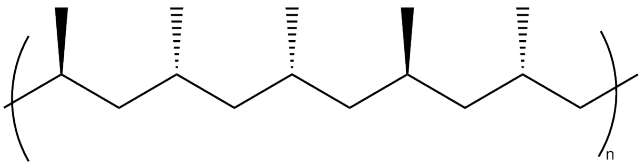

Figure 2.3: Basic structure for atactic polypropylene

Studies that have been done on different types of polypropylenes have found that analysis of the physical properties and molecular structure of the fractions of the samples will give information regarding the inter- and intra-molecular heterogeneity of the polymers, simply based on the inter- and intra-chain tacticity distributions. [3]

It is commonly known that heterogeneous Ziegler-Natta catalysts have multiple active sites, and when used to produce polypropylene, a polymer with varying degree of stereoregularity is obtained. Information regarding the catalyst and the polymerization mechanism can be obtained when investigating specific factors such as the isotacticity, stereodefects and the distribution thereof, and the stereoregular sequences in a polymer. [4,5] Investigation of these aforementioned factors can be done using analysis techniques such as ^{13}C nuclear magnetic resonance spectroscopy (NMR), high temperature size exclusion chromatography (HT-SEC), differential scanning calorimetry (DSC), attenuated total reflectance Fourier transform infrared spectroscopy (ATR-FTIR), X-ray diffraction (XRD) and more. [3,5–8]. There has been a lot of effort put into determining the exact structures of the active sites present on the catalyst, however, no definitive result has emerged except for some progress made using a molecular modelling approach. [4,9–11] A common method used is the more indirect study of the polymer structure, where information on the catalyst can be obtained if the polymer characterization is done thoroughly. The fine structure of the polymer contributes largely to the properties of the polymer material, and it has been observed that not only average isotacticity, but the way in which the tacticity is distributed among the chains in a polymer has an effect on the final properties. [4] It is thus necessary to obtain quantitative information on the complex polymer structure obtained by using a heterogeneous Ziegler-Natta catalyst, by fractionating the sample and conducting analysis and characterizations of the fractions in order to determine the distribution of stereodefects within the sample. [4,12]

2.1.1 Catalyst

Polypropylene can be produced exclusively by utilizing a transition metal catalyst. These catalysts could be either heterogeneous Ziegler-Natta catalysts or homogeneous metallocene catalysts. The heterogeneous Ziegler-Natta catalysts have been widely implemented in industry for the production of polypropylene. [9,13] Ziegler-Natta catalysts have come a long way since their inception as low stereospecific catalysts with low activity, and have evolved to have high stereospecificity together with a high activity. [3] Ziegler-Natta catalysts are by far the most widely used catalyst for the production of polypropylene, and is estimated to account for more than 99 % of all polypropylene production, which in 2004, exceeded 30 million tonnes per annum. [14]

Throughout history, heterogeneous Ziegler-Natta catalysts have been used to produce iPP and it has been found that these catalysts are multi-sited. [14] Each of the active sites of the catalyst will end up producing polymer molecules that differ, depending on the activity of each site, in both molecular weight and tacticity. Due to this, the polymer will contain both atactic material, which consists of isotactic sequences interrupted by stereo-defects, and highly isotactic material, which consists of higher molecular weight isotactic sequences with fewer stereo-defects. It has also been shown that iPP produced with Ziegler-Natta

catalysts will have an increasing amount of stereo-defects as the molecular weight decreases, leading to a non-homogeneous system of polymer molecules. [15]

Catalysts typically consist of $MgCl_2$, $TiCl_3$, an internal donor used together with a co-catalyst of the aluminium alkyl type, and finally an external donor which is generally added during polymerization. It was the discovery of $MgCl_2$ supported $TiCl_4$ which lead to high activity of the catalyst and the later discovery of electron donors in the form of a Lewis base, that allowed for the increase of the stereospecificity of the catalyst. [13] This increased stereospecificity meant that highly isotactic polypropylene could be produced. The use of a highly active $MgCl_2$ supported catalyst is critical for propylene polymerization. [16,17] In addition to the $MgCl_2$ support and the main active component, which is typically $TiCl_3$, an internal- and an external donor are needed for effective polymerization as well.

As mentioned previously, the high activity Ziegler-Natta catalysts are typically made up of $MgCl_2$, $TiCl_4$, a cocatalyst which is typically $AlEt_3$, and an ”internal” and an ”external” electron donor which are added during polymerization. [9,13,14] Internal electron donors have two functions in $MgCl_2$ supported catalysts. Firstly, the internal donor functions in stabilizing the primary crystallites of $MgCl_2$, and secondly it is needed to regulate the $TiCl_4$ amount and distribution in the catalyst. [13] An external donor is needed when the internal donor used is an ester. This is due to a loss of internal donor upon contact with the co-catalyst due to alkylation and complexation reactions. The presence of an external donor allows for the replacement of the internal donor by an external donor upon contact with the catalyst constituents, which preserves the stereoselectivity of the catalyst. The absence of an external donor will lead to a low stereoselective catalyst having more freedom of movement on the catalyst surface. [13] Some of the catalysts used in earlier years used an ethyl benzoate internal donor, with a second aromatic ester as the external donor. The newer catalysts, however, make use of a diester internal donor such as a diisobutyl phthalate and an alkoxysilane external donor of the type $RR'Si(OMe)_2$ or $RSi(OMe)_3$. [14] Some catalysts have been introduced that showcase high isospecificity which don't use an external donor at all, but needed a bidentate internal donor having appropriate oxygen-oxygen distance which need not be removed from the support after contact with $AlEt_3$. [18] These internal donors are hindered diethers, and have preferential affinity to $MgCl_2$ rather than the aluminium alkyl co-catalyst, and as a result aren't displaced from the catalyst surface upon contact with the co-catalyst. [13] This means that highly isotactic polypropylene can be produced without the need for an external donor. In past years, a $MgCl_2$ supported catalyst family was developed, which didn't use a phthalate ester, but rather a succinate, while still using an alkoxysilane as external donor. These succinate type catalyst systems lead to the production of a polypropylene which have a broader molar mass distribution compared to the phthalate ester catalyst systems. [14]

The regio- and stereoselectivity of catalyst systems will thus be affected by internal and external donor

combinations. These effects need to be considered thoroughly, as well as the steric hindrance effect which might occur due to the presence of donor molecules in the catalyst vicinity. Ultimately, the strength of the donor coordination will directly affect the propagation and chain transfer characteristics of a polymerization reaction. [13]

An indication of the evolution of Ziegler-Natta catalysts used for propylene polymerization can be seen in the Table 2.1.

Table 2.1: Evolution of Ziegler-Natta catalysts [17]

Catalyst	Co-catalyst	External donor
$MgCl_2/TiCl_4$/ethyl benzoate	AlR_3	Aromatic ester
$MgCl_2/TiCl_4$/dialkyl phthalate	AlR_3	Alkoxy silane
$MgCl_2/TiCl_4$/diether	AlR_3	

When a comprehensive understanding of the fundamental aspects of $MgCl_2$ supported catalysts is achieved, a relationship can be set up from the catalyst to the resulting polypropylene structure and properties. [14] Some noteworthy progress has been made recently with regards to understanding the fundamental factors which have an influence on $MgCl_2$ supported catalyst performance, related to catalyst selectivity, activity as well as sensitivity to hydrogen. [13] A crucial aspect in understanding $MgCl_2$ supported catalysts, is the control of molecular weight by using a chain transfer agent such as hydrogen. The effect that the presence of hydrogen has on the molecular weight of a polymer isn't consistent throughout all catalyst systems. Looking specifically at diether containing catalysts, it has been observed that small amounts of hydrogen are required for molecular weight control, as these types of systems have high sensitivity to the presence of hydrogen. [14] Generally it is known that chain transfer reactions occur following primary (1,2-) insertion, however, these catalyst systems lead to chain transfer occurrences following secondary (2,1-) insertions. [19]

As mentioned previously, Ziegler-Natta catalysts have multiple active sites, a property which means that the nature and position distributions of the active species will directly affect the molar mass and molar mass distribution of a polymer. It is reported that compared to phthalate-, benzoate-, and succinate-based systems, catalyst systems containing diether give polymers with a narrower molecular weight distribution. [14] The effect of molar mass and dispersity on the end properties of polymer materials is quite significant. For example, when fiber spinning applications are the end use of the polymer, it would be advantageous to have a polymer with a lower molar mass as well as a narrow molar mass distribution. When the final polymer material needs to be used for the extrusion of sheets and pipes, a polymer with higher molar mass and

broader molar mass distribution is required as these polymers showcase better melt strength properties. For high rigidity end uses, a polymer with broad molecular weight distribution, and high stereoregularity is required, as it will have higher isotacticity and concommitant higher crystallinity. [14]

2.2 Fractionation of the bulk samples

2.2.1 TREF

It is known that fundamental properties of polymers cannot be determined accurately simply by using average values, and it is thus necessary to fractionate the bulk polymer in order to delve deeper into specific properties of a polymer. [3] Temperature rising elution fractionation or TREF, is a technique that fractionates semi-crystalline samples according to crystallizability and relies on the differences of chain crystallizabilities in a dilute solution. TREF is probably the most comprehensive analytical technique that has been implemented in order to characterize polyolefins worldwide. [20] TREF could be described in more detail as a technique that fractionates semi-crystalline polymers according to their temperature-solubility relationships, a factor which is directly affected by the molecular structures of a polymer. [21] It should also be mentioned that TREF does not fractionate polypropylene by tacticity, but rather by the longest crystallizable sequences present in the chain which could ultimately reflect on the tacticity within the sample. [3] It is accepted that polymer chains, in this case isotactic polypropylene chains, with higher crystallizabilities will be fractionated at higher temperatures compared to the polymer chains that have low crystallizability. [21,22]

The fractionation mechanism of TREF will be discussed here as it is of critical importance to understand the differences in TREF fractions, which will be analysed and characterized throughout the project. There are two temperature cycles involved in the process.
First, the bulk polymer is dissolved in a suitable solvent at high temperature for a couple of hours, after which the solution is added to a support within a column at equally high temperature. This column is then allowed to cool down at an extremely low rate (1 °C/hour) and serves as the crystallization step and the first temperature cycle. During the crystallization step, layers of decreasing crystallizability are deposited on the support and fractionation is thus achieved.
The following step is required to physically obtain or quantify the fractions, which is where the second temperature cycle becomes relevant. This is achieved by adding the support with crystallized material surrounding it into a column and into an oven. Fresh solvent is then pumped through the column starting at room temperature increasing up to a specified higher temperature, which will selectively dissolve fractions of increasing crystallizability. These fractions are then physically collected, which is the basis for preparative

TREF (*p*-TREF), after which the solvent is removed, leaving the fractionated polymer behind. The fractions could alternatively be monitored by some detector in order to produce a crystallizability distribution curve, which is the basis for analytical TREF (*a*-TREF). [4,20] For this study preparative TREF is implemented as it gives more information compared to analytical TREF despite the much longer experimental times, as the fractions can be further analysed using various analytical techniques.

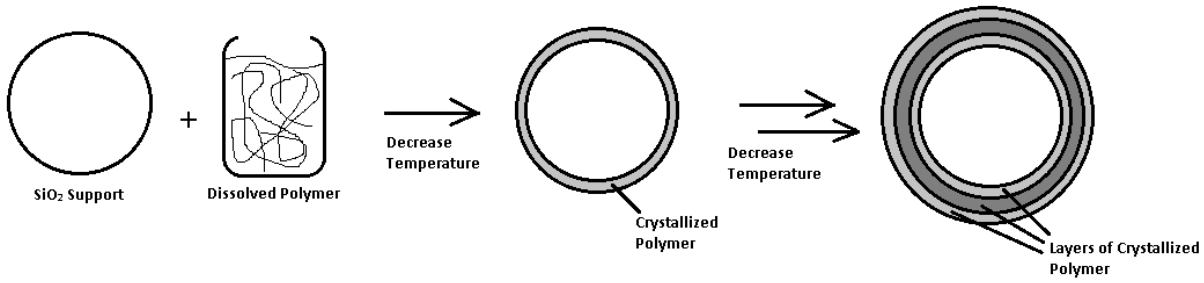

Figure 2.4: Schematic of TREF fractionation mechanism

The schematic in Figure 2.4 serves as a basic explanation of the TREF procedure. The dissolved polymer is added to the preheated support, and the reactor containing the polymer and support is then placed in a preheated oil bath. The temperature is then decreased, causing a layer of polymer material to crystallize onto the support. This layer consists of the most crystallizable material present in the polymer sample. The temperature is then decreased further, causing subsequent layers of decreasing crystallizability to crystallize onto the support. When this process is done the support with polymer material surrounding it is added to a column and placed in an oven. Fresh solvent is then pumped through the column at increasing temperatures, causing each subsequent layer of crystalline material on the support to dissolve and elute out of the column. The solvent containing the polymer is collected, after which the solvent is removed, and the fractionated polymer remains.

2.2.2 CRYSTAF

Crystallization analysis fractionation or CRYSTAF, like TREF, is a technique that fractionates the polymer chains in a dilute solution according to crystallizability. CRYSTAF is mainly used as an analytical technique and is based on the crystallization of polymer chains at varying temperatures. [23,24] The instrument measures the concentration of the polymer in solution during the crystallization step, as a function of temperature. [25] This then relates to a cumulative concentration curve, of which the derivative is related to the fraction of polymer that has crystallized at that temperature, and information is thus obtained about the distribution of chain crystallizability within the polymer sample. [22,26,27] Due to the applicability of CRYSTAF it has become

a rather important technique for the characterization of olefinic materials. [27] A typical CRYSTAF is shown in Figure 2.6.

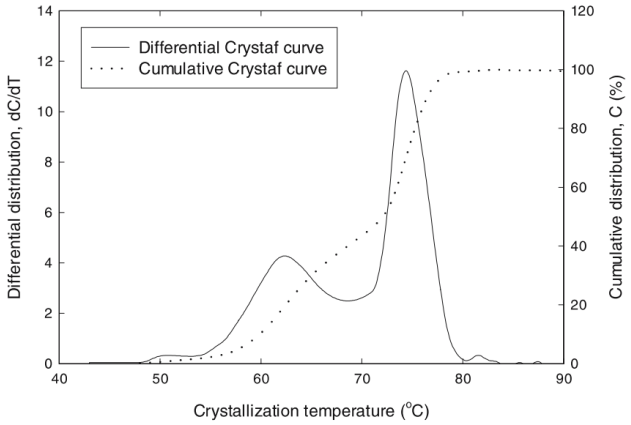

Figure 2.5: Typical example of a CRYSTAF graph [22]

CRYSTAF was originally developed to serve as an alternative to TREF, as TREF procedures are extremely time consuming. [26,27] CRYSTAF analysis could be done much faster, as it only has one temperature cycle compared to TREF, which needs two temperature cycles to complete an experiment. With CRYSTAF it is also possible to analyse multiple polymer samples simultaneously (depending on the instrument) and significantly less solvent is needed compared to TREF. [28] Both techniques have similar fractionation mechanisms and this means that the results of the two techniques are comparable. [22] The graph obtained from CRYSTAF is thus commonly used in order to observe where the most crystallizable material within a polymer sample occurs. This enables the user to roughly determine the elution temperatures to be implemented during the second temperature cycle of *p*-TREF (assuming that the crystallization and re-dissolution occur at relatively the same temperature), as CRYSTAF analysis can be done on polymer samples in a much shorter time than TREF itself. The data from CRYSTAF can thus be used to see where the majority of polymer will elute when TREF elution is conducted, however, it should be noted that there is a delay period and the elution temperature of TREF could be up to 10 °C higher than the corresponding temperature on CRYSTAF, and the technique should thus only be used as a guideline and not as a definitive explanation.

An alternative to using CRYSTAF for this purpose, is to use solution crystallization analysis by laser light scattering or SCALLS. SCALLS works by detecting the intensity of light from several lasers as a function of temperature. These lasers are pointed through a glass vial containing polymer and solvent, and will be reflected due to the crystalline material that forms in the solution when the polymer crystallizes. [30] A schematic of the experimental setup can be seen in Figure 2.6. [30] A graph is thus obtained of the scattered light intensity versus temperature, and this information can thus be related to the temperatures at which

crystalline material will elute during TREF elution. SCALLS is mentioned here for completeness, but was not used in this project as initial experiments showed that the homopolymers studied in this project crystallized onto the stirrer bar rather than into the solvent, leading to inaccurate results.

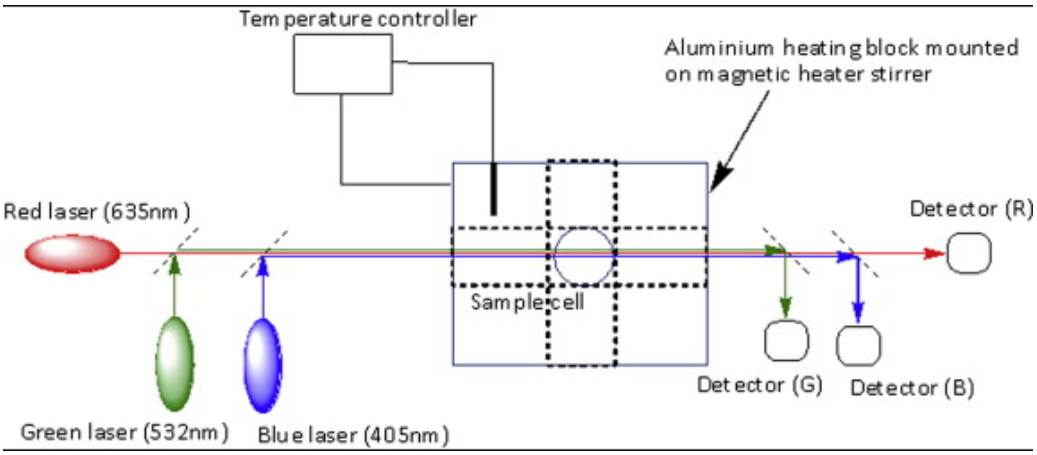

Figure 2.6: Experimental setup of a SCALLS experiment [30]

2.3 Characterisation techniques

2.3.1 DSC

Differential scanning calorimetry or DSC, is a method used for measuring the thermal behaviour of materials, such as the glass transition temperature (T_g), the melting temperature (T_m) and the crystallization temperature (T_c). [15] DSC also enables the determination of the corresponding enthalpy and entropy changes of these phase transitions, and other effects that have changes in the heat capacity or latent heat. DSC is widely used due to its simplicity, and the properties measured via calorimetry gives clear information regarding the thermal behaviour properties of the polymer. DSC has many advantages compared to other calorimetric analytical techniques. The main advantage, compared to other calorimetric methods, lies in the usability of the instrument, i.e the easy manipulation of the heating and cooling rates. The main disadvantage of the method is most probably the determination of the baseline heat capacity, which leads to uncertainties when calculating the percentage crystallinity of a sample. Uncertainties are a critical factor in the determination of crystallinity from DSC thermograms, and can be minimized to below 1 $\%$ if the temperature of the instrument is below room temperature. In the case of polymers, which have low thermal conductivity and require higher temperatures, or in the case when heat capacity becomes time dependant, some other problems occur. This leads to a heat capacity measurement with a significantly higher percentage of uncertainty. [31]

There are some important thermodynamic equations used to allow for the description of some important material properties, and these include the enthalpy H, calculated as $H = \int_0^T C_p dT$ and the entropy S, calculated as $S = \int_0^T C_p/T dT$. In the aforementioned equations, C_p is the heat capacity of the sample, and T is the temperature in Kelvin. If the heat capacity of the sample is known accurately, the thermodynamic properties of a material are thus known as a result thereof. [31]

The setup for the instrument used in this study is a conventional heat flux DSC, where the calorimeter has two sample positions within a furnace, one occupied by a reference sample and the other occupied by the sample under investigation. The reference sample consists of an empty DSC pan with a lid, while the sample under investigation contains the polymer sample within the pan, closed with a lid. The heating rate within the furnace is controlled and the thermocouple situated below each sample then measures the difference in temperature between the sample under investigation and the reference sample, which ultimately gives a heat flow value. These heat flow values are plotted as a function of time to give a DSC thermogram, from where the relevant properties of the samples are ultimately calculated. A schematic of the DSC setup can be seen in Figure 2.7.

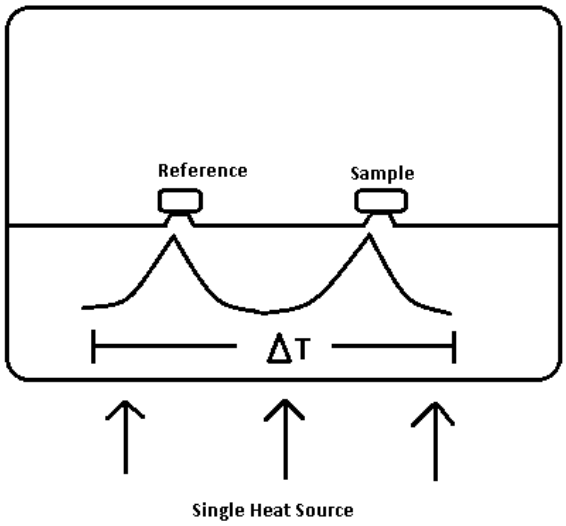

Figure 2.7: Experimental setup of a heat flux DSC instrument

It was previously mentioned that various properties can be determined from DSC, and these properties can be classified as either first- or second order thermal transitions. T_m and T_c are first order thermal transitions, as it has latent heat associated to the property, and is observed as a physical peak on the DSC thermogram, while the T_g is a second order thermal transition, only observed as a baseline shift on the curve of the DSC thermogram. Only the melting temperature (T_m) and crystallization temperature (T_c) are of interest in the DSC measurements to be done for this project. The enthalpy associated with the melting event for each

sample will be used to calculate the percentage crystallinity of the sample. The enthalpy of melting of each sample is calculated by integrating the area under the crystalline melt endotherm peak and is used in the equation below to determine the percentage crystallinity of the sample: [32]

$$\frac{\Delta H_m}{\Delta H_{0\,100\,\%\,crystalline}} \times 100 = \%\,crystallinity \tag{2.1}$$

Where ΔH_m is the enthalpy of the melting peak and $\Delta H_{0\,100\,\%\,crystalline}$ is the theoretical melt enthalpy value for a 100 $\%$ crystalline polymer sample.

DSC has previously been implemented in order to obtain qualitative data that could correlate with the chemical composition distribution of a polymer. It can't, however, replace TREF as a preparative technique in the sense that it is purely a qualitative technique that does not provide an ideal environment for polymer crystallization and thus can't give quantitative mass measurements. [20]

2.3.2 HT-SEC

Size exclusion chromatography (SEC) is a liquid chromatographic technique that is the most widely used technique for the determination of molar mass related properties of synthetic polymers. This method is used so often in part due to it being relatively simple to use, relatively inexpensive, fast and repeatable. SEC is extremely valuable as it allows for highly accurate determination of molar mass and molar mass distribution of polymers, more specifically linear homopolymers. SEC is, however, not a flawless method as incorrect use of the technique will lead to poor quality of results, and is often the result of uninformed decisions regarding use of the technique. [33]

There are three main groups of molecular characteristics for linear homopolymers. These are the molar mass, chemical structure and physical architecture of polymers. The molar mass of a polymer is defined as the mass of one mole of the chemical substance under consideration, and is generally expressed in either g/mol or kg/mol. The molar mass of macromolecules can range from the low hundreds for oligomer materials, up to a few million for higher molar mass polymers. Chemical structure includes the composition of polymer backbones and the functionality of these chemical groups. [3] Macromolecules that consist of one type of monomer such as polypropylene are termed as homopolymers. The third molecular characteristic to be discussed is the molecular architecture of polymers. This includes the topology, spatial arrangement and stereoregularity of polymers. The relative orientation of side groups on polymer backbones, which will be methyl groups in the case of polypropylene, is directly responsible for stereoregularity of a polymer. Stereoregularity will lead to a polymer being classified as isotactic, syndiotactic or atactic and will have an influence on the crystallizability of a polymer. This means that the stereoregularity will have an effect on the solubility of a polymer, and thus on the enthalpic interactions of polymer chains within a liquid

chromatographic system. Synthetic polymers don't show homogeneous molecular characteristics, rather having a distribution thereof and thus represent a mixture of macromolecules of varying components. These distributions can be described as being unimodal, bimodal, broad, narrow etcetera by distribution functions. [33]

A SEC instrument typically consists of a pump, sample injector, column, stationary phase and detector. The pump typically allows for solvent throughput of 1 mL/min and needs to be kept consistent for accurate results. The sample injector will allow for automatic injection of the sample into the column so as to eliminate the opportunity for human error. The stationary phase within the column is important as the size of the pores on the stationary phase particles will play a big role in polymer absorption, and ultimately affects the retention time of the polymer. Ultimately the detector also plays a major role for obvious reasons. A refractive index detector is typically used that allows for the detection of the concentration of polymer at each elution time.

As is the case with all liquid chromatographic techniques, the sample being analysed needs to be dissolved, and this is no different for SEC. The polymers need to be dissolved at higher concentrations compared to what is needed for liquid chromatography of small molecules, often higher than 1 mg/mL. In thermodynamic terms for a polymer to be dissolved, is dependent on properties such as the Gibbs free energy ΔG, which is further related to thermodynamic values such as the entropy ΔS, and the enthalpy ΔH. For macromolecules the contribution of entropy of mixing is negligible and thus the enthalpy interactions are the driving factor in determining polymer solubility. Thermodynamically good solvents show a high solvating power to polymers, as the solvent molecules have more favourable interactions with the polymer chains than the polymer chains have with themselves. The crystallites found in a solid polymer sample need to disband, or high temperature needs to be used to melt the crystals for the polymer to be completely soluble. [33]
Polypropylene is a polymer material that is only soluble at high temperatures using strong solvents such as 1,2,4-trichlorobenzene and needs to be dissolved at temperatures between 130 and 160 °C. For polymers such as polypropylene we thus use a high temperature variation of SEC called high temperature size exclusion chromatography or HT-SEC. [2] A schematic of how low- and high molar mass polymer chains move through a SEC column can be seen in Figure 2.8. It can be seen that the lower molar mass chains have more interactions with the porous stationary phase particles, due to a larger fraction of the pores being accessible, and will thus elute after higher molar mass polymer chains, which have fewer interactions with the stationary phase.

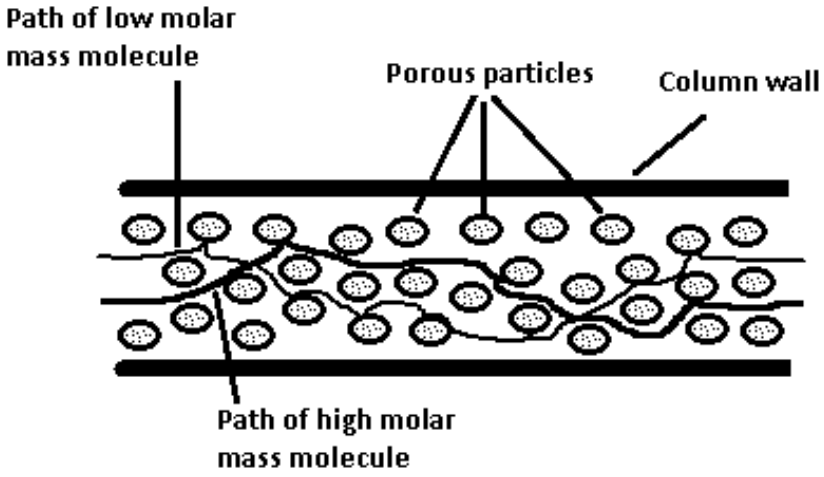

Figure 2.8: Movement of polymer chains of varying molar mass through SEC column

The dissolved polymer sample is transported through the column using a solvent that acts as the mobile phase. When utilizing a good solvent, the variation in size is bigger for polymer samples that have different molar mass and similar architecture and chemical composition, compared to when a poor solvent is used. A good solvent system is thus implemented in HT-SEC due to the fact that polymers are separated based on their size in solution, also called the hydrodynamic volume. The column packing, which serves as the stationary phase, is porous and is thus also important as it has enthalpic interactions with both the polymer chains and the solvent molecules. The dissolved polymer chains will absorb into these pores to different degrees dependant on the nature of the interactions. The mobile phase should be chosen to have such a nature that the polymer chains have preferential interaction with the solvent rather than with the stationary phase. This will allow for molar mass separation, as higher molar mass polymer chains will then elute first due to more preferential interactions with the mobile phase, followed by the lower molar mass polymer chains. There aren't a wide variety of column stationary phases available, and as a result the nature of the mobile phase is the easier parameter to vary during analysis. SEC mobile phases thus need to be chosen for their interaction to stationary phase and polymer chains. [33]

Number- and weight-average molar mass values are obtained for molecular characteristics such as molar mass, by adding the molar mass of polymer chains of the same type and calculating an average value. Average molar mass can be defined as the total mass of the polymer divided by the total number of molecules and can be calculated in two ways to give number- and weight-average values. The number-average molar mass is calculated using the equation: $M_n = \frac{\sum N_i M_i}{\sum N_i}$ with the weight-average molar mass being calculated using the equation: $M_w = \frac{\sum N_i M_i^2}{\sum N_i M_i}$. A useful parameter to determine for polymers is the dispersity of the polymer chains and is defined as the ratio between the weight- and number-average molecular weights.

The dispersity is calculated using the equation: $PDI = \frac{M_w}{M_n}$. These average values don't say much about the actual shape of the distribution, as the dispersity value might be the same for polymers with both a unimodal and a bimodal distribution. [33]

2.3.3 FTIR spectroscopy

Fourier transform infrared spectroscopy or FTIR spectroscopy is a characterization technique that is sensitive to the structure and folding method of polypropylene chains, and is thus a method implemented to characterize the changes in helical conformation of polypropylene. [34,35] It has been well established in recent years that a set relationship exists between specific regularity bands found on an FTIR spectrum, and the critical helix length of polypropylene. For example, regularity bands at 1220, 840, 998 and 973 cm^{-1} have helical structures with a decreasing degree of order and have minimum n values (critical helix length) of 14, 12, 10 and 5 monomer units respectively. Thus, higher n values correspond to higher ordered degree of regularity. The differences in absorbance of several regularity bands could thus be calculated to obtain information regarding the conformational changes in polypropylene. [34,36]

Regularity bands occur due to intramolecular vibration within a single chain, and is the type of infrared band most commonly observed for polypropylene. [36] Crystalline bands also occur, however, will not be discussed in the scope of this study. The critical helix length can be described as the minimum number of monomers that have to be present in order for the regularity band to be present on the FTIR spectrum. Furthermore, if it is known that the thermal history of samples are identical, then differences in conformational order degree can be attributed to differences in structural regularities in the sample. [5] This allows for the use of FTIR to investigate the structural regularities in various polypropylene samples and can be used alongside other techniques to obtain valuable information about polymer catalysts and polymer forms.

2.3.4 XRD

X-ray diffraction or XRD, is a method wherein a sample is radiated with X-rays and the angle at which these rays are scattered are measured. This technique is generally used to determine the crystallinity of a sample, however, it could be employed to achieve many other applications such as the orientation of crystals and corresponding mass fractions thereof. [37] The technique is widely implemented to determine sample crystallinity as it measures the crystallinity directly, rather than measuring properties related to crystallinity. Another interesting application of XRD is to determine the type of crystal lattice present within the sample. Polypropylene crystals occurs in at least three forms namely the monoclinic (α), hexagonal

(β), and triclinic/orthorhombic (γ) forms. [15,38–42] A schematic of the diffraction patterns of these forms can be seen in Figure 2.9. [43] The XRD instrument can be used in two settings, namely the wide-angle X-ray diffraction (WAXD) or the small angle X-ray scattering (SAXS) settings. These settings only differ in the deviation angle of the incident beam measured in degrees as the 2θ angle. [38]

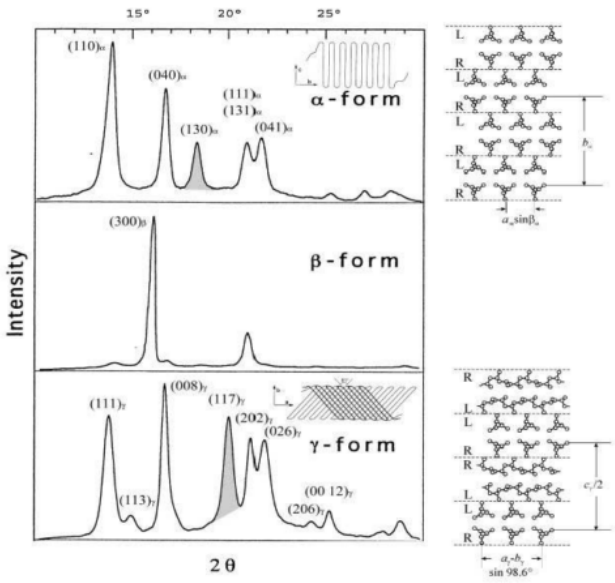

Figure 2.9: Typical diffraction patterns of alpha, beta and gamme forms of iPP

From an XRD diffractogram it is possible to obtain some properties of polymers by simply utilizing Braggs Law: $n\lambda = 2dsin\theta$, as well as the Debye-Scherrer Equation: $L = \frac{0.9\lambda}{\beta cos\theta}$. [34] From Bragg's Law it is possible to determine the crystal-spacing *d* between the crystals, and from the Debye-Scherrer equation the crystallite size *L* could be determined. The *d*-spacing of the crystals give us relevant information regarding the distance between single crystals. The intensity of the diffracted X-ray beams is affected by the relative positions of atoms within the unit cell. [38] The full width at half maximum (FWHM) of each peak is related to the crystallinity of the sample in that the thinner the FWHM the higher the crystallinity of the sample. Finally, from Braggs' Law it can be derived that the larger the sinθ value for a specific peak, the closer the individual crystals will be to each other. A schematic of how the instrument works can be seen in Figure 2.10.

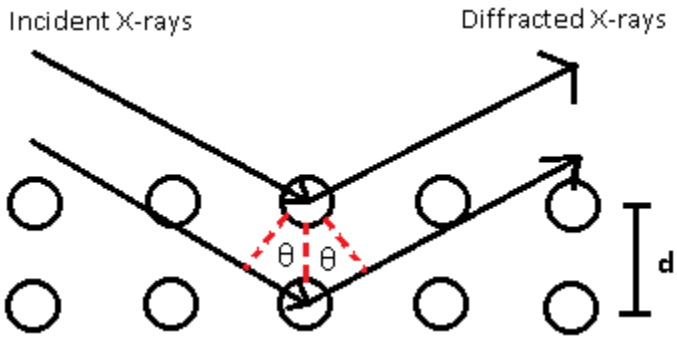

Figure 2.10: Representation of how X-rays are reflected in an XRD experiment

It is known that the crystallization behaviour of polypropylene is complicated, as thermal history and detailed microstructure of the polymer chains determine the morphology and properties of the polymer after it has crystallized. [15] From literature it is possible to assign the relevant peaks as α, β or γ peaks. For example, with α-iPP five peaks will occur in a WAXD diffractogram at 2θ angles of about 14.3, 17.1, 18.5, 21.2 and 21.9 ° corresponding to the α(110), α(040), α(130), α(111) and α(-131) peaks respectively. [34] The specific crystal structures that form during solution crystallization are called quadrites and are present in the -monoclinic form with cell parameters a = 6.65, b = 20.78 and c = 6.50 Å and a rough representation of how these lattices occur can be seen in Figure 2.11. [44,45]

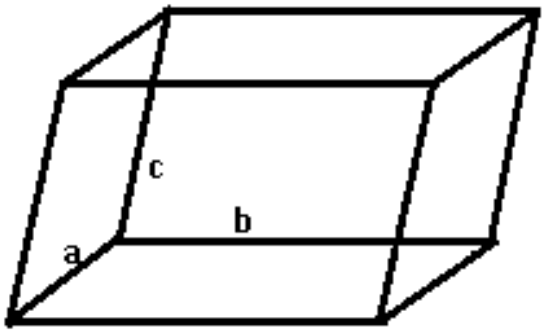

Figure 2.11: Unit cell paramters for isotactic polypropylene

The diffraction pattern that occurs due to the orientation of the crystal lattices are characteristically monoclinic, as the a1 and c1 axes are parallel to c2 and a2 respectively. The actual crystalline structure of polypropylene is unique in the sense that it has a characteristic lamellar branching, which has not been seen in other semi-crystalline polymers. This characteristic branching is mostly present in the α-monoclinic form, while it could be present in the γ-triclinic form and not at all in the γ-hexagonal form, which is strange as all the forms of iPP have a threefold helical configuration. [44,45] A representation of how α-monoclinic crystal reflections occur can be seen in Figure 2.12.

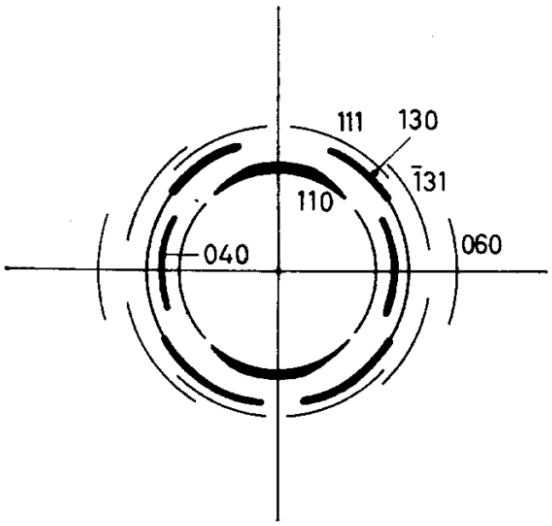

Figure 2.12: Representation of α-monoclinic crystal reflections [45]

Polypropylene exists as a lamellar stacking of spherulites and is very different to the crystal structure of polyethylene and other semi-crystalline polymers, which exists as a radiating lamellar structure. When crystallized from the molten state, polypropylene generally forms the α-monoclinic crystal structure and in some cases, β-modification may be present. For both the α- and β-modifications a threefold helical configuration is observed, where the left or right handed conformation of the helix is determined by the succession of the methyl groups on the polypropylene chain. [45]

As mentioned before, the α-monoclinic form is the most common form present in polypropylene. Generally, the β and γ forms will only be formed under special conditions. The β-hexagonal form can be made using nucleating agents or a temperature gradient during crystallization, while the γ-triclinic form can be produced when propylene is polymerized with Ziegler-Natta catalysts at elevated pressures or by incorporating low molecular weight polymer that has very little chain folding present. [15,40] The β -crystals found in polypropylene are fairly interesting as they showcase excellent toughness properties, and as a result have received a fair amount of attention in the industry. [46] The form has been seen to have a higher modulus and tensile strength. Up to this point, the best way to obtain β crystals in polypropylene was to add a β-nucleating agent, and is widely implemented in industrial production. [40–42,46,47]

2.3.5 SSA

Successive self-nucleation and annealing is a thermal fractionation technique developed by Muller et al. [48] in 1997. Since the introduction of SSA, the technique has been widely used throughout the world as SSA could yield both quantitative and qualitative data regarding various distributions within a sample, such as the lamellar thickness in the sample. [49] This technique is based on the application of successive nucleation and annealing steps to a sample in order to thermally fractionate the sample. It is a fractionation technique vastly different from solution fractionation techniques such as TREF and CRYSTAF in the sense that it does not use any solvents, and it cannot physically fractionate the sample. Using SSA leads to the production of a distribution of lamellar crystals within each sample, the sizes of which give information regarding the distribution of the methyl sequence length (MSL) within a sample. Fractionation occurs due to defects in a sample which are generally found in the amorphous regions of a sample, while the more regular structures are found inside the lamellar crystals. [48–50]

The use of DSC to employ SSA was developed by Fillon et al. [51] and the procedure for self-nucleation and annealing is described as follows: [51,52] Firstly the thermal history of the sample needs to be erased and this is achieved by heating the sample to 25-30 °C above its melting temperature and keeping the temperature constant for at least three minutes. The sample is then cooled down at a constant rate to a predetermined temperature low enough for the sample to completely crystallize, that is called the standard semi-crystalline state. The sample is then heated again at a constant rate to a thermal conditioning temperature (T_s) where the sample is melted, nucleating and allowed to anneal at the temperature for five minutes. The sample is then cooled down from T_s down to the standard T_c at a constant cooling rate and held at this temperature for five minutes. The heating and cooling steps is then repeated for the amount of self-nucleation and annealing steps that the operator needs and the T_s is decreased by an increment of 4 or 5 °C for each step. The final step implemented is a heating cycle at a constant rate up to the same temperature it was heated to in the first heating step. A final multiple melting endotherm is then obtained showing the melting peaks relevant to the thermally fractionated sample. [49]

Fillon et al. [51] described three specific domains pertaining to the self-nucleation and annealing of isotactic polypropylene. These domains are described as follows: Domain I is the melting domain, where complete melting has occurred and the thermal history of the sample has been erased. This is thus the temperature range from the lowest temperature directly following a melting peak, up to the temperature at which the sample is kept, removing all thermal history. Domain II is the self-nucleation domain. Thermal annealing at the T_s temperature leads to the self-nucleation of the polymer sample and the T_c subsequently shifts to a higher temperature. Domain III is the self-nucleation and annealing domain where T_s is too low and

as a result a partially melted sample is obtained and thus the unmolten crystals will anneal. This will lead to a melting endotherm with a small peak at a high temperature as a result of the annealed crystals that melt.

2.3.6 NMR spectroscopy

2.3.6.1 High temperature ^{13}C solution NMR spectroscopy

It is of critical importance to be able to characterize the microstructure of polymers in order to understand amongst other, polymer properties and the mechanism of polymerization. Nuclear magnetic resonance- or NMR spectroscopy is one of, if not the most important method, for analysing and characterizing microstructure of chemical molecules. When analysing polymers, ^{13}C-NMR is very often used, especially for olefinic polymer molecules. [53–56] Due to the nature of olefinic materials, ^{13}C-NMR analysis has to be done at high temperatures to ensure that the sample doesn't crystallize within the NMR tube. The technique can thus be referred to as high temperature ^{13}C-NMR, or HT-^{13}C NMR. The primary advantage of ^{13}C NMR comes in the chemical shift range, it being approximately 20 times that which it would be for ^{1}H-NMR. Well separated resonances also allow for high levels of structural sensitivity with different types of carbon atoms. The low abundance of ^{13}C nuclei (about 1 %), can be seen as both an advantage and a problem. This is because the low abundance will allow for specific carbons to be observed, however, very long analysis times are needed due to the low abundance. Proton interactions can be easily eliminated by hetero-nuclear decoupling, allowing for the observation of a specific polymer moiety at each chemical shift. In this sense, ^{13}C-NMR nearly resembles mass spectrometry, as each NMR peak represents a fragment of the polymer molecule. [57,58]

The technique of course has some difficulties that need to be overcome in order to fully utilize the power of the method. The sensitivity of ^{13}C-NMR leads to the presence of a cluster of structural information which relates to sequences ranging from three to seven units in length. The structural information obtained thus has to be assigned and sorted which might take some time initially. As Fourier transform and signal averaging techniques are generally used to obtain the ^{13}C-NMR spectra, it is necessary to have good knowledge of the characteristics of the polymer under investigation. The equilibrium conditions need to be set correctly to avoid distorted spectral information and the nuclear Overhauser effect (NOE) also needs to be considered. If the NOE is equal or otherwise taken into consideration, then the intensities of the spectra can be used to obtain the concentration of specific pentads within the polymer molecule. It has been observed through the years that for polymers the NOE is at a maximum and as a result distorts the

NMR peaks equally throughout the spectra. [57,58]

Pentads are the result of four dyads next to each other. A dyad can be defined as the relative orientation of two adjacent chemical groups, which in the case of polypropylene are methyl groups. A meso dyad configuration is present when two methyl groups next to each other have the same configuration, while a racemic configuration is when the two methyl groups have opposite configurations. A dyad could thus be classified as either 'm' or 'r' and gives structural information regarding the relative configurations of two adjacent methyl groups. Depending on the strength of the NMR instrument that is used, different levels of sensitivity can be obtained, however, we will only concern ourselves with the pentad sensitivity level where methyl carbon resonances are influenced by the adjacent methyl groups as well as the next nearest methyl groups. When observing pentads on a ^{13}C NMR spectrum, we can find ten different methyl regions, ranging from the 'mmmm' to the 'rrrr' pentads with several variations in-between. This classification of pentads is now also only relevant to the methyl region of the ^{13}C-NMR spectrum. In semi-crystalline polypropylene there are three main regions to be seen on the ^{13}C-NMR spectrum, namely the methylene region occurring at about 46 ppm, the methine region occurring at about 28 ppm and the methyl region occurring at about 20 ppm, all measured relative to an internal tetramethylsilane (TMS) reference. [57,58]

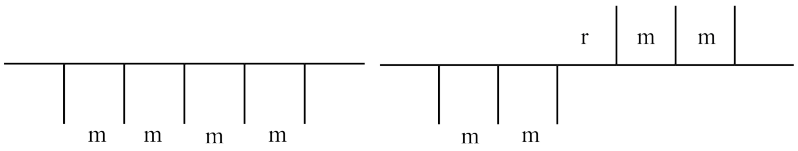

Figure 2.13: Aid to explanation of polypropylene pentads

The small schematics in Figure 2.13 serve as explanation to how pentads work. On the left we have an 'mmmm' pentad (or four consecutive 'm' dyads), which consists of five methyl groups all oriented in the same direction relative to each other. On the right we see that there are two methyl groups that are oriented in opposite directions relative to each other, and we thus have an 'r' dyad present. When considering the methyl orientations that occur when a Ziegler-Natta catalyst is used we can consult the schematic in Figure 2.14.

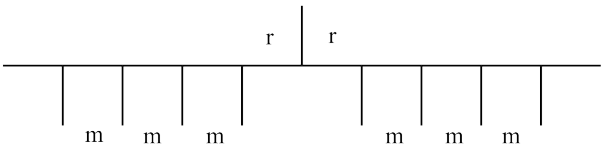

Figure 2.14: Ideal pentad conformation using Ziegler-Natta catalyst

When a stereo-error occurs during polymerization with a Ziegler-Natta catalyst, i.e when a methyl group ends up in an opposite orientation to its adjacent methyl group and forms an 'r' dyad, then in an ideal Ziegler-Natta setup the catalyst would 'correct' the error, which leads to another 'r' dyad. Ideally the chain would then continue producing 'm' dyads, leading to highly isotactic polypropylene. From this schematic above it is possible to predict three pentads that would occur in the methyl region of a ^{13}C NMR spectrum, due to stereodefects in the polymer chain. These are the 'mmmr', 'mmrr' and 'mrrm' pentads. A further six pentads might occur whose presence will lead to the formation of atactic material. These are the 'rmmr', 'mmrm', 'rmrm', 'rmrr', 'mrrr' and 'rrrr' pentads. Together with the purely isotactic 'mmmm' pentads we now have ten pentads which might occur in the spectrum.

2.3.6.2 Solid-state NMR spectroscopy

Solid-state NMR spectroscopy, is a powerful analytical technique employed for characterizing the crystalline and non-crystalline regions of semi-crystalline polymer materials in their solid state. [59] We will employ this technique as a method to determine chain conformation along with the molecular dynamics of the polymer chains. This is convenient as it enables us to compare the results to other solid-state techniques such as DSC and XRD. NMR was for a long period of time mainly conducted on solution state samples, because nuclear resonance lines had large widths when analysing solids. [60] This problem was resolved by the development of a technique that reduced the linewidths by three orders of magnitude and thus paved the way for solid-state NMR to become a valuable technique for the analysis and characterization of solid polymer samples. [61–63] These techniques included the use of cross polarization magic angle spinning (CPMAS) experiments. CP is applied in order to remove the effects of chemical shift anisotropy (CSA) and heteronuclear dipolar coupling which leads to an increase in the resolution of the solid state resonances. [64]

Several solid state ^{13}C NMR studies has been conducted on isotactic polypropylene. [59,60,65,66] Polypropylene will have peaks present in similar regions in the solid state compared to solution NMR, namely a methyl peak (-CH_3) at about 22 ppm, a methine peak (-CH-) at about 26 ppm and a methylene peak (-CH_2-) at about 44 ppm. A system was developed for assignment of peaks and changes specifically within the methylene region, relating to the disorder in the chain packing by Comotti et al. [67] Solid-state NMR can be used as a complementary technique to solution state NMR in that it obtains information on the chain conformations in the solid state, similar to how we can elucidate chain microstructure in solution NMR. This is possible because the polymer chains exist in different environments, thus there are chain segments in different environments which will have different molecular dynamics. These molecular dynamics can be picked up on by solid-state NMR as we can utilize the technique to give us information of the crystalline, as well as the mobile areas of the polymer. [68]

Isotactic polypropylene is known to exist in different crystal structures or allomorphs such as the α, β and γ forms. These allomorphs all have a 3_1 helix conformation, however, the crystal packing of these helices differ. The α allomorph has helices of alternating handedness that stack together, which leads to the methyl and methylene carbons experiencing non-equivalent environments. This ultimately leads to a splitting of the methylene peak in a 2:1 ratio. [67] The methylene peak could potentially be deconvoluted into three separate peaks, where one would relate to the disordered phase, and two peak (on alternating sides of the first peak) would represent the ordered α phase, in a 2:1 ratio as mentioned previously. [67]

While the CPMAS experiments are mostly sensitive to rigid crystalline components of low mobility, there is a different solid-state NMR experiment that can be executed in order to visualise the mobile components of the polymer system. This technique is called dipolar dephasing or interruptive decoupling and will be referred to further on as IDREF. This technique observes the decay of dipolar carbon-proton interactions, where stronger dipolar coupling will have a faster decay. If there is mobility, the coupling will be weaker, and the decay will be slower, allowing us to observe these segments on an IDREF spectrum.

2.3.7 SEM

It is known that there are difficulties related to analysis of polymers by microscopic techniques, and as a result there aren't many simple techniques that can be used to obtain contrast in orthodox electron microscopes. As polymers mainly consist of carbon and hydrogen they are low density materials, and together with having low atomic number atoms present, leads to poor electron scattering and ultimately low contrast images. [69] Scanning electron microscopy (SEM) is a technique employed to look at the surface morphology of polymers at high resolution. The use of field-emission SEM (FE-SEM) is an effective method to look at the surface morphology of polymers as it gives high resolution at low voltages. The field emission gun is an improvement to the technique which has a small spot size and a low energy spread and allows for high resolution SEM. These advancements in SEM technology is promising for morphological characterizations of polymers as in theory resolution could be obtained at 50 angstrom at a charge of 1.0 keV. [69] Low voltages (0.5-5.0 keV) are necessary when analysing polymers by SEM, as polymers are poor conductors, and as a result charge builds up on the sample when exposed to the electron beam. [69,70] The accumulation of heat and electric charge decreases sample stability and is called 'charging'. Polymer samples are coated with a conductive carbon layer prior to exposure to the electron beams to minimize the effects of charging. The coating has the disadvantage of concealing some fine topographical features on the sample surface. [69] SEM will be mainly used to investigate the surface morphology as well as individual particle size of the isotactic polypropylene powder samples.

2.4 References

1. Mamun, A., Mujibur Rahman, S. M. & Aiken, C. Influences of the chemical defects on the crystal thickness and their melting of isothermally crystallized isotactic polypropylene. *J. Polym. Res.* **24**, 19 (2017).
2. Macko, T. & Pasch, H. Separation of linear polyethylene from isotactic, atactic, and syndiotactic polypropylene by high-temperature adsorption liquid chromatography. *Macromolecules* **42**, 60636067 (2009).
3. Viville, P., Daoust, D., Jonas, A.M., Nysten, B., Legras, R., Dupire, M., Michel, J. & Debras, G. Characterization of the molecular structure of two highly isotactic polypropylenes. *Polymer (Guildf)*. **42**, 19531967 (2001).
4. Virkkunen, V., Laari, P., Pitknen, P. . & Sundholm, F. Tacticity distribution of isotactic polypropylene prepared with heterogeneous Ziegler-Natta catalyst. 1. Fractionation of polypropylene. *Polymer (Guildf)*. **45**, 30913098 (2004).
5. Kang, J., Yang, F., Wu, T., Li, H., Liu, D., Cao, Y., Xiang, M. Investigation of the crystallization behavior of isotactic polypropylene polymerized with different Ziegler-Natta catalysts. *J. Appl. Polym. Sci.* **129**, 26632670 (2013).
6. Kang, J., Chen, J., Cao, Y., Li, H. Investigation of the Stereodefect Distribution and Conformational Behavior of Isotactic Polypropylene Polymerized with Different ZieglerNatta Catalysts. *Polym. Polym. Compos.* **125**, 30763083 (2012).
7. Cheruthazhekatt, S., Pijpers, T. F. J., Harding, G. W., Mathot, V. B. F. & Pasch, H. Multidimensional analysis of the complex composition of impact polypropylene copolymers: Combination of TREF, SEC-FTIR-HPer DSC, and high temperature 2D-LC. *Macromolecules* **45**, 20252034 (2012).
8. Nikolaeva, M., Matsko, M. & Zakharov, V. Comparative Study of Distribution of Active Sites According to Their Stereospecificity in Propylene Polymerization over the Traditional TiCl 3 and Supported Titanium-Magnesium Catalysts with Different Composition. *Macromol. Chem. Phys*. 1700488, 1700488 (2018).
9. Virkkunen, V., Pietil, L. O. & Sundholm, F. DFT investigation of the regiospecificity of a model catalyst site for propene polymerisation. *Polymer (Guildf)*. **44**, 31333139 (2003).
10. Boero, M., Parrinello, M., Hffer, S. & Weiss, H. First principles study of propene polymerization in Ziegler-Natta heterogeneous catalysis. *J. Am. Chem. Soc.* **122**, 501509 (2000).
11. Cavallo, L., Guerra, G. & Corradini, P. Mechanisms of propagation and termination reactions in classical heterogeneous Ziegler-Natta catalytic systems: A nonlocal density functional study. *J. Am. Chem. Soc.* **120**, 24282436 (1998).
12. Soares, J. B. P. Mathematical modelling of the microstructure of polyolefins made by coordination polymerization: A review. *Chem. Eng. Sci.* **56**, 41314153 (2001).

13. Chadwick, J. C., Morini, G., Balbontin, G., Camurati, I., Heere, J.J.R., Mingozzi, I., Testoni, F. Effects of Internal and External Donors on the Regio- and Stereoselectivity of Active Species in MgCl 2 - Supported Catalysts for Propene Polymerization. *Macromol. Chem. Phys* **202**, 19952002 (2002).

14. Chadwick, J. C., van der Burgt, F.P.T.J. & Rastogi, S. Influence of ziegler-natta catalyst regioselectivity on polypropylene molecular weight distribution and rheological and crystallization behavior. *Macromolecules* **37**, 97229727 (2004).

15. Bond, E. B., Spruiell, J. E. & Lin, J. S. WAXD/SAXS/DSC study on the melting behavior of Ziegler-Natta and metallocene catalyzed isotactic polypropylene. *J. Polym. Sci. Part B Polym. Phys.* **37**, 30503064 (1999).

16. Stukalov, D. V., Zakharov, V. A., Potapov, A. G. & Bukatov, G. D. Supported Ziegler-Natta catalysts for propylene polymerization. Study of surface species formed at interaction of electron donors and TiCl4with activated MgCl2. *J. Catal.* **266**, 3949 (2009).

17. Andoni, A., Chadwick, J. C., Niemantsverdriet, H. J. W. & Thne, P. C. The role of electron donors on lateral surfaces of MgCl2-supported Ziegler-Natta catalysts: Observation by AFM and SEM. *J. Catal.* **257**, 8186 (2008).

18. Albizzati, E., Giannini, U., Morini, G., Galimberti, M., Barino, L. & Scordamaglia, R. Recent advances in propylene polymerization with MgCl2 supported catalysts. *Macromol. Symp.* **89**, 7389 (1995).

19. Chadwick, J. C., Morini, G., Albizzati, E., Balbontin, G., Mingozzi, I., Cristofori, A. Aspects of hydrogen activation in propene polymerization using MgCl2/TiCl4/diether catalysts. **2510**, 25012510 (1996).

20. Monrabal, B. Temperature Rising Elution Fractionation and Crystallization Analysis Fractionation. Encycl. *Anal. Chem.* 80748094 (2006). doi:10.1002/9780470027318.a2035

21. Soares, J. B. P. & Hamielec, A. E. Temperature rising elution fractionation of linear polyolefins. *Polymer (Guildf).* **36**, 16391654 (1995).

22. Anantawaraskul, S., Soares, J. B. P. & Wood-Adams, P. M. Fractionation of semicrystalline polymers by crystallization analysis fractionation and temperature rising elution fractionation. *Adv. Polym. Sci.* **182**, 154 (2005).

23. Monrabal, B. Crystallization analysis fractionation: A new technique for the analysis of branching distribution in polyolefins. *J. Appl. Polym. Sci.* **52**, 491499 (1994).

24. Monrabal, B. lZ0,81-86 (1996). *Macromol. Symp.* **86**, 8186 (1996).

25. Brll, R., Pasch, H., Wahner, U. & Monrabal, B. Analysis of polyolefin blends by CRYSTAF. *Macromol. Symp.* **178**, 8191 (2002).

26. Anantawaraskul, S., Soares, J. B. P. & Wood-Adams, P. M. An experimental and numerical study on crystallization analysis fractionation (Crystaf). *Macromol. Symp.* **206**, 5768 (2004).

27. Soares, J. B. P. & Anantawaraskul, S. Crystallization analysis fractionation. J. Polym. Sci. Part B *Polym. Phys.* **43**, 15571570 (2005).

28. Britto, L. J. D., Soares, J. B. P., Penlidis, A. & Monrabal, B. Polyolefin Analysis by Single-Step Crystallization Fractionation. J. Polym. Sci. Part B *Polym. Phys.* **37**, 539552 (1999).

29. Cheruthazhekatt, S., Robertson, D. D., Brand, M., Van Reenen, A. & Pasch, H. Solution crystallization and dissolution of polyolefins as monitored by a unique analytical tool: Solution crystallization analysis by laser light scattering. *Anal. Chem.* **85**, 70197023 (2013).

30. Robertson, D. Studying crystallization kinetics using Solution Crystallization Analysis by Laser Light Scattering (Scalls). (Stellenbosch University, 2012).

31. Schick, C. Differential scanning calorimetry (DSC) of semicrystalline polymers. *Anal. Bioanal. Chem.* **395**, 15891611 (2009).

32. Mathot, V. B. F. & Pijpers, M. F. J. Heat capacity, enthalpy and crystallinity of polymers from DSC measurements and determination of the DSC peak base line. *Thermochim. Acta* **151**, 241259 (1989).

33. Berek, D. Size exclusion chromatography - A blessing and a curse of science and technology of synthetic polymers. *J. Sep. Sci.* **33**, 315335 (2010).

34. Kang, J., Chen, J., Cao, Y. & Li, H. Effects of ultrasound on the conformation and crystallization behavior of isotactic polypropylene and -isotactic polypropylene. *Polymer (Guildf).* **51**, 249256 (2010).

35. Su, Z., Wang, H., Dong, J., Zhang, X., Dong, X., Zhao, Y., Yu, J., Han, C.C., Xu, D. & Wang, D. Conformation transition and crystalline phase variation of long chain branched isotactic polypropylenes (LCB-iPP). Polymer (Guildf). 48, 870876 (2007).

36. Zhu, X., Yan, D. & Fang, Y. In Situ FTIR Spectroscopic Study of the Conformational Change of Isotactic Polypropylene during the Crystallization Process. *J. Phys. Chem. B* **105**, 1246112463 (2001).

37. Somani, R. H., Hsiao, B. & Nogales, A. Structure development during shear flow induced crystallization of i-PP: In situ wide-angle X-ray diffraction study. *Macromolecules* **34**, 59025909 (2001).

38. Reid, J. Introduction to Crystallography. (2012).

39. Varga, J. Supermolecular structure of isotactic polypropylene. *J. Mater. Sci.* **27**, 25572579 (1992).

40. Cai, Z., Zhang, Y., Li, J., Shang, Y., Huo, H., Feng, J., Funari, S.S. & Jiang, S. Temperature-dependent selective crystallization behavior of isotactic polypropylene with a -nucleating agent. *J. Appl. Polym. Sci.* **128**, 628635 (2013).

41. Yang, S., Yu, H., Li, J., Guo, S., Wu, H., Shen, J., Xiong, Y. & Chen, R. Formation Mechanism and Morphology of -Transcrystallinity of Polypropylene Induced by Two-Dimensional Layered Interface. *Macromolecules* **48**, 39653973 (2015).

42. Varga, J. -Modification of Isotactic Polypropylene: Preparation, Structure, Processing, Properties, and Application. *J. Macromol. Sci.* Part B **41**, 11211171 (2002).

43. van der Burgt, F. P. T. J. Crystallization of isotactic polypropylene: The influence of stereo-defects. (Technische Universiteit Eindhoven, 2002). doi:10.6100/IR559498

44. Lotz, B. & Wittmann, J. C. The molecular origin of lamellar branching in the (monoclinic) form of isotactic polypropylene. *J. Polym. Sci.* Part B *Polym. Phys.* **24**, 15411558 (1986).

45. Binsbergen, F. L. & de Lange, B. G. M. Morphology of polypropylene crystallized from the melt. *Polymer (Guildf).* **9**, 2340 (1968).

46. Yang, S. G., Chen, Y., Deng, B., lei, J., Li, L. & Li, Z. Window of Pressure and Flow to Produce -Crystals in Isotactic Polypropylene Mixed with -Nucleating Agent. *Macromolecules* **50**, 48074816 (2017).

47. Stocker, W., Schumacher, M., graff, S., Thierry, A., Wittmann, J. & Lotz, B. Epitaxial crystallization and AFM investigation of a frustrated polymer structure: Isotactic poly(propylene), phase. *Macromolecules* **31**, 807814 (1998).

48. Muller, a J., Hernandez, Z. H., Arnal, M. L. & Sanchez, J. J. A novel technique to study molecular segregation during crystallization. *Polym. Bull.* **472**, 465472 (1997).

49. Mller, A. J., Michell, R. M., Prez, R. A. & Lorenzo, A. T. Successive Self-nucleation and Annealing (SSA): Correct design of thermal protocol and applications. *Eur. Polym. J.* **65**, 132154 (2015).

50. Virkkunen, V., Laari, P., Pitknen, P. & Sundholm, F. Tacticity distribution of isotactic polypropylene prepared with heterogeneous Ziegler-Natta catalyst. 2. Application and analysis of SSA data for polypropylene. *Polymer (Guildf).* **45**, 46234631 (2004).

51. Fillon, B., Wittmann, J. C., Lotz, B. & Thierry, A. Selfnucleation and recrystallization of isotactic polypropylene (phase) investigated by differential scanning calorimetry. *J. Polym. Sci.* Part B *Polym. Phys.* **31**, 13831393 (1993).

52. Mller, A. J. & Arnal, M. L. Thermal fractionation of polymers. *Prog. Polym. Sci.* **30**, 559603 (2005).

53. Zhou, Z., Kummerle, R., Stevens, J.C., Redwine, D., He, Y., Qiu, X., Cong, R., Klosin, J., Montanez, N. & Roof, G. 13C NMR of polyolefins with a new high temperature 10 mm cryoprobe. *J. Magn. Reson.* **200**, 328333 (2009).

54. Inoue, Y., Nishioka, A. & Chujo, R. Carbon-13 Nuclear Magnetic Resonance Spectroscopy of Polypropylene. *Die Makromol. Chemie* **152**, 1526 (1972).

55. Busico, V., Cipullo, R., Monaco, G., Vacatello, M. & Segre, A. L. Full Assignment of the 13 C NMR Spectra of Regioregular Polypropylenes: Methyl and Methylene Region. *Macromolecules* **30**, 62516263 (1997).

56. Busico, V., Cipullo, R., Monaco, G., Talarico, G. & Vacatello, M. High-resolution 13C NMR configurational analysis of polypropylene made with MgCl2-supported Ziegler-Natta catalysts. 1. The model system MgCl2/TiCl4-2,6-dimethylpyridine/Al(C2H5)3. *Macromolecules* **32**, 41734182 (1999).

57. Randall, J. C. Carbon - 13 NMR and Polymer Stereochemical Configuration. *Am. Chem. Soc.* **9**, 7183 (1979).

58. Randall, J. C. & Petroleum, P. Distribution of Monomer Configurations in Polypropylene as Determined with 13C NMR. *J. Polym. Sci.* **12**, 703712 (1974).

59. Saito, S., Moteki, Y., Nakagawa, M., Horii, F. & Kitamaru, R. High-Resolution Solid-State13c NMR Study of Isotactic Polypropylenes Isothermally Crystallized from the Melt. *Macromolecules* **23**, 32563260 (1990).

60. Lyeria, J. R. & Yannoni, C. S. High-resolution carbon-13 NMR of polymers in the solid state. *IBM J. Res. Dev.* **27**, 302312 (1983).

61. Yannoni, C. S. High-Resolution NMR in Solids: The CPMAS Experiment. *Acc. Chem. Res.* **15**, 201208 (1982).

62. Schaefer, J., Stejskal, E. O. & Buchdahl, R. Magic-Angle 13C NMR Analysis of Motion in Solid Glassy Polymers. *Macromolecules* **10**, 384405 (1977).

63. Lyerla, J. R., Yannoni, C. S. & Fyfe, C. A. Chemical Applications of Variable-Temperature Cpmas Nmr Spectroscopy in Solids. *Acc. Chem. Res.* **15**, 208216 (1982).

64. Colletti, R. F. & Mathias, L. J. in Solid State NMR of Polymers 2360 (Springer, 1991).

65. Bunn, A., Cudby, M. E. ., Harris, R. . & Say, B. . High resolution 13C n.m.r, spectra of solid isotactic polypropylene. *Polymer (Guildf).* **23**, 694698 (1982).

66. Gomez, M. a., Tanaka, H. & Tonelli, A. E. High-resolution solid-state 13C nuclear magnetic resonance study of isotactic polypropylene polymorphs. *Polymer (Guildf).* **28**, 22272232 (1987).

67. Comotti, A., Simonutti, R., Bracco, S., Castellani, L. & Sozzani, P. Simultaneous crystallization of isotactic and syndiotactic sequences of polypropylene. *Macromolecules* **34**, 48794885 (2001).

68. Botha, L. The effect of in-process ethylene incorporation on the evolution of particle morphology and molecular characteristics of commercial heterophasic ethylene propylene copolymers (HEPCs). (Stellenbosch University, 2014). doi:10.1016/j.eurpolymj.2013.04.020

69. Vezie, D. L., Thomas, E. L. & Adams, W. W. Low-voltage, high-resolution scanning electron microscopy: a new characterization technique for polymer morphology. *Polymer (Guildf).* **36**, 17611779 (1995).

70. Butler, J. H., Joy, D. C., Bradley, G. F. & Krause, S. J. Low-voltage scanning electron microscopy of polymers. *Polymer (Guildf).* **36**, 17811790 (1995).

Chapter 3

Materials and Methodology

This chapter will summarize the specifications of the materials studied in this project. It will also contain detailed experimental procedures followed during the project as well as a detailed example of the sample preparation required for each technique.

3.1 Materials

Bulk samples of 20 different isotactic polypropylene polymers were received from *Sasol*. A total of five different grades were received, with four variations of each relating to the catalyst used during polymerization as well as the final form of the polymer. These grades and some basic properties are summarised and can be seen in Table 3.1.

Table 3.1: Grades of polypropylene investigated during study

Grade	MFI (g/10min)	Tensile modulus (MPa)	Charpy impact strength (kJ/m^2)
HKQ 205	3	1400	4.5
HKR 102	3.5	1600	3.5
HMR 127	8.5	1550	3
HNR 100	12	1550	2.8
HNR 101	12	1550	2.8

3.2 Methodology

3.2.1 Fractionation techniques

3.2.1.1 TREF

Preparative temperature rising elution fractionation was used as the primary fractionation technique for the project. There are two main temperature cycles for TREF, namely the cooling cycle used for crystallization, and the heating cycle used for elution of polymer material. First, about 4 g of polymer and 0.08 g Irganox 1010/ Irgafos 165 stabilizer (2 wt$\%$) was dissolved in 400 mL p-Xylene (100 mL/g) at 130 ^{circ}C. During the dissolution time the support (quartz sea sand, Sigma Aldrich, 50-70 mesh particle size) is heated in a temperature blanket to approximately the same temperature as the dissolution. Following dissolution, the support is then added through a funnel into the reactor containing the dissolved polymer. Enough sand is added so as to cover the solvent surface completely. The reactor is then transferred into an oil bath preheated to 130 °C. This procedure is repeated for four separate reactors, as four reactors can fit in the oil bath simultaneously. Once all the reactors have been placed in the oil bath, the temperature is programmed to decrease at 1 °C/hour until the temperature reaches 25 °C.

Following the cooling cycle, the sand is then removed from the reactor and placed in a column. This column is then placed in an oven and is fitted with an inlet and an outlet for fresh solvent. Fresh solvent is then

pumped through the column at a rate of approximately 40 mL/min, while the oven temperature is increased. 500 mL of xylene is then collected for each temperature fraction which contains dissolved polymer. Fractions were collected at 30, 50, 70, 90 100, 110 and 140 °C for a total of 7 fractions. The solvent is then removed making use of rotary evaporation with the water bath kept at 80 °C. The polymer that stays behind in the round bottom flask after rotary evaporation is then transferred to a polytop and left to dry in a vacuum oven overnight. Three columns were eluted per sample, and the three fractions of the same temperature were combined.

3.2.1.2 SCALLS

Solution crystallization analysis by laser light scattering analysis was done on an instrument built within the department. A sample of 20 mg was placed in a quartz vial, together with a smooth stirrer bar and 20 mL o-dichlorobenzene was added. The temperature profile for analysis had cycles ranging from 130 °C to 30 °C and back to 130 °C at rates of either 5 or 10 °C/min. The polymer was found to crystallize onto the stirrer bar which led to inaccurate results and use of the technique was abandoned. CRYSTAF was used as an alternative

3.2.1.3 CRYSTAF

Crystallization analysis by fractionation was carried out using a Polymer Char model 200 instrument. Five samples weighing 20 mg were dissolved with 35 mL TCB/oDCB (1,2,4-trichlorobenzene/ortho-dichlorobenzene) at a temperature of 160 °C, each in a separate stainless-steel reactor. The polymer solutions were then allowed to cool down at a rate of 0.1 °C/min until it reached 30 °C, during which the concentration of the polymer was measured as a function of temperature.

3.2.2 Characterization techniques

3.2.2.1 DSC

For this characterization technique a heat-flux DSC instrument (*TA Instruments*, Q100) was used. Samples of approximately 4 mg were weighed off and added to an aluminium DSC pan and closed off with an aluminium lid. The samples were then analysed using a three-cycle temperature profile. In the first cycle the temperature in the heat chamber is increased at 10 °C/min up to 200 °C in order to erase all thermal history of the polymer. The temperature is then kept constant for five minutes at 200 °C. During the second

cycle, the temperature is then decreased at 10 °C/min down to 0 °C. The temperature is then kept constant for five minutes at 0 °C. During the third and final cycle, the temperature is increased at 10 °C/min up to 200 °C which signifies the end of the DSC analysis. The DSC instrument was calibrated using benzophenone as well as Indium standards. The chamber is kept under an inert N_2 atmosphere, flowing at 50 mL/min during the run.

3.2.2.2 HT-SEC

The molar mass properties of the samples were determined with High-Temperature Size Exclusion Chromatography using a Polymer Laboratories PL-GPC 220 instrument. A differential refractive index (RI) detector is coupled to the instrument. Samples weighing 4 mg were dissolved in 2 mL 1,2,4-trichlorobenzene (TCB) stabilized with 0.0125 % BHT, to prevent sample degradation to occur within the instrument as the instrument is kept at a temperature of 150 °C. Styrene-divinylbenzene (10 μm particle size) was used as the stationary phase, while the mobile phase consisted of TCB with 0.0125 % BHT operating at a flow rate of 1 mL/min. The column system consisted of three 300 x 7.5 mm^2 columns (PLgel Olexis, *Agilent Technologies*) together with a 50 x 7.5 mm^2 guard column (PLgel Olexis, *Agilent Technologies*). Samples of 200 μL were injected into the column. Narrow distribution polystyrene standards (*Agilent Technologies*) and polyethylene standards (*Polymer Standards Services*) were used to calibrate the system and thus allowed for accurate determination of molar masses.

3.2.2.3 ATR-FTIR

For this characterization technique a Thermo-Fischer Nicolet iS10 FTIR instrument was used. The instrument is equipped with a Smart iTR ATR sampling accessory which is configured to a diamond. The diamond crystal has a refractive index of 2.4 and an incident angle of 42 °. For the pellet bulk samples, a single pellet was cut in half using a scalpel to ensure optimal contact and placed on the diamond for analysis. The powder bulk samples were analysed as received. The fractionated samples were also analysed in their natural form.

All spectra obtained were acquired and baseline corrected using *Omnic* 8.1 software. Each spectrum produced was the result of 32 individual scans added together, with a spectral resolution of 4 cm^{-1}. The background was also generated using 32 individual scans. All spectra were recorded from 4000 cm^{-1} to 650 cm^{-1}.

3.2.2.4 XRD

X-ray diffraction analysis was done using a *Bruker* D2 Phaser X-ray diffractometer. Analysis was only done on fractions, and the fractions were used as is in the solid state and flattened onto the XRD disk using a glass microscope slide in order to ensure consistency. The analysis was carried out at room temperature, at a continuous scan from 2θ angles of 5-30 °C at a rate of 2 °/min and a scanning step of 0.02 °. [2] The X-rays are produced from a Copper source and the α wavelength, K_α is 1.54184.

3.2.2.5 SSA

Successive self-nucleation and annealing was done on some samples using the same DSC instrument discussed above. The difference is in the temperature profile used, and an outline of the temperature profile applied can be seen below: [1]

1. Increase temperature at 10 °C/min to 200 °C
2. Kept isothermally at 200 °C for 5 minutes
3. Decrease temperature at 10 °C/min to 0 °C
4. Increase temperature at 10 °C/min to 170 °C
5. Kept isothermally at 170 °C for 5 minutes
6. Decrease temperature at 10 °C/min to 0 °C
7. Increase temperature at 10 °C/min to 166 °C
8. Kept isothermally at 166 °C for 5 minutes
9. Decrease temperature at 10 °C/min to 0 °C
10. Repeat steps 7-9, each time increasing the temperature to 4 °C less than the previous heating cycle until the temperature is increased to 130 °C
11. Kept isothermally at 130 °C for 5 minutes
12. Decrease temperature at 10 °C/min to 0 °C
13. Increase temperature at 10 °C/min to 200 °C

A total of 25 cycles is applied for SSA analysis. As for DSC, samples weighing 4 mg were used for the analysis. All other factors are kept the same as for normal DSC.

3.2.2.6 HT - ^{13}C NMR

High temperature - ^{13}C NMR analysis was done in the solution state using a 600 MHz *Varian Unity Inova* NMR spectrometer. A 5 mm inverse detection pulsed field gradient probe was used for the analysis. Samples were prepared by adding approximately 60 mg of sample into an NMR tube. TCE-d_2 (deuterated 1,1,2,2-tetrachloroethane) was used as the solvent and 0.6 mL was added to each NMR tube. The tubes were then placed in an oil bath heated to 120 °C and left to dissolve the sample in the tube. The samples were then heated with a heating gun to homogenize the sample and ensure all sample in the tube was present in the solution at the bottom of the tube. The samples were then submitted and stored in a fridge until the time of analysis. The samples were then run at 120 °C overnight to produce the NMR spectrum.

3.2.2.7 Solid-state NMR

Solid-state nuclear magnetic resonance was done using a 500 MHz *Varian* VNMRS NMR spectrometer. The instrument is equipped with a 4 mm *Chemagnetics* T3 HX MAS probe and two channels. Sample preparation included packing the samples into zirconia rotors. The ^{13}C experiments were conducted at room temperature using cross polarization, with a magic angle spinning (MAS) of 5 kHz and dipolar decoupling. Adamantane was used as the external chemical shift standard. The same conditions that were used for the cross-polarization experiments were used for the interrupted decoupling experiments. [3]

3.2.2.8 SEM

Scanning electron microscopy analysis was done using a *Zeiss* Merlin SEM microscope. All the samples were bulk powder samples and were prepared for SEM analysis using the same method. A small piece of double sided tape was placed on a clean SEM stub. A few grains of the polymer powder were then added to the tape, and a second piece of tape was placed over approximately half of the area where the grains were found. The stub was then 'bumped' at an angle to ensure any loose grains will fall off the stub. The prepared SEM stubs were then placed in a carbon coater and subsequently coated with a single layer of carbon under vacuum. The samples were finally analysed separately using the SEM microscope and images were saved using *Zeiss* SmartSEM software. The SEM images throughout the thesis contain the further specific instrument settings applied for each individual sample.

3.3 References

1. Mller, A. J. & Arnal, M. L. Thermal fractionation of polymers. Prog. Polym. Sci. 30, 559603 (2005).

2. Kang, J., Chen, J., Cao, Y. & Li, H. Effects of ultrasound on the conformation and crystallization behavior of isotactic polypropylene and -isotactic polypropylene. Polymer (Guildf). 51, 249256 (2010).

3. Botha, L. The effect of in-process ethylene incorporation on the evolution of particle morphology and molecular characteristics of commercial heterophasic ethylene propylene copolymers (HEPCs). (Stellenbosch University, 2014). doi:10.1016/j.eurpolymj.2013.04.020

Chapter 4

Analysis and characterization: Bulk samples

*This chapter will relay and discuss selected results of the fractionation and analysis of the bulk polymer samples investigated during this project. This chapter will serve as **part 1** of the results of the thesis.*

4.1 Results and discussion

A total of twenty isotactic polypropylene samples were received from *Sasol*. These samples comprised five different grades. Two different catalyst systems (Lynx and NHP), were used to produce each grade and samples were supplied as the ”as-is” reactor powder and the pelletized form (containing the relevant additives that are added prior to extrusion and pellitization). A summary of these twenty samples can be seen in Table 4.1. The analysis of these bulk samples, as well as the fractionation and analysis of these samples, will be discussed during this chapter and will serve as **part 1** of the results from this project. The experimental procedures employed for the fractionation and analysis of the samples, which include TREF, DSC, HT-SEC, FTIR and NMR have been discussed in detail in Chapter 3. The analysis of the bulk samples results in a representation of the average composition of these samples and will thus serve as an overview of the average molecular properties within the bulk polymer samples. In order to delve deeper into the microstructural properties of polymers, these bulk samples needed to be fractionated to allow for the investigation of chemically homogeneous fractions. The results and discussion of the fractionated samples will serve as **part 2** of the results from this project and can be seen in Chapter 5.

Table 4.1: Summary of twenty bulk polymer samples investigated

#	Grade	Form	Catalyst	#	Grade	Form	Catalyst
1	HKQ 205	Powder	Lynx	11	HKQ 205	Pellet	Lynx
2	HKR 102	Powder	Lynx	12	HKR 102	Pellet	Lynx
3	HMR 127	Powder	Lynx	13	HMR 127	Pellet	Lynx
4	HNR 100	Powder	Lynx	14	HNR 100	Pellet	Lynx
5	HNR 101	Powder	Lynx	15	HNR 101	Pellet	Lynx
6	HKQ 205	Powder	NHP	16	HKQ 205	Pellet	NHP
7	HKR 102	Powder	NHP	17	HKR 102	Pellet	NHP
8	HMR 127	Powder	NHP	18	HMR 127	Pellet	NHP
9	HNR 100	Powder	NHP	19	HNR 100	Pellet	NHP
10	HNR 101	Powder	NHP	20	HNR 101	Pellet	NHP

4.2 DSC

Each of the bulk samples were analysed to determine their solid-state crystallinity and melting properties using differential scanning calorimetry (DSC). Isotactic polypropylene is known to have a high melting temperature (> 150 °C), and thus the temperature range for the analysis was chosen to be between 0 and

200 °C. The samples were found to have a fairly broad melting endotherm. This is due to the diversity of polymer chains present within each sample, leading to a variety of crystallite sizes during cooling. Smaller, less perfect crystallites start melting at lower temperatures. The cooling and heating cycles of the four variations of the HKQ 205 grade sample can be seen in Figure 4.1.

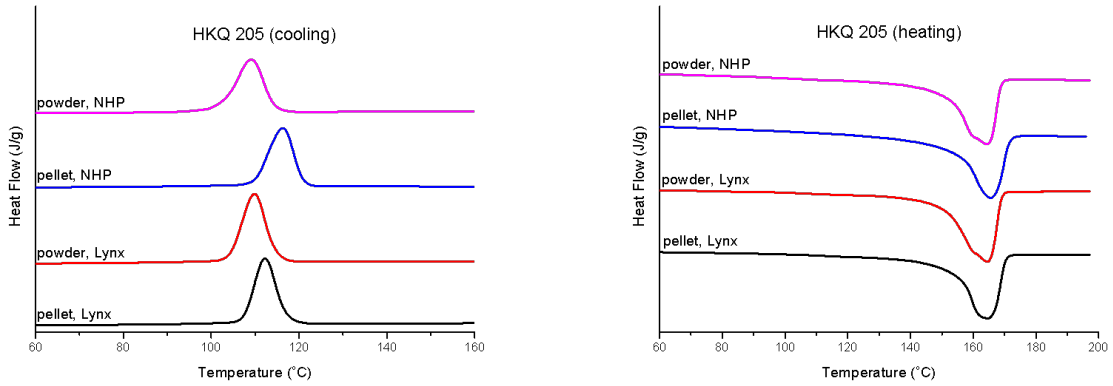

Figure 4.1: DSC cooling (left) and heating (right) cycles of HKQ 205 bulk samples

Table 4.2: Tabulated DSC data of HKQ 205 grade bulk samples

	Sample	Crystallization temperature (°C)	Melting temperature (°C)	% Crystallinity	Melt enthalpy (J/g)
HKQ 205	Powder, Lynx	109.86	164.29	38.52	79.74
	Powder, NHP	109.16	164.00	35.51	73.51
	Pellet, Lynx	112.23	164.80	34.84	72.12
	Pellet, NHP	116.29	164.45	34.01	70.40

From the data in Table 4.2 and on the cooling cycles in Figure 4.1, we can see that the pellet samples crystallize at a higher temperature compared to the powder samples, indicating that the pellet samples crystallize to a greater extent than the powder samples in the solid state. [1] Our main point of focus, however, won't be on the differences between the pellet and powder samples, but rather between the same form samples polymerized with different catalysts. Furthermore, we can observe that for the powder samples, the crystallization temperature (T_c) is fairly similar, however, the NHP catalysed sample has a broader peak compared to the Lynx catalysed sample. This is indicative that the NHP catalysed sample has a wider distribution of crystallizable chains and we consequently might expect the NHP catalysed samples to have a wider molar mass dispersity as well (Section 4.3). For the pellet samples, we can observe that the T_c of the NHP catalysed sample is significantly higher than that of the Lynx catalysed sample.

Initially it doesn't seem as if there are any differences present on the heating cycle in Figure 4.1, however, there are some observations to take note of. Firstly, we observe that the size and position of the melting endotherm in each case is very similar, which is indicative that similar size crystals are produced during the crystallization event. The percentage crystallinity values shown in Table 4.2 show that the Lynx catalysed powder sample has a slightly higher crystallinity (3 $\%$) while the crystallinities of both pellet samples are similar. For the pellet samples we observe a broad homogeneous melting endotherm. This indicates that there are definite variations in the size of crystals produced during the cooling cycle, as the melting temperature (T_m) is determined by the size of the crystal being melted. The melting endotherms of the powder samples are indicating a slight tendency to some heterogeneity as we can see the melting event containing two subtle peaks. These peaks typically occur due to molecular segregation within the samples, resulting in the formation of two different size crystals. [2] These segregation effects were observed again and much clearer for the other grades of polymers. The heating curves of these grades can be seen in Figures 4.2-4.3.

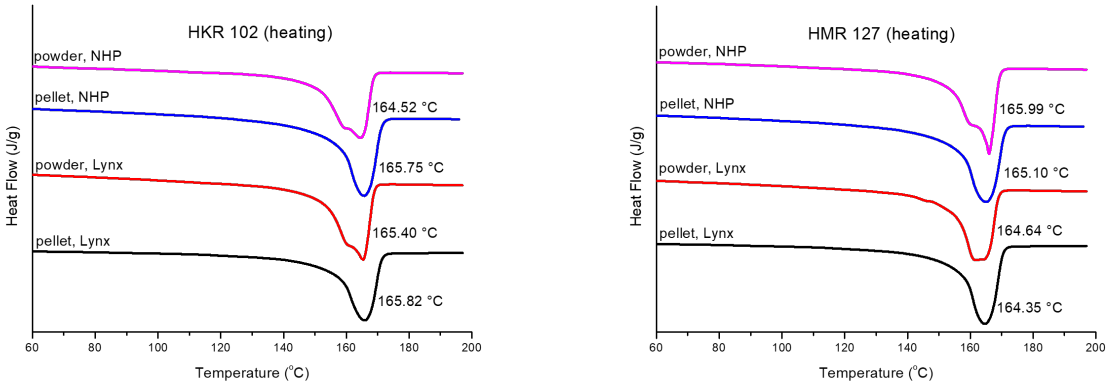

Figure 4.2: DSC heating cycles of HKR 102 (left) and HMR 127 (right) bulk samples

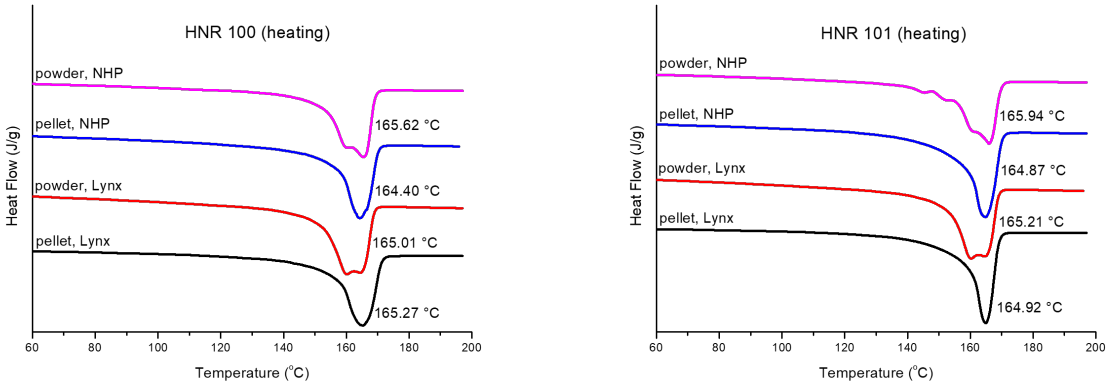

Figure 4.3: DSC heating cycles of HNR 100 (left) and HNR 101 (right) bulk samples

It can be observed that the melting endotherms of all the powder samples in Figures 4.2-4.3, have double melting endotherms due to molecular segregation. In addition, it can be seen that the bimodality of the melting peak for the powder samples is different for the polymers produced by the two catalysts; for the HNR 100 and 101 samples it seems that the peak at lower temperature is relatively larger for the polymers produced by the Lynx catalyst as opposed to the NHP catalyst (Figures 4.3). The pellet samples, as seen before, only have one homogeneous peak, albeit a broad peak. The presence of the split in the melting peaks of the powder samples and the broad uniform melting peak for the pellet samples may be explained be considering what happens during processing of the polymer samples. The powder samples are received as is from the reactor, while stabilizers are added to the powder samples and sent through an extruder in order to pelletize the pellet samples which may affect the solid state crystallization properties of the pellet samples. The entire set of DSC thermograms of the bulk samples have been added to the Annexure on Page 124.

From the results in Figures 4.1 and Table 4.2 regarding specifically the HKQ 205 grade, it can be observed that there are some variations present. The T_c values are consistent for the two powder samples, and increase for the pellet samples, with the NHP catalysed pellet sample having a T_c of 4 °C higher than that of the Lynx catalysed pellet sample. The T_m values for the four variations of the HKQ 205 grade display very similar values, indicating that all the samples produce crystals of roughly the same size. The melt enthalpy values are used to determine the percentage crystallinity in the samples and it is found that the crystallinity values are fairly similar, differing by no more than 3 $\%$ for samples of the same form. Similar trends are observed for the other grades of samples in that there aren't any major anomalies present. It is clear that larger differences between the grades produced by the two different catalysts are visible in the reactor powder samples than in the pellet samples. As the pellets represent the materials as sold and used, it was decided to first focus on the fractionation and analysis of these materials and then to focus on the reactor powders in cases where molecular differences are visible in the pellet samples. Further work on the fractions of these bulk samples will be discussed in Chapter 5. The entire set of results from DSC analysis of the bulk samples have been added to the Annexure on Page 124.

4.3 HT-SEC

Each of the twenty bulk samples received was analysed to determine their molar mass related properties using high temperature size exclusion chromatography (HT-SEC). Isotactic polypropylene, being a polyolefin is only soluble in selected solvents at elevated temperature, and SEC analyses were conducted in TCB at 150 °C. The SEC curves obtained for the HKQ 205 and HKR 102 grades are shown in Figure 4.4.

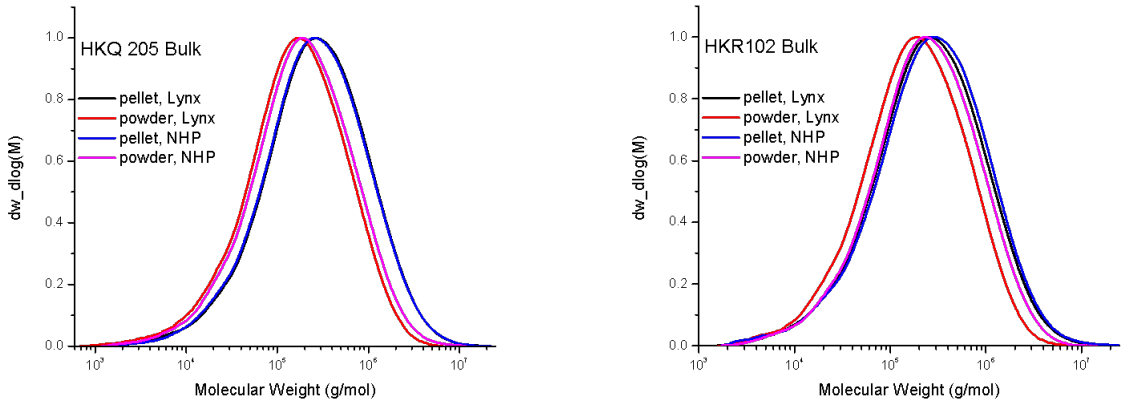

Figure 4.4: HT-SEC chromatograms for HKQ 205 and HKR 102 bulk samples

It is clear from the Figure 4.4 above and Table 4.3 below that the molar mass of the pellets appears to be larger than that of the reactor powders. This phenomenon was observed throughout the study and there appears to be no explanation for this. We can only speculate that the fact that the pelletized samples are a result of in-silo blending before extrusion contributes to this observation. In addition the dispersity values for the powder samples are generally slightly lower than that of the pellet samples.

In addition, we can see that there are no real trends with regards to the molar mass or dispersity values when comparing the polymers produced by the Lynx catalyst or the NHP catalyst. In Table 4.3 the results of the HKQ 205 grade is given for illustrative purposes. The entire set of HT-SEC curves for the bulk samples have been added to the Annexure on Page 137.

Table 4.3: Summary of SEC data for HKQ 205 bulk samples

	Sample	M_n	M_w	M_z	PDI
HKQ 205	Powder, Lynx	58056	298116	850163	5.13
	Powder, NHP	69473	355829	1172527	5.12
	Pellet, Lynx	91440	516902	1771901	5.65
	Pellet, NHP	92361	512639	1790059	5.55

Further work on the fractions of these bulk samples will be discussed in Chapter 5. The entire set of results from HT-SEC analysis of the bulk samples have been added to the Annexure on Page 137.

4.4 FTIR

The bulk samples were analysed to investigate their lamellar structure and helical conformation using attenuated total reflectance - Fourier-transform infrared spectroscopy (ATR-FTIR). [3,4] This technique was further employed to investigate the possibility of developing a protocol during which a quick FTIR scan will give production companies a more significant result regarding their product, compared to the basic information usually obtained from simple FTIR analysis. This was unsuccessful, however, as no significant differences were observed on the FTIR spectra between the different grades of bulk samples. An example of the FTIR spectra obtained for the bulk samples can be seen in Figure 4.5.

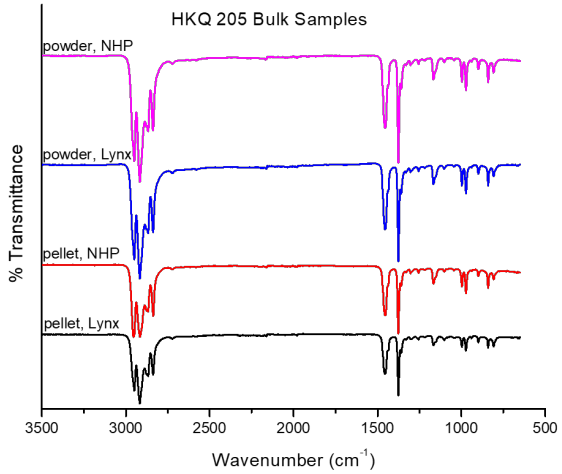

Figure 4.5: FTIR spectra of HKQ 205 bulk samples

As a means to determine the relative amount of all length of helical sequences, the intensities of several regularity bands were measured and compared to the same grade and form of sample, differing only in the catalyst used to produce that sample. This allowed us to investigate if any trends were present in helical sequences due to the type of catalyst used. The results of the HKQ 205 grade have been showed in Figure 4.6.

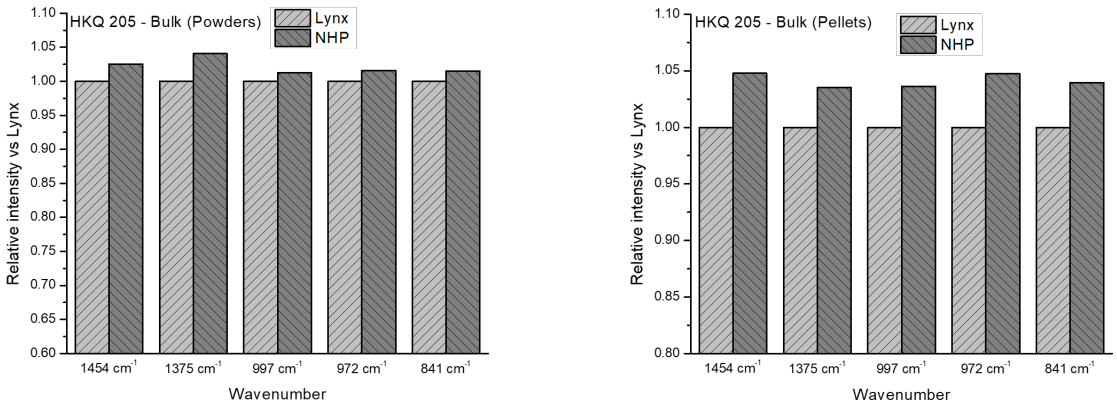

Figure 4.6: Comparison of FTIR peak intensity between samples of different catalyst composition

What we can see from these graphs, is that the NHP catalysed sample in both the powder and pellet forms consistently has a higher intensity for all the regularity bands investigated. This allows us to infer that the NHP catalysed sample has higher contents of all lengths of helical sequences. Furthermore, if we assume that there is an equal amount of stereodefects present within the samples, then we can speculate that the Lynx catalysed samples have a more uniform distribution of stereodefects, as the presence of stereodefects interrupts helical sequences and would lead to a lower intensity in the regularity bands observed. [1] This trend, however, isn't observed throughout all the grades and thus no definitive conclusion could be made regarding the effect of the catalyst on the helical sequences within the bulk polymer sample. An example of this inconsistency can be seen in the HNR 101 grade shown in Figure 4.7.

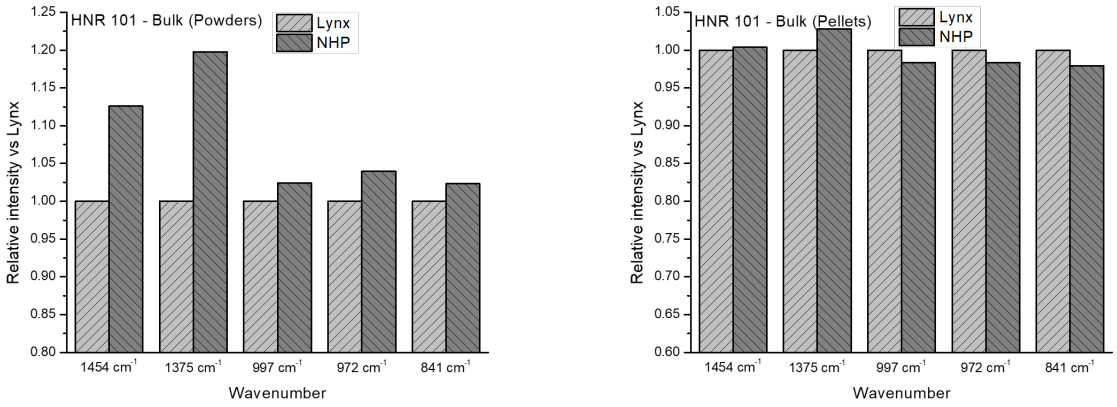

Figure 4.7: Comparison of FTIR peak intensity between HNR 101 bulk powder and pellet samples

For the HNR 101 grade we can see in the powder samples that the NHP catalysed sample consistently has

a significantly higher intensity of regularity band compared to the Lynx catalysed powder. For the pellets, however, we see a more even distribution of intensities, with the intensities varying slightly between each regularity band investigated. We see thus that the inconsistencies between the HNR 101 grade samples are too significant to allow for a definite conclusion to be made regarding the effect of catalyst on the helical sequences within the bulk polymer samples.

4.5 CRYSTAF

The bulk samples were analysed to determine their solution crystallization properties using crystallization analysis by fractionation (CRYSTAF). This technique allows us to observe the crystallization behaviour of our samples in solution and is also used as an aid to TREF fractionation which will be discussed in Section 4.6. The CRYSTAF graphs of the HKQ 205 grade are shown in Figures 4.8-4.9.

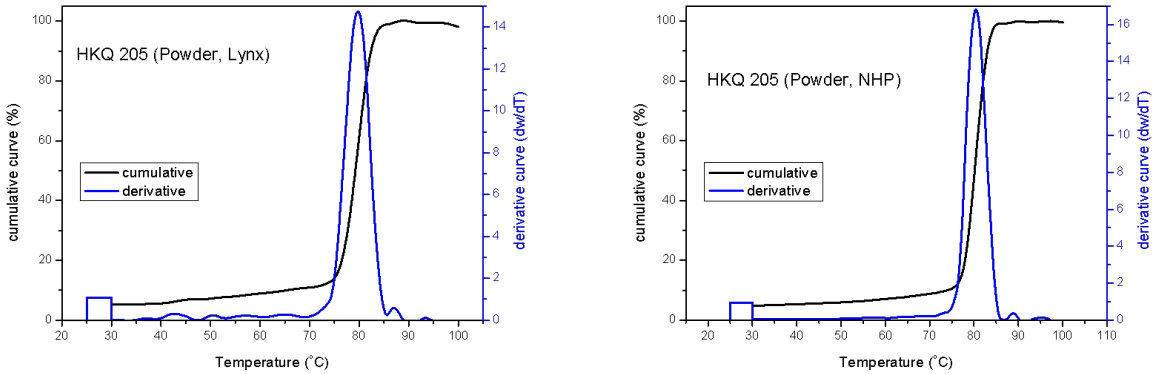

Figure 4.8: CRYSTAF graphs of HKQ 205 bulk powder samples

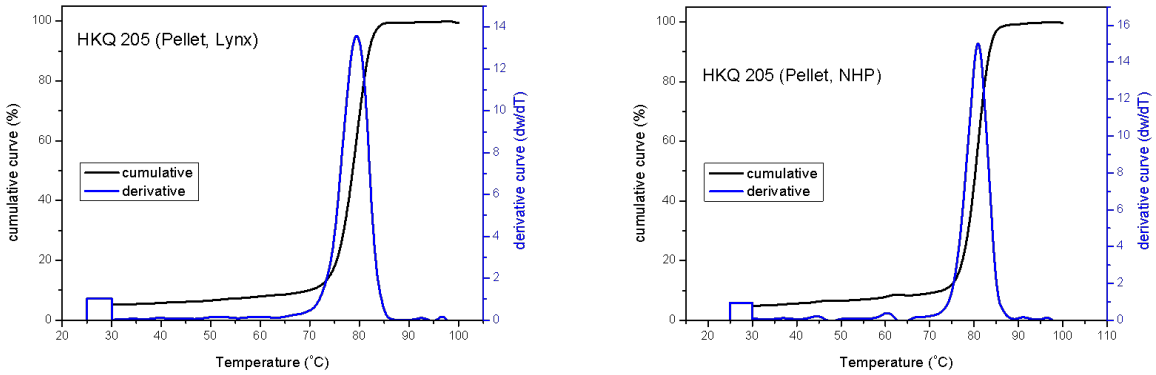

Figure 4.9: CRYSTAF graphs of HKQ 205 bulk pellet samples

There is a similar trend in the graphs, in that the major crystallization event occurs at about 80 °C, which in actuality is around 90 °C due to the undercooling effect of the CRYSTAF technique. The differences that are present between the variations of the HKQ 205 grade occur in the temperatures before and after the major crystallization event. We can observe in for example, the HKQ 205 Lynx catalysed powder sample, that there are a couple of smaller crystallization events occurring at lower temperatures as well as a small event just before the main crystallization event. This also occurs, to a lesser extent, in the HKQ 205 NHP catalysed pellet sample. These smaller crystallization events at lower temperatures may be due to some lower molar mass polymer chains that crystallize at these temperatures, or to the presence of chains of lower isotacticity index. These smaller crystallization events can be seen to occur more clearly in some other samples, a couple of which are shown in Figure 4.10.

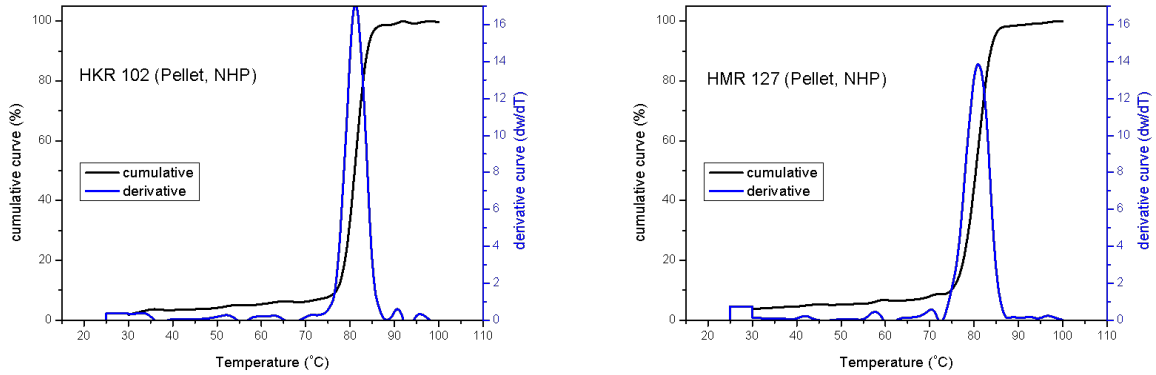

Figure 4.10: CRYSTAF graphs of a HKR 102 bulk sample (left) and a HMR 127 bulk sample (right)

For these results we can clearly see the presence of these smaller crystallization events, however, these

events aren't present in each sample. Some samples which didnt show smaller crystallization events can be seen in Figure 4.11. It was typically found that the Lynx catalysed pellet samples had far fewer small crystallization events, with the other grades and variations thereof showing varying amounts of these events. These results, even though they do not occur as a rule, clearly indicate that there is a significant difference in the solution crystallization properties of samples that differ not only in grade and form, but importantly between samples varying only in catalyst used. The entire set of CRYSTAF graphs of the bulk samples have been added to the Annexure on Page 121.

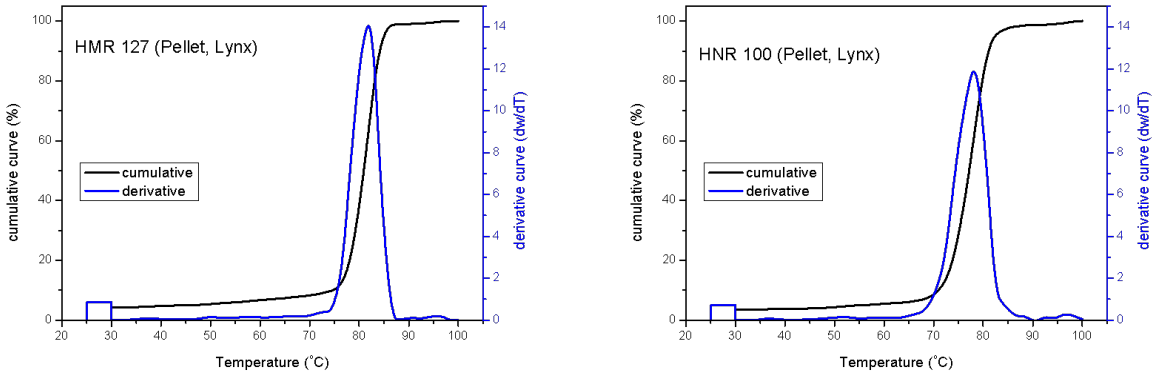

Figure 4.11: CRYSTAF graphs of a HMR 127 bulk sample (left) and a HNR 100 bulk sample (right)

4.6 TREF

The values that are obtained when analysing bulk polymer samples, are an average of all the polymer chains present within the bulk sample. These average values give some insight into the polymer samples but are limited in the sense that more detailed information regarding the polymer microstructure and chemical composition distribution is lacking. In order to overcome this problem, it is necessary to fractionate these samples, which allows us to obtain specific fractions of the bulk polymer which are more homogeneous in nature. These fractions can then be further analysed to give more detailed information regarding the microstructure present within a polymer sample. These fractions will be discussed in Chapter 5.

The bulk samples were fractionated based on their crystallizability using temperature rising elution fractionation (TREF). TREF allows us to obtain fractions of the bulk polymer which crystallize within the same temperature range, starting with the highly crystallizable material which elutes at 140 and 110 °C, down to the non-crystallizable amorphous material which elutes at 30 °C. As mentioned previously, CRYSTAF was used as an aid to TREF elution, as the crystallization profiles from CRYSTAF were used to

determine the temperatures at which fractions were eluted in the TREF experiment. The TREF fractograms of the HKQ 205 powder samples can be seen in Figure 4.12.

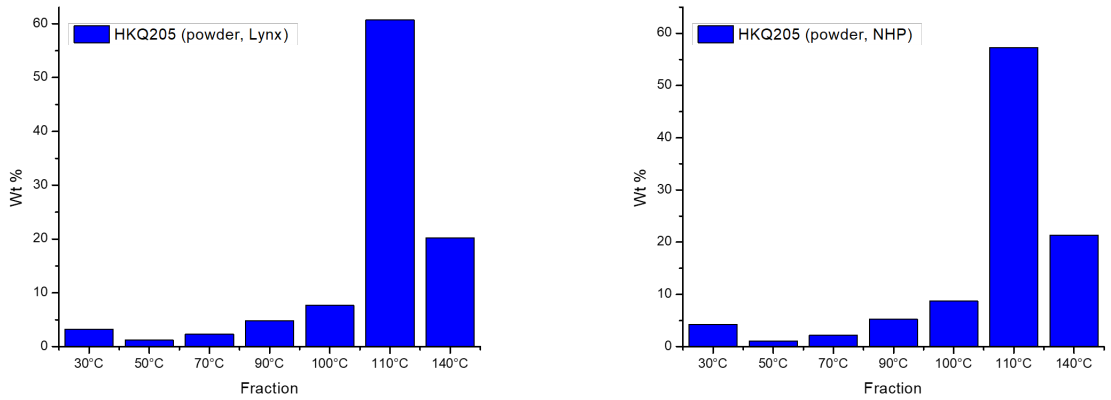

Figure 4.12: TREF fractograms of HKQ 205 powder bulk samples

It is clear that the majority of material crystallizes at 110 and 140 °C, indicating that the samples are highly crystalline. Typically, more than 80 % of the sample consisted of highly crystalline material as determined from TREF elution, which isn't unexpected, as isotactic polypropylene is known to be a semi-crystalline material. There is also a noticeable amount of non-crystallizable amorphous material eluting at 30 °C. This amorphous fraction typically made up between 2,5 - 5 % of the sample. What is also noticeable is that the relative amounts eluting at each temperature differ between the polymers produced by different catalysts. This is noticeable when comparing the fractions obtained at 100, 110 and 140 °C. The entire set of TREF fractograms for the bulk samples have been added in the Annexure on Page 117. To ease the process of comparing between samples the graphs were plotted using a marked line graph and the results from the HKQ 205 grade samples can be seen in Figure 4.13.

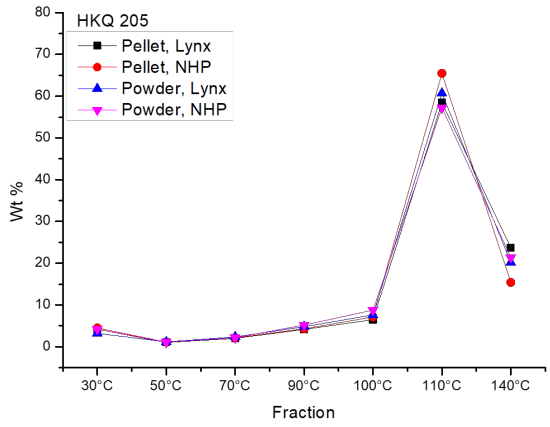

Figure 4.13: Comparison of HKQ 205 grade TREF fractograms

This graph clearly shows the same trend for all the HKQ 205 grade samples, with the only significant variations occurring in the 100, 110 and 140 °C fractions. The exact weight percentages of each fraction for the HKQ 205 grade samples can be seen in Table 4.4.

Table 4.4: Summary of TREF elution results for HKQ 205 grade bulk samples

		Weight percentage (%)						
	Sample	30 °C	50 °C	70 °C	90 °C	100 °C	110 °C	140 °C
HKQ 205	Powder, Lynx	3.18	1.18	2.34	4.78	7.62	60.71	20.18
	Powder, NHP	4.20	1.10	2.18	5.21	8.76	57.20	21.35
	Pellet, Lynx	4.18	1.04	2.00	4.16	6.51	58.41	23.70
	Pellet, NHP	4.49	1.11	2.14	4.32	7.14	65.43	15.37

From the results in Table 4.4 we can see that for the fractions from 30 °C up to the 100 °C, we have similar values across all variations for the same fraction. Some variations occur within the 110 and 140 °C fractions, however, if you add these two fractions together for each sample we find that the values are all somewhere around 80 %. The main variations thus occur in the high temperature fractions, observing that the higher the 110 °C weight fraction the lower the 140 °C fraction for each sample. The comparison graphs for the other grades can be seen in Figures 4.14-4.15.

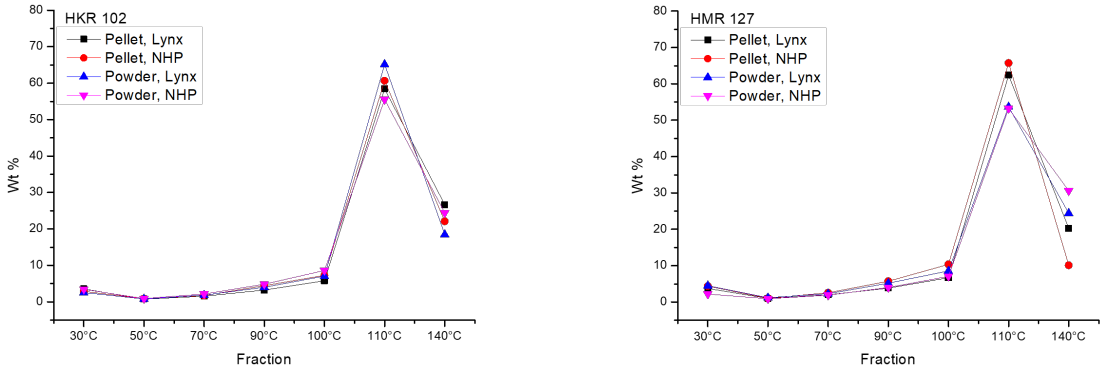

Figure 4.14: Comparison of HKR 102 grade (left) and HMR 127 grade (right) TREF fractograms

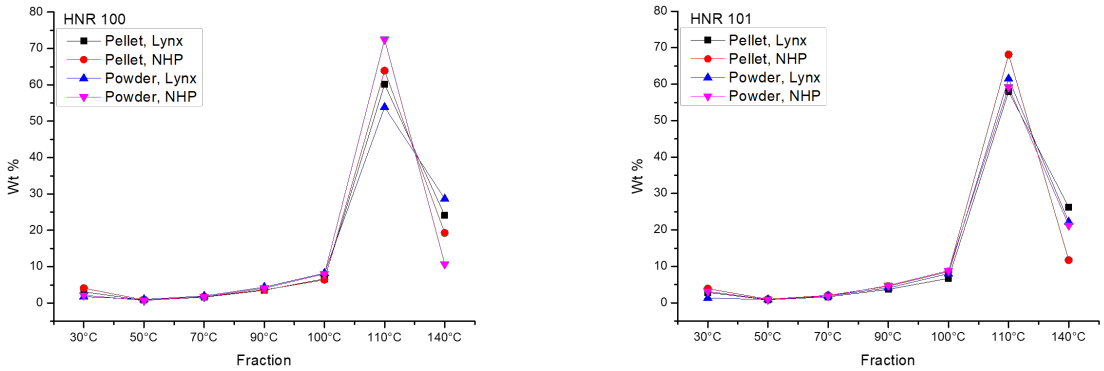

Figure 4.15: Comparison of HNR 100 grade (left) and HNR 101 grade (right) TREF fractograms

From these graphs we can see the same trend that was observed for the HKQ 205 grade in that the variations occur mainly in the 100, 110 and 140 °C fractions. It should be noted that there were spill accidents with the 110 and 140 °C NHP catalysed pellet samples of the HMR 127 and HNR 101 grades, and thus the results for these specific samples have been omitted. These results show that there are definite variations within each grade simply by observing that the highest weight percentage sample of the 110 °C fraction varies between each grade, i.e for the HKR 102 grade we see that the Lynx catalysed powder sample has the highest weight percentage value, but for the HNR 100 grade the NHP catalysed powder sample has the highest value. This specific result and others indicate that the catalyst definitely plays a role in the distribution of crystallizable chains within the bulk polymers.

4.7 Solid-state NMR

Solid-state nuclear magnetic resonance spectroscopy (Solid-state NMR) was used to gain information regarding chain conformations in the solid state. The solid-state techniques will focus on selectively observing both crystalline and amorphous regions of the polymers, in order to gain a better understanding of the dynamics associated with the molecules in the solid state. The first solid-state NMR experiment conducted was cross-polarization magic angle spinning (CPMAS), which is sensitive to the proton density and mobility of components within the sample. [5] CPMAS experiments were conducted on the powder samples of the HKQ 205 and HKR 102 grades, and the results can be seen in Figure 4.16.

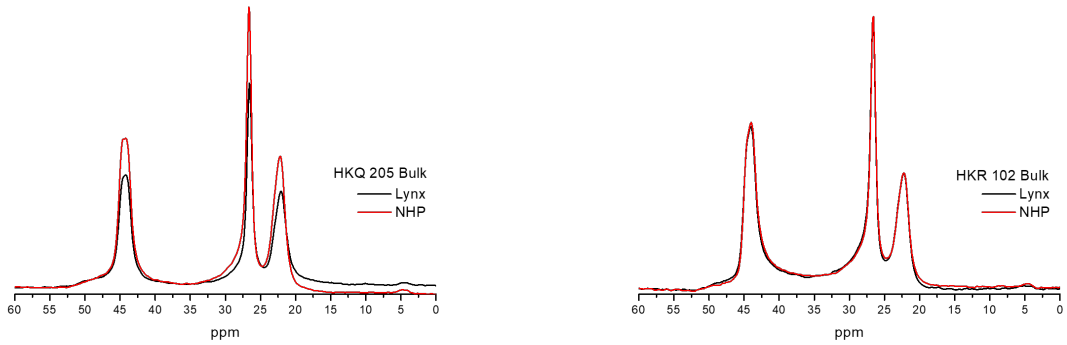

Figure 4.16: CPMAS results of HKQ 205 and HKR 102 bulk powder samples

On these spectra we can see the appearance of the methyl CH_3 peak at about 22 ppm, the methine CH peak at about 26 ppm and a methylene CH_2 peak at about 44 ppm. Due to the nature of the CPMAS experiment, the methine peak is the sharpest peak due to its low mobility, being hindered by the methyl and methine groups. The methyl and methylene peaks can be seen to be broader and less resolved due to the groups having some mobility.

Looking specifically at the methylene peak we see that there is a hint of a shoulder, which is more pronounced in the HKR 102 samples. From literature we would expect the methylene peak to split as the methylene carbons exist in different environments, due to the 3_1 helix structure of the α allomorph of isotactic polypropylene. [6] These two peaks are expected to occur at 44.7 and 43.8 ppm respectively, representative of the ordered α phase. From a pure crystalline form, these two peaks should exist in a 2:1 ratio, however, might differ due to the presence of atactic sequences. [5] An example of how the deconvolution of the methylene peak was done can be seen in Figure 4.17.

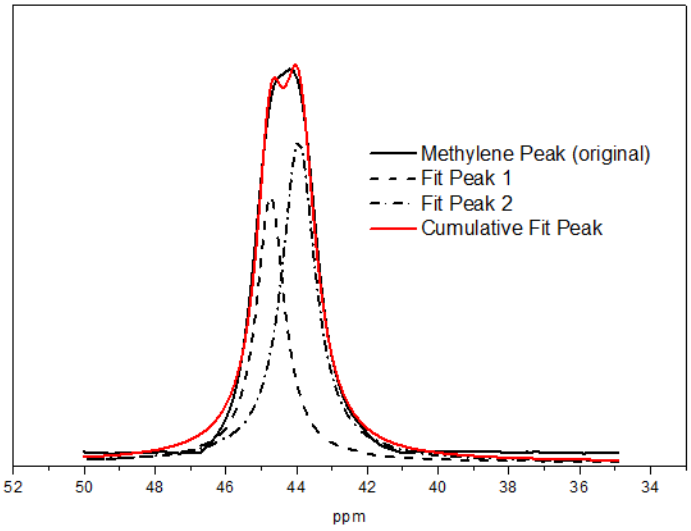

Figure 4.17: Example of deconvolution of solid-state NMR methylene peak

The data obtained from the deconvolution of the methylene peaks, together with other relevant data from the CPMAS experiments can be seen in Table 4.5. A Lorentz fit was used throughout processing to deconvolute the methylene peak.

Table 4.5: Summary of data from CPMAS experiments

Sample	Chemical shift (ppm)		CH_2 Peak		
	CH_3	CH	CH_2	% Area	Ratio
HKQ 205 Lynx	22.07	26.57	45.59	41.17	1.43
			44.19	58.83	
HKQ 205 NHP	22.19	26.63	44.20	40.91	1.44
			44.46	59.09	
HKR 102 Lynx	22.25	26.63	44.54	17.87	4.60
			44.03	82.13	
HKR 102 NHP	22.25	26.62	44.61	26.03	2.84
			44.00	73.97	

From Table 4.5 we see that the values for the two methylene peaks are slightly closer together than predicted, and the ratios between the peaks are also not close to 2:1 as predicted. We will further investigate these samples by looking at solid-state NMR results of the fractions of these bulk samples in Chapter 5.

We can conduct another experiment in solid-state NMR in order to selectively visualise areas in our samples with higher mobility. These experiments are called interruptive decoupling or dipolar dephasing and will further be referred to as IDREF experiments. These IDREF experiments make use of dipolar carbon-proton interactions, of which there is a faster decay in strongly coupled regions. These strongly coupled regions typically occur in areas of lower mobility, and thus we can observe the areas of higher mobility which have weaker dipolar interactions and slower decay times. The IDREF spectra obtained for the powder samples of the HKQ 205 and HKR 102 grades can be seen in Figure 4.18.

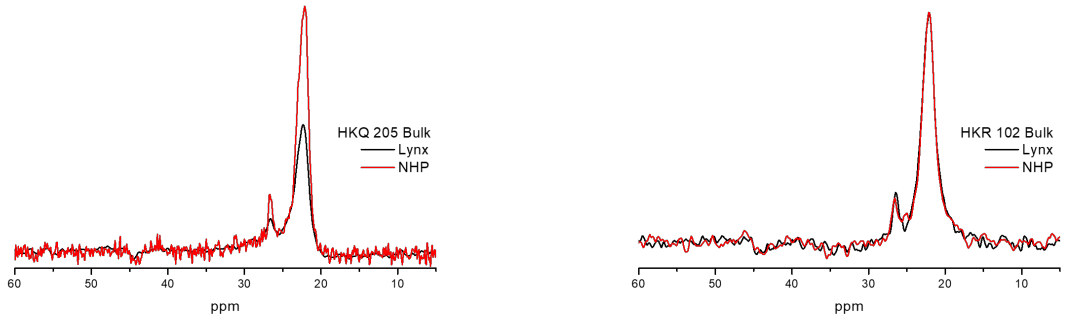

Figure 4.18: IDREF results of HKQ 205 and HKR 102 bulk powder samples

We see for these figures, as we did for the CPMAS experiments, that the peaks for the Lynx catalysed HKQ 205 sample has lower intensity compared to the NHP catalysed HKQ 205 sample, while the peaks for the HKR 102 grade samples are nearly identical in intensity. We can observe that the methylene peak isn't present at all on the IDREF spectra, and the methine peak nearly completely disappeared. This is to be expected as the methylene and methine carbons form part of the polypropylene backbone and are expected to have low mobility. The methyl carbons are observed as a very pronounced peak, which is also expected due to it not being part of the backbone and will thus have inherent mobility. The most exciting result here is surely the presence of the methine peak which appears in the IDREF spectra. As it is part of the backbone of the polymer, we typically won't expect the methine peak to have mobility, but it seems they do experience some mobility. These peaks in the IDREF spectra are enlarged, however, and for reference an overlay between a CPMAS and IDREF spectra of the same sample has been shown in Figure 4.19 to show the relative amounts of these groups present. From there we can see that the IDREF peaks are very small in comparison to the CPMAS peaks, which is indicative of the low amount of mobile components present within the sample.

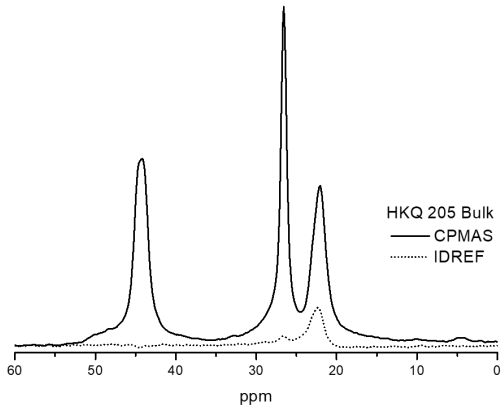

Figure 4.19: Comparison of CPMAS and IDREF spectra for HKQ 205 powder Lynx samples

4.8 SEM

The surface morphology of the powder samples was analysed using scanning electron microscopy (SEM). This allowed us to see if there are any morphological or structural differences in the reactor powders prepared with different catalysts. The SEM images of the Lynx catalysed (Figure 4.20) and NHP catalysed (Figure 4.21) samples of the HKQ 205 grade can be seen below.

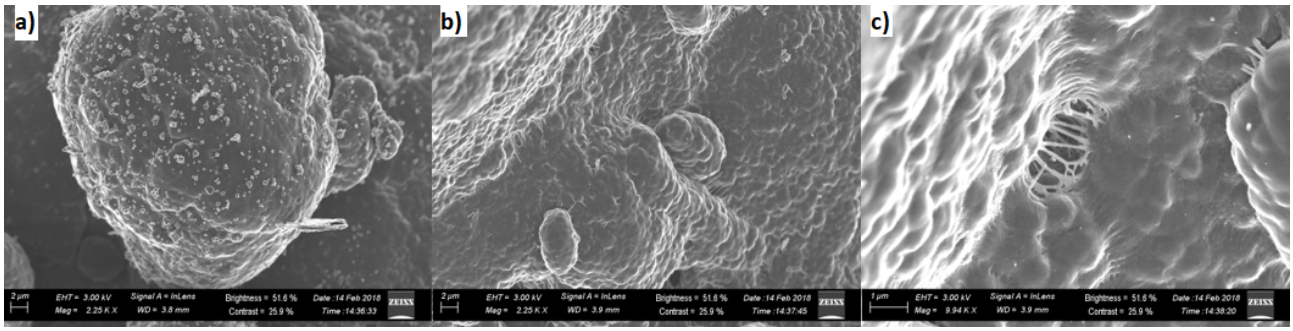

Figure 4.20: SEM images of HKQ 205 Lynx catalysed powder samples

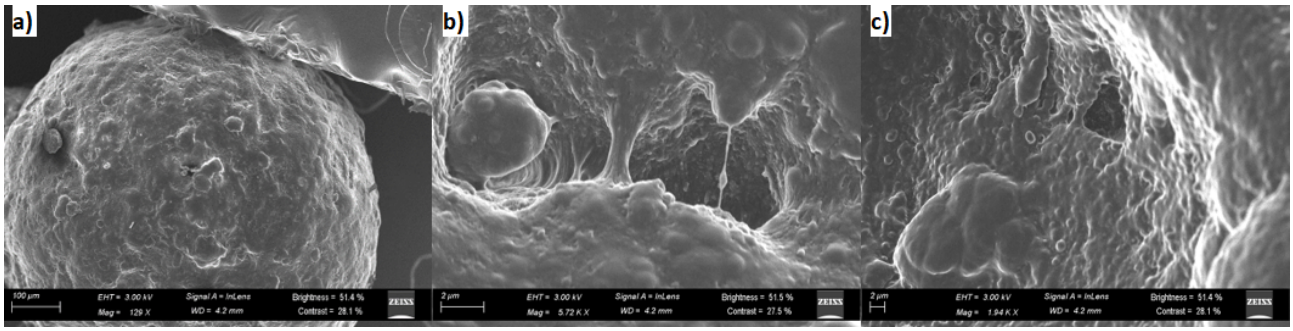

Figure 4.21: SEM images of HKQ 205 NHP catalysed powder samples

There are some clear morphological differences for the powder samples catalysed by the Lynx and NHP catalysts. Both samples show some porous structures. These pores can be classified as both submicron sized micropores, or as macropores, the presence of which was observed and discussed previously by Kakugo et al. [7,8] The porous structures have not been quantified and thus we can't say which catalyst leads to samples of higher porosity.

The main difference between the samples is in the smoothness of the particle surface. For the Lynx catalysed samples, the surface consists of individual particles packed closely together to form a 'bumpy' surface. For the NHP catalysed samples, we see that the surface is slightly smoother, with individual particles scattered on the surface. These occurrences can be seen throughout the other grades of polymers as well, and some selected results can be seen in Figures 4.22-4.23.

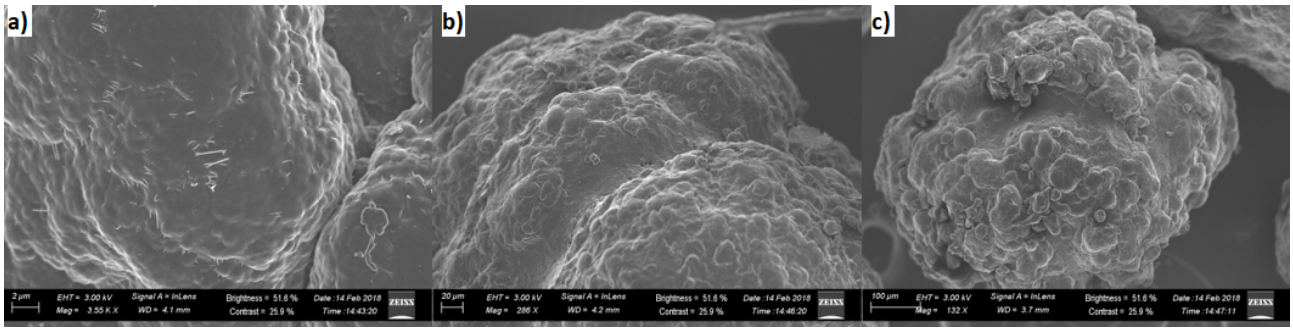

Figure 4.22: SEM images of HKR 102 (a), HMR 127 (b) and HNR 100 (c) Lynx catalysed samples

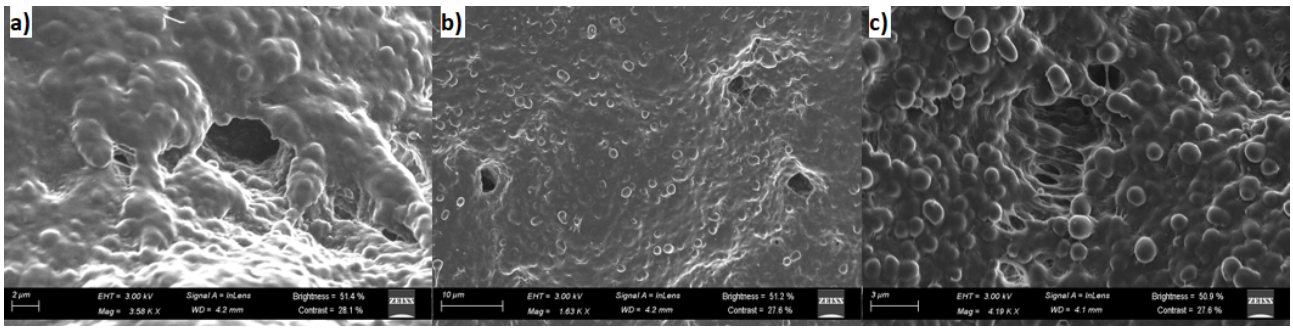

Figure 4.23: SEM images of HKR 102 (a), HMR 127 (b) and HNR 101 (c) NHP catalysed samples

These results clearly show the difference in surface morphology for the samples catalysed with different catalysts, an effect which is potentially of great significance if considering that these samples may be used in the future for production of for example impact polypropylene. The porous structures present within these samples are also consistent throughout all the samples. Some further examples of these porous structures can be seen in Figure 4.24.

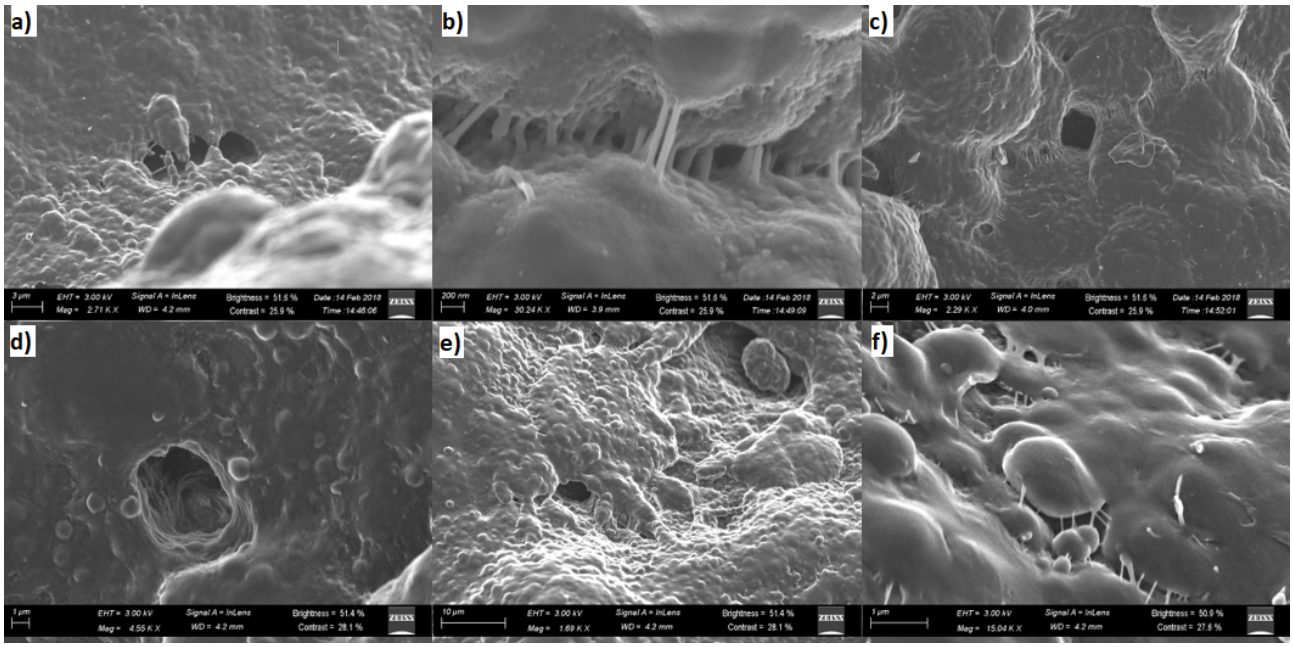

Figure 4.24: SEM images of HMR 127 (a), HNR 100 (b), HNR 101 (c) Lynx catalysed samples and HKQ 205 (d), HKR 102 (e), HNR 100 (f) NHP catalysed samples

These figures clearly show the presence of porous structures throughout the bulk powder samples. Finally, it was observed that when zooming in to the nanometer scale, the surfaces of the individual particles aren't smooth but are somewhat jagged. This phenomenon can be seen in Figures 4.25.

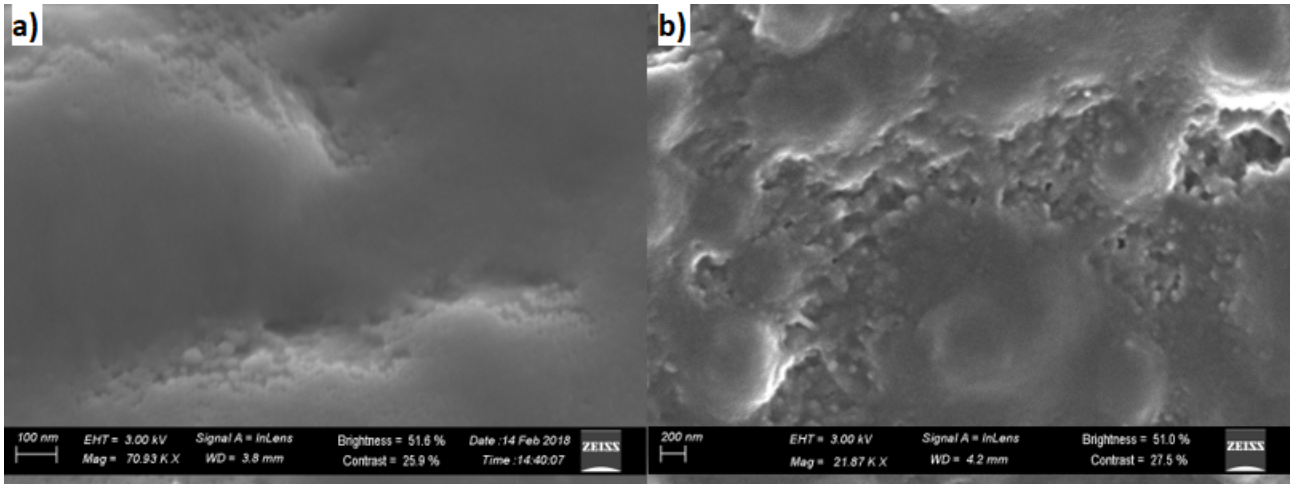

Figure 4.25: SEM images of HKQ 205 Lynx catalysed (a) and HMR 127 NHP catalysed (b) samples

4.9 Summary

The entire set of bulk samples received were analysed and characterized thoroughly using the techniques available to set up a comprehensive set of results regarding the average molecular properties within the bulk polymer samples. Not only did we find that distinct differences in molecular properties are present between the reactor powder samples and the extruded pellet samples, but we also found that the pellets of the same form had clearly different properties when catalysed with catalysts of different composition, namely the Lynx and the NHP catalysts.

From DSC analysis we found that the powder samples had a different shape melting endotherm compared to the pellet samples, and that the Lynx catalysed samples of both the powder and pellet samples had slightly higher crystallinities compared to the NHP catalysed samples. From HT-SEC analysis we observed that the pellet samples had higher molar mass and dispersity values compared to the powder samples, while the NHP catalysed samples had higher molar mass and similar dispersity values compared to the Lynx catalysed samples of the same form. FTIR analysis proved somewhat inconclusive, however, the fractionation of the bulk samples using TREF and CRYSTAF delivered results that were more significant. CRYSTAF analysis showed that our samples had distinctly different crystallization behaviours in solution. This was noteworthy, because even though the main crystallization event was similar for most of the samples, we could clearly see differences in the smaller crystallization events surrounding the main crystallization peak. These differences occurred between both the powder and pellet samples, as well as between same form samples catalysed by the Lynx and NHP catalysts. The final three fractions (100, 110 and 140 °C) of the TREF fractograms was where we observed the differences in elution behaviour of our bulk samples. It was in these fractions that we could see the distribution of crystallizable material differing between samples of different form and catalyst.

Penultimately, solid-state NMR analysis of our bulk samples showed information regarding the solid-state dynamics of our polymer chains, as we found that the chains have mobility in both the methyl pendant group carbon as well as our methine carbon found in the backbone. Furthermore, we observed a splitting of our methylene carbon in the CPMAS experiments, which is indicative that our chains with alternating helices exist in slightly different environments. Differences among samples could not be observed clearly as only four powder samples were analysed.

Finally, using SEM we could observe the surface morphologies of our powder polymers to find that distinct differences exist between samples catalysed with the Lynx and NHP catalysts for all grades of polymers investigated, with regards to the actual surface morphology and porosity of the samples.

4.10 References

1. Kang, J., Yang, F., Wu, T., Li, H., Liu, D., Cao, Y. & Xiang, M. Investigation of the Stereodefect Distribution and Conformational Behavior of Isotactic Polypropylene Polymerized with Different ZieglerNatta Catalysts. *Polym. Polym. Compos.* **12** 30763083 (2012).

2. Zhu, X., Li, Y., Yan, D., Zhu, P. & Lu, Q. Influence of the order of polymer melt on the crystallization behavior: I. Double melting endotherms of isotactic polypropylene. *Colloid Polym. Sci.* **279**, 292296 (2001).

3. Kang, J., Chen, J., Cao, Y. & Li, H. Effects of ultrasound on the conformation and crystallization behavior of isotactic polypropylene and -isotactic polypropylene. *Polymer (Guildf)*. **51**, 249256 (2010).

4. Su, Z., Wang, H., Dong, J., Zhang, X., Dong, X., Zhao, Y., Yu, J., Han, C.C., xu, D. & Wang, D. Conformation transition and crystalline phase variation of long chain branched isotactic polypropylenes (LCB-iPP). *Polymer (Guildf)*. **48**, 870876 (2007).

5. Botha, L. The effect of in-process ethylene incorporation on the evolution of particle morphology and molecular characteristics of commercial heterophasic ethylene propylene copolymers (HEPCs). (Stellenbosch University, 2014). doi:10.1016/j.eurpolymj.2013.04.020

6. Comotti, A., Simonutti, R., Bracco, S., Castellani, L. & Sozzani, P. Simultaneous crystallization of isotactic and syndiotactic sequences of polypropylene. *Macromolecules* **34**, 48794885 (2001).

7. Kakugo, M., Sadatoshi, H., Sakai, J. & Yokoyama, M. Growth of Polypropylene Particles in Heterogeneous Ziegler-Natta Polymerization. *Macromolecules* **22**, 31723177 (1989).

8. Kakugo, M., Sadatoshi, H. & Sakai, J. Morphology of Nascent Polypropylene Produced by MgCl2Supported Ti Catalyst. Stud. Surf. *Sci. Catal.* **56**, 345354 (1990).

Chapter 5

Analysis and characterization: Fractionated samples

*This chapter will relay and discuss selected results of the analysis of the fractionated polymer samples investigated during this project. This chapter will serve as **part 2** of the results of the thesis.*

5.1 Results and discussion

A total of twenty isotactic polypropylene samples were received from Sasol to be used during this project. These samples comprised five different grades, each polymerized with two different catalysts and each obtained in both as a reactor powder and in extruded pellet form. A summary of these samples can be seen in Table 5.1. The bulk samples were fractionated based on their crystallizability using temperature rising elution fractionation (TREF). Seven fractions were obtained in each case. These fractions were collected at elution temperatures of 30, 50, 70, 90, 100, 110 and 140 °C. The bulk samples were analysed and characterized as discussed in Chapter 4. The experimental procedures employed for the fractionation and analysis of the samples, which include TREF, DSC and HT-SEC are discussed in detail in Chapter 3. The investigation of the fractionated samples will allow us to delve deeper into the microstructural properties of the polymers. The analysis and characterization of the fractionated samples will serve as **part 2** of the results of the project.

Table 5.1: Summary of twenty bulk polymer samples investigated

#	Grade	Form	Catalyst	#	Grade	Form	Catalyst
1	HKQ 205	Powder	Lynx	11	HKQ 205	Pellet	Lynx
2	HKR 102	Powder	Lynx	12	HKR 102	Pellet	Lynx
3	HMR 127	Powder	Lynx	13	HMR 127	Pellet	Lynx
4	HNR 100	Powder	Lynx	14	HNR 100	Pellet	Lynx
5	HNR 101	Powder	Lynx	15	HNR 101	Pellet	Lynx
6	HKQ 205	Powder	NHP	16	HKQ 205	Pellet	NHP
7	HKR 102	Powder	NHP	17	HKR 102	Pellet	NHP
8	HMR 127	Powder	NHP	18	HMR 127	Pellet	NHP
9	HNR 100	Powder	NHP	19	HNR 100	Pellet	NHP
10	HNR 101	Powder	NHP	20	HNR 101	Pellet	NHP

5.2 DSC

Each of the fractionated samples was analysed to determine their solid-state crystallinity and melting properties using differential scanning calorimetry (DSC). The fractionated samples were analysed within the same temperature range (0-200 °C) that was used for the bulk polymer samples to maintain consistency throughout the results. The fractions within a sample showed clear variations, which is what we would expect due to the manner in which the bulk samples were fractionated. It is important to remember that TREF

doesn't fractionate based on molar mass or crystallinity but rather based on crystallizability. Crystallizability is in turn influenced by factors such as molar mass, crystallinity, and presence and distribution of stereodefects. [1,2] These effects will be discussed later, as we will start by investigating the physical shape of the DSC thermograms of the HKQ 205 grade fractions shown in Figures 5.1-5.4.

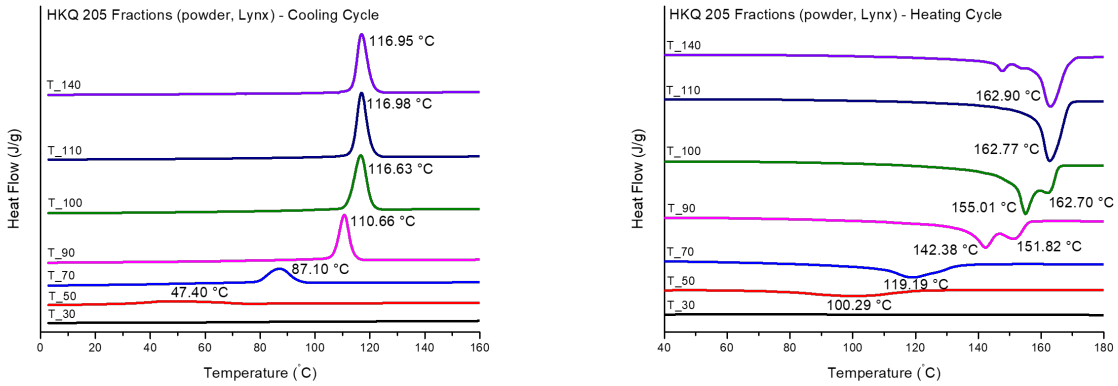

Figure 5.1: DSC cooling (left) and heating (right) curves of Lynx catalysed HKQ 205 powder fractions

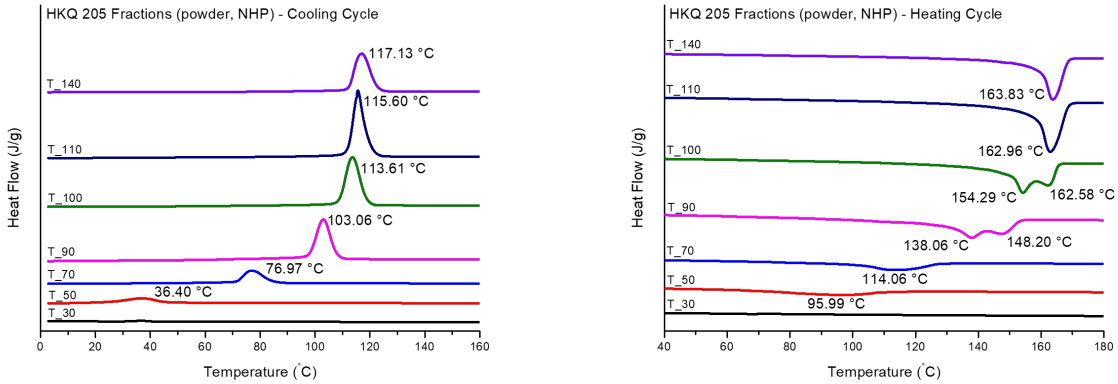

Figure 5.2: DSC cooling (left) and heating (right) curves of NHP catalysed HKQ 205 powder fractions

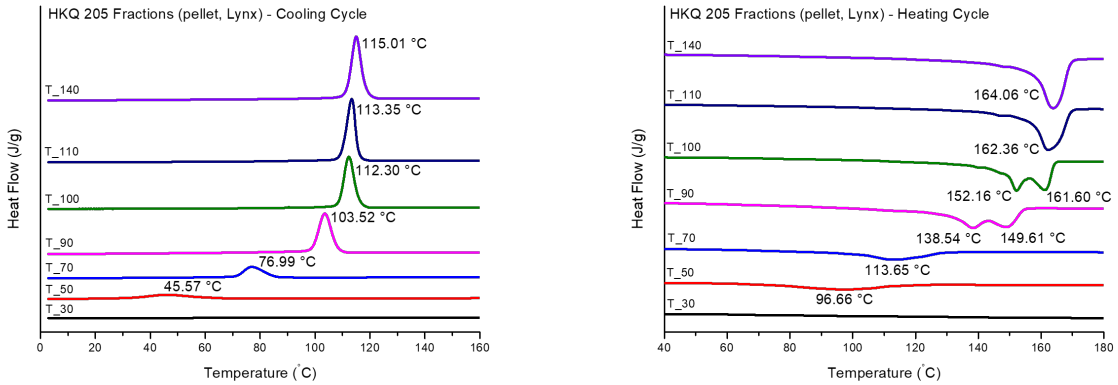

Figure 5.3: DSC cooling (left) and heating (right) curves of Lynx catalysed HKQ 205 pellet fractions

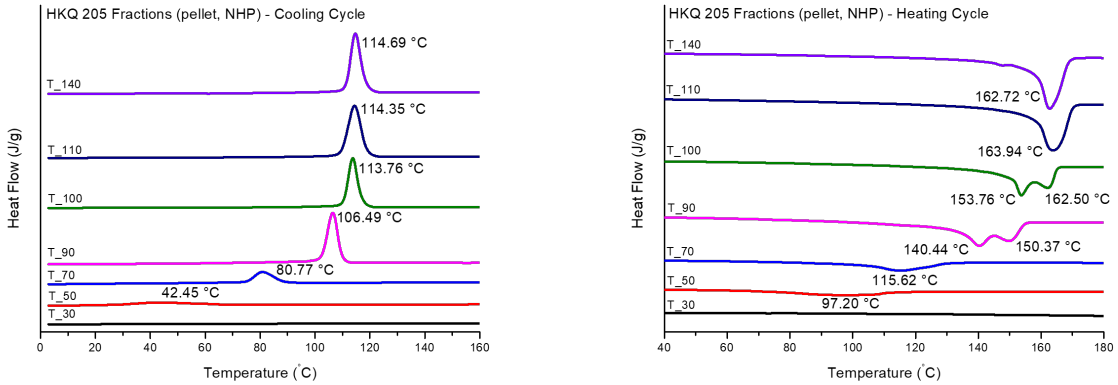

Figure 5.4: DSC cooling (left) and heating (right) curves of NHP catalysed HKQ 205 pellet fractions

If we look at the cooling cycles of these graphs we observe that each sample has the same trend, in that the temperature of the crystallization peak shifts to higher temperatures as a higher temperature fraction is analysed. This is essentially what we would expect if we compare this to the manner in which the fractions crystallize during TREF cooling. The 140 °C fraction crystallizes first during TREF cooling, as it only elutes in the final fraction at 140 °C, and we would thus expect this sample to crystallize at the highest temperature in the solid state as it did in the solution state. Caution should be exercised when predicting these events, however, as crystallization events in the solid- and solution-states aren't directly comparable. This is confirmed when observing that samples which elute at three different temperatures, namely 100, 110 and 140 °C all crystallize at approximately the same temperature in the solid state.

The cooling cycle of the 30 °C fractions show no crystallization peaks. This is due to the 30 °C fractions consisting of non-crystallizable chains and we can thus refer to the 30 °C fraction as the amorphous fraction. We would expect the amorphous fractions to have low molar mass, high dispersity and many stereodefects.

We will characterize the molar mass characteristics of the samples when we discuss the HT-SEC results in Section 5.3. The 50 °C fractions show a very broad crystallization peak at low temperature, indicating that there are some crystallizable chains present within the fractions. A steady increase in the size and temperature of the crystallization peaks are observed up to the 100 °C fraction, after which the next two fractions, namely the 110 and 140 °C fractions, have similar size peaks and crystallization temperature. The values related to these observations can be seen in Table 5.2 after which it will be discussed.

We now look at the heating cycles where we can again observe a trend, however, this trend for the heating cycles of the fractions aren't as similar as what we observed for the cooling cycles. We find that the 30 °C fractions don't show a melting endotherm. This is expected, as there are no crystallization peaks for these fractions, and thus there aren't any crystals present which can melt to form a melting endotherm. We see broad melting peaks for the 50 and 70 °C fractions, in line with what we would expect after looking at their corresponding crystallization peaks. The first interesting results from these heating cycles are the double melting endotherms that we observe for the 90 and 100 °C fractions. This is observed throughout all the grades of polymer analysed and for each variation within that specific grade, and can be seen in the Annexure on Page 124. The temperature at which the melting endotherm occurs is dependent on the size of crystal that is being melted, and thus we can say that for the 90 and 100 °C fractions, there is a significant amount of two sizes of crystals present after the crystallization event. This could typically occur due to some molecular segregation within the fractions, as they crystallize at the same temperature. [3] These 'segments' of different molar mass will then crystallize at the same temperature but will form crystals of different sizes. This is in line with what we would expect from TREF, as these polymer chains present within the same fraction have the same crystallizability, which is what we observe from DSC in that there is a single crystallization event for these fractions.

We can then investigate these double melting events further by looking at the sizes of the two peaks relevant to each other. It is observed that the size of the first melting peak of the powder samples are slightly larger compared to the second peak for both the 90 and 100 °C fractions, while these same peaks are more similar in size compared to each other for the pellet samples. When we compare the Lynx and NHP catalysed 100 °C powder samples of the same grade we see that the Lynx catalysed samples consistently have a first melting peak much larger than that of the second melting peak. The NHP catalysed 100 °C powder samples, however, generally have two melting peaks that are more equal in size. Some examples of these observations can be seen in Figures 5.5-5.6. It should be mentioned that these observations don't occur in every case, however, seems to be the general trend and have been pointed out in order to highlight that there are differences that exist in the DSC melting endotherms of samples catalysed by the Lynx and NHP

catalysts. These trends and others can be further investigated for the other variations of samples by looking at the complete set of DSC results found in the Annexure on Page 124.

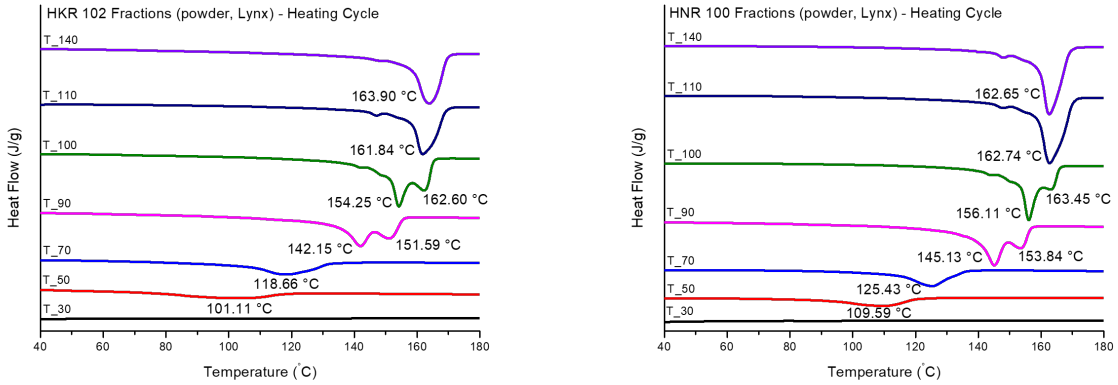

Figure 5.5: DSC heating curves of Lynx catalysed HKR 102 (left) and HNR 100 (right) powder fractions

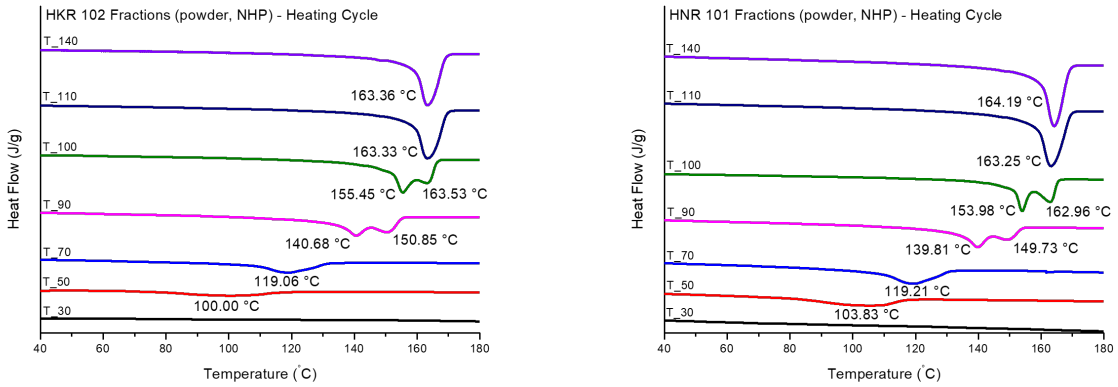

Figure 5.6: DSC heating curves of NHP catalysed HKR 102 (left) and HNR 100 (right) powder fractions

The melting events for the 110 and 140 °C fractions are fairly similar, in line with what we would expect from their corresponding crystallization peaks. We can further investigate these results by looking at the values for these DSC thermograms (T_c, T_m, percentage crystallinity, melt enthalpy) summarized in Table 5.2. The entire set of DSC results of the fractions can be seen in the Annexure on Page 124.

Table 5.2: DSC results: HKQ 205 Fractionated samples

Sample		Crystallization Temp (°C)	Melting Temp (°C)	% Crystalline	Melt Enthalpy (J/g)
HKQ 205 Powder, Lynx	T30	-	-	-	-
	T50	47.40	100.29	13.39	27.72
	T70	87.10	119.19	19.12	39.58
	T90	110.66	142.38 & 151.82	27.09	56.08
	T100	116.63	155.01 & 162.70	38.78	80.28
	T110	116.98	162.77	35.62	73.72
	T140	116.95	147.69/153.73/162.90	31.64	65.49
HKQ 205 Powder, NHP	T30	36.39	-	-	-
	T50	36.40	95.99	12.68	26.26
	T70	76.97	114.06	13.05	27.00
	T90	103.06	138.06/148.20	23.96	49.60
	T100	113.61	154.29/162.58	32.63	67.55
	T110	115.60	162.96	34.89	72.22
	T140	117.13	163.83	26.76	55.40
HKQ 205 Pellet, Lynx	T30	-	-	-	-
	T50	45.57	96.66	11.68	24.18
	T70	76.99	113.65	13.00	26.91
	T90	103.52	138.54/149.61	25.01	51.77
	T100	112.30	152.16/161.60	29.40	60.86
	T110	113.35	162.36	30.34	62.80
	T140	115.01	164.06	33.70	69.76
HKQ 205 Pellet, NHP	T30	-	-	-	-
	T50	42.45	97.20	14.27	29.55
	T70	80.77	115.62	16.77	34.72
	T90	106.49	140.44/150.37	36.15	74.83
	T100	113.76	153.76/162.50	34.62	71.66
	T110	114.35	163.94	45.47	94.11
	T140	114.69	162.72	43.56	90.18

The results in Table 5.2 will be used to confirm the assumptions we made previously simply by looking at the DSC thermograms. Firstly, if we look at the crystallization temperatures (T_c) we observe that the T_c does indeed occur at higher temperatures for the higher temperature fractions. We also notice that the crystallization temperature of the three highest temperature fractions are fairly close to one another,

as we observed from the thermograms. The same trend can be observed for the melting temperatures (T_m) in that the T_m is higher for higher temperature fractions, with the T_m of the two highest temperature fractions very close to one another. A value that we didn't discuss previously is that of the percentage crystallinity of the sample, which is calculated using the melt enthalpy of the melting endotherm. These crystallinity results are rather interesting as we would typically make the mistake of assuming that the highest temperature TREF fraction would have the highest percentage crystallinity, however, that isn't necessarily the case as we can see with these results. We observe from these results that there is a definite increase in crystallinity from the 50 °C fraction up to the 100 °C fraction, however, the crystallinity results for the two highest temperature fractions are not always what we would expect. We find that the 140 °C fraction only has the highest crystallinity for the Lynx catalysed pellet variation of the HKQ 205 grade. The 110 °C fraction has the highest crystallinity for both the NHP catalysed samples and the 100 °C fraction has the highest crystallinity for the Lynx catalysed powder variation of the HKQ 205 grade. This confirms that TREF doesn't fractionate according to crystallinity per se, but rather by crystallizability. The entire set of results from DSC analysis of the fractionated samples can be seen in the Annexure on Page 124.

Following the investigation of the DSC results, we can now make some conclusions regarding these polymers, in order to determine the effect that the catalyst has on the solid-state melting and crystallization properties of these fractionated samples. The crystallization temperatures vary between the Lynx and NHP catalysed samples of the same form, and thus no conclusion can be made regarding the strength of crystallization from these results. The melting temperatures are also too similar to make a conclusion regarding the size of the crystals produced in each case. The crystallinity results of the two catalysts have been discussed previously. We can thus conclude for the DSC results of specifically the HKQ 205 grade, that there are noticeable differences between samples catalysed between both the Lynx and NHP catalysts, however, these differences don't occur consistently across all variations of all grades and has been highlighted simply to show that there are differences, however small, between the thermal properties of samples catalysed by Lynx and NHP catalysts.

5.3 HT-SEC

Each of the fractionated samples were analysed to determine their molar mass related properties using high temperature size exclusion chromatography (HT-SEC). The samples, even though fractionated, are still olefinic in nature and are thus difficult to dissolve. The same sample preparation that was needed for the bulk samples (Chapter 3) was applied to the fractionated samples, using a strong solvent (TCB) and

high temperature (150 °C) to be able to dissolve the samples and subsequently perform the analysis. The SEC curves obtained for the HKQ 205 grade samples have been shown in Figures 5.7-5.8.

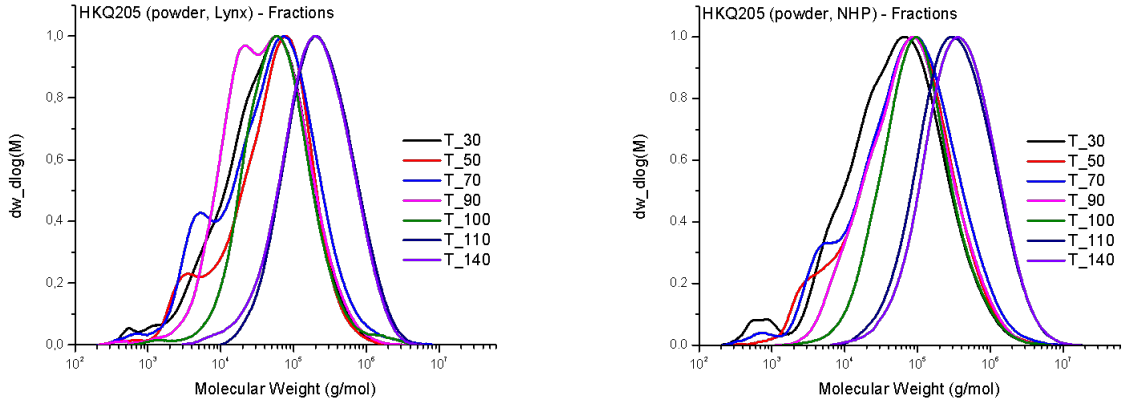

Figure 5.7: HT-SEC chromatograms of Lynx catalysed (left) and NHP catalysed (right) HKQ 205 powder fractions

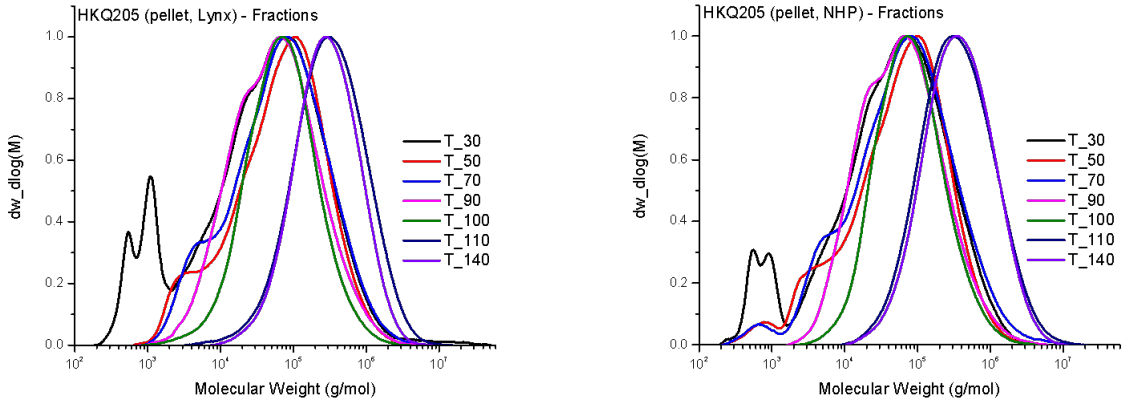

Figure 5.8: HT-SEC chromatograms of Lynx catalysed (left) and NHP catalysed (right) HKQ 205 pellet fractions

Looking at the SEC curves of the fractions of the HKQ 205 grade, we can observe some similarities as well as some differences. First, we can observe for all the chromatograms that from the 30 °C amorphous fraction up to the 140 °C fraction we have a transition from broad low molar mass to narrow high molar mass samples. The broadness of the peak relates to the dispersity of the sample, i.e. a narrow peak indicates a low dispersity. We can also consistently see that the 110 and 140 °C fractions are isolated in terms of molar mass, however, the 100 °C fractions have similar dispersities to the high temperature fractions in some cases. For the 50, 70, 90 and 100 °C fractions we have a large overlap of molar mass, with the lower temperature fractions showcasing bimodal distributions. The most noticeable difference between the variations of the HKQ 205 grade, however, is found in the amorphous 30 °C fraction. This fraction

consistently shows at least a tetramodal distribution, with the two lower molar mass peaks being the easiest to distinguish from each other. The amorphous fraction of the pellet samples shows two distinct peaks in the low molar mass region, while the amorphous fractions of the powder samples show little resolution in the low molar mass region. Typically, it is observed throughout the samples that the NHP catalysed amorphous fractions show less detail in the low molar mass region compared to the Lynx catalysed samples. This effect can be seen in an example of both powder and pellet samples in Figures 5.9-5.10. The entire set of HT-SEC chromatograms can be seen in the Annexure on Page 137.

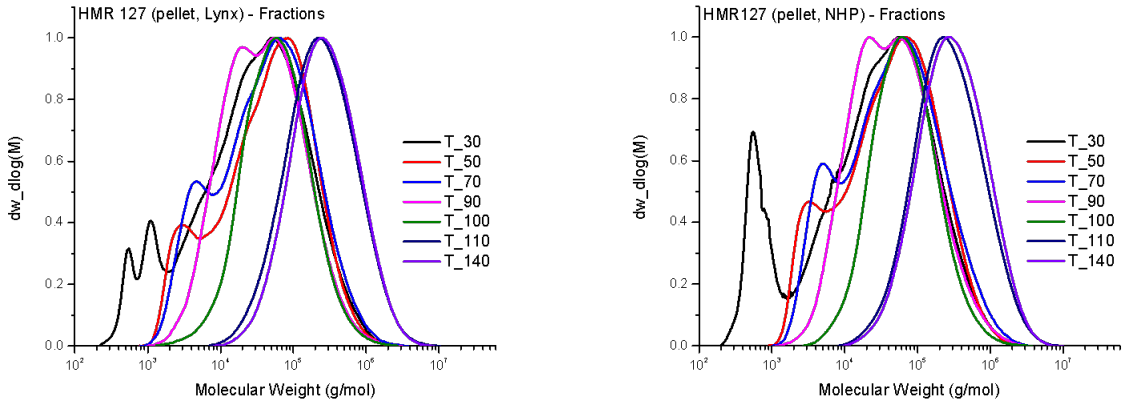

Figure 5.9: HT-SEC chromatograms of Lynx catalysed (left) and NHP catalysed (right) HMR 127 pellet fractions

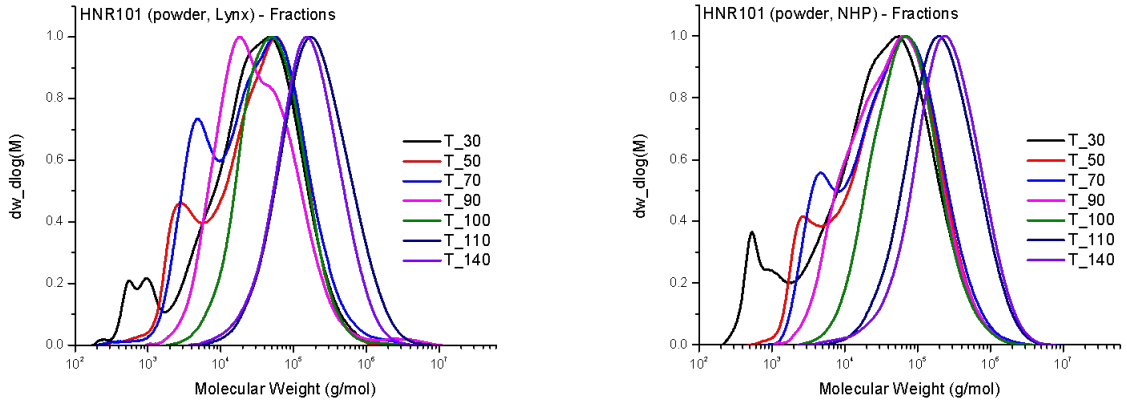

Figure 5.10: HT-SEC chromatograms of Lynx catalysed (left) and NHP catalysed (right) HNR 101 powder fractions

There are some fractions present on the SEC curves which deviate from the normal trends observed, such as for example the 50 °C fraction of the HKR 102 grade NHP catalysed pellet sample (Figure 5.11 left) or the 100 ^{circ}C fraction of the HKR 102 grade Lynx catalysed powder sample (Figure 5.11 right).

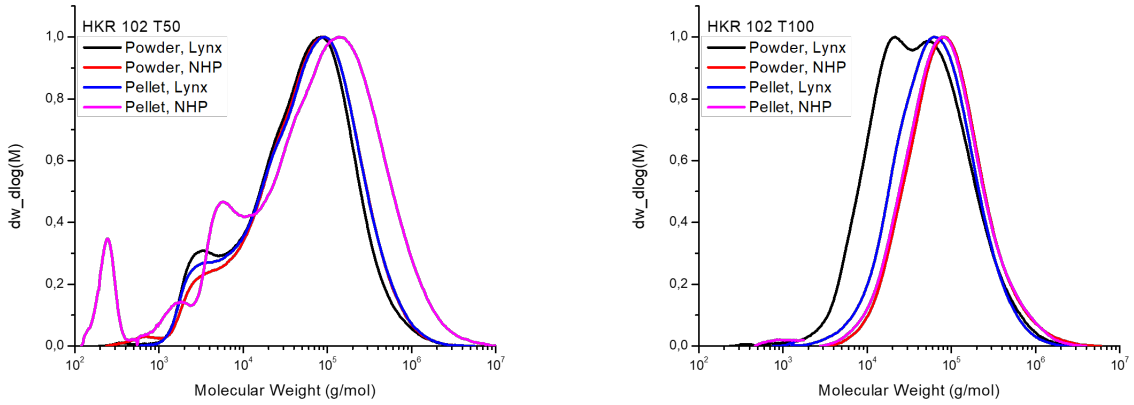

Figure 5.11: HT-SEC chromatograms of 50 °C fraction (left) and 100 °C fraction (right) of HKR 102 grade samples

To be able to further investigate the effect that the catalyst has on the molar mass properties of polymers we need to look at the values associated with the HT-SEC curves, as investigation simply by observation doesn't tell the full story. The summarised values for the HKQ 205 grade can be seen in Table 5.3.

If we focus on the three highest temperature fractions in Table 5.3, we can see that the NHP catalysed samples have a higher molar mass compared to the Lynx catalysed samples of the same form. This being said, the observation is then made that the dispersity values are typically lower for the Lynx catalysed samples. When taking the other samples into account we find that the NHP catalysed samples don't necessarily always have higher molar mass, although it is very often found that the sample with higher molar mass has the higher dispersity value. We thus can't make an overall conclusion as to the effect that the catalyst has on molar mass, however, there are clear differences between HKQ 205 grade samples catalysed with the Lynx and NHP catalysts. These conclusions don't necessarily reflect on all the variations of all the grades but have been highlighted simply to show that some differences exist between samples catalysed with Lynx and NHP catalysts. The entire set of data values for HT-SEC can be seen in the Annexure on Page 137.

Table 5.3: HT-SEC results: HKQ 205 Fractionated samples

Sample		M_n [a]	M_w [b]	M_z [c]	PDI [d]	Sample		M_n [a]	M_w [b]	M_z [c]	PDI [d]
HKQ 205 Powder, Lynx	T30	12188	81950	273750	6.72	HKQ 205 Powder, NHP	T30	11592	123939	744891	10.69
	T50	14048	86849	237699	6.18		T50	17942	147501	672927	8.22
	T70	12576	111754	736406	8.89		T70	15528	171762	895379	11.06
	T90	17902	82242	296737	4.59		T90	33072	159040	614448	4.81
	T100	31233	110874	546445	3.55		T100	51498	172580	613969	3.35
	T110	130569	354261	849024	2.71		T110	165710	579439	1689115	3.45
	T140	98158	324231	776555	3.30		T140	190797	630313	1743015	3.30
HKQ 205 Pellet, Lynx	T30	4755	176214	5633286	37.06	HKQ 205 Pellet, NHP	T30	6025	123887	505108	20.56
	T50	18091	140828	507543	7.78		T50	11311	126223	466151	11.16
	T70	19482	155791	670665	8.00		T70	12642	175380	1272850	13.87
	T90	24245	123887	529188	5.11		T90	28200	128554	605676	4.56
	T100	35462	119472	370686	3.37		T100	44934	134571	440679	2.99
	T110	149523	526341	1412784	3.52		T110	178624	614004	1952471	3.44
	T140	161384	426851	945725	2.64		T140	193644	588056	1493864	3.07

[a] - Number average molar mass

[b] - Weight average molar mass

[c] - Z-average molar mass

[d] - Dispersity value (M_w/M_n)

5.4 Summary

Having looked at the DSC and HT-SEC results of the fractions of our bulk polymer samples it is clear to see that some significant differences exist in the molecular properties between powder and pellet samples as well as between same form samples catalysed with different catalysts, namely the Lynx and NHP catalysts. This isn't unexpected as we found in Chapter 4 that the bulk polymer samples also have significant differences in the molecular properties of the varying samples. Earlier in this chapter we discussed the relative difference in size of the two melting peaks of the 90 and 100 °C fractions of these samples. These differences could be related back to the TREF fractograms that we discussed during the results of the bulk polymer samples in Chapter 4. We know that the size of the melting peak is dependent on the amount of a certain size crystal present within the sample, and thus the differences in relative sizes observed in the melting endotherms are due to there being varying amounts of each crystal present within the samples. The TREF fractograms show some slight variations in the amount of material eluted of the 90 and 100 °C fractions. These slight

differences might be indicative of for example, higher (or lower) percentages isotacticity present within these samples and the distribution thereof will then cause the size of the melting peaks to vary.

Due to the high number of samples investigated during this study, it was impossible to do further experimental analysis on all the fractionated samples. It was decided to look more in depth at some specific samples in order to elucidate some further molecular information. The samples chosen were the 90 and 100 °C fractions of the HKQ 205 and HKR 102 grades and all variations thereof. The investigation of these samples with advanced techniques such as XRD, SSA and NMR allowed us to further study the effects that catalyst composition has on the molecular properties of isotactic polypropylene samples. The results of this study will be discussed in Chapter 6 and will serve as **part 3** of the results of the project.

5.5 References

1. Soares, J. B. P. & Hamielec, A. E. Temperature rising elution fractionation of linear polyolefins. *Polymer (Guildf)*. **36**, 16391654 (1995).

2. Viville, P., Daoust, D., Jonas, A.M., Nysten, B., Legras, R., Dupire, M., Michel, J. & Debras, G. Characterization of the molecular structure of two highly isotactic polypropylenes. *Polymer (Guildf)*. **42**, 19531967 (2001).

3. Zhu, X. & Yan, D. In situ FTIR spectroscopy study on the crystallization process of isotactic polypropylene in isotactic polypropylene/polyethylene-glycol blends. *Macromol. Chem. Phys* **202**, 11091113 (2001).

Chapter 6

In depth studies

This chapter will serve as an in-depth investigation into a smaller set of samples, to gain detailed knowledge regarding the fine molecular structure present within the samples. The results obtained from this study will be documented and discussed comprehensively throughout the chapter. This chapter will serve as ***part 3*** *of the results of the thesis.*

6.1 Results and Discussion

Due to the sheer volume of samples used during this study, it was impossible to do extensive analysis on each sample. It was thus decided after investigating the DSC and HT-SEC results of all the fractions, to further investigate only a couple of specific fractions, in order to further probe the molecular properties of our polypropylene samples. These samples were divided into two sets of 8 samples, 8 powder and 8 pellet samples, each consisting of the 90 and 100 °C fractions of both the Lynx and NHP catalysed samples of the HKQ 205 (MFI 3g/10min) and HKR 102 (MFI 3.5g/10min) grades. This gave us a total of 16 samples, and a breakdown of these samples can be seen in Tables 6.1 & 6.2 below.

Table 6.1: Summary of powder samples studied in depth

Sample				
#	Grade	Form	Catalyst	Temp Fraction (°C)
1	HKQ 205	Powder	Lynx	90
2	HKQ 205	Powder	NHP	90
3	HKQ 205	Powder	Lynx	90
4	HKQ 205	Powder	NHP	90
5	HKR 102	Powder	Lynx	100
6	HKR 102	Powder	NHP	100
7	HKR 102	Powder	Lynx	100
8	HKR 102	Powder	NHP	100

Table 6.2: Summary of pellet samples studied in depth

Sample				
#	Grade	Form	Catalyst	Temp Fraction (°C)
1	HKQ 205	Pellet	Lynx	90
2	HKQ 205	Pellet	NHP	90
3	HKQ 205	Pellet	Lynx	90
4	HKQ 205	Pellet	NHP	90
5	HKR 102	Pellet	Lynx	100
6	HKR 102	Pellet	NHP	100
7	HKR 102	Pellet	Lynx	100
8	HKR 102	Pellet	NHP	100

This chapter will consist of an in-depth analysis and characterization of these samples, starting with the 8 powder samples followed by the 8 pellet samples. These discussions will be done as a comparative study, directly comparing samples differing solely on their catalyst (e.g. comparison of sample **1** vs sample **2**). This will allow us to directly investigate the effect that the catalyst has on the molecular properties of the polymers.

The results will be discussed based on what can be seen from the graphs of the samples added within this chapter. Where further insights are mentioned, a reference will be given as to where the data can be found. Comprehensive results from XRD, SSA and NMR will thus be summarized in tables and added to the Annexure of the thesis from Page 145 onwards.

The experimental procedures employed for the analysis of these samples, which include DSC, HT-SEC, FTIR, XRD, SSA and NMR are discussed in detail in Chapter 3.

6.2 Powders

6.2.1 Background

Table 6.3: General results of HKQ 205 90 °C powder samples

HKQ 205 powder - T90	Lynx (**1**)	NHP (**2**)
TREF weight fraction (%)	4.78	5.21
HT-SEC M_w (g/mol)	82242	159040
HT-SEC PDI	4.59	4.81
^{13}C NMR mmmm (%)	87.66	83.23

Table 6.4: General results of HKR 102 90 °C powder samples

HKR 102 powder - T90	Lynx (**3**)	NHP (**4**)
TREF weight fraction (%)	4.03	4.85
HT-SEC M_w (g/mol)	84737	121318
HT-SEC PDI	4.09	4.33
^{13}C NMR mmmm (%)	83.38	88.64

Table 6.5: General results of HKQ 205 100 °C powder samples

HKQ 205 powder - T100	Lynx (**5**)	NHP (**6**)
TREF weight fraction (%)	7.62	8.76
HT-SEC M_w (g/mol)	110874	172580
HT-SEC PDI	3.55	3.35
^{13}C NMR mmmm (%)	95.95	94.20

Table 6.6: General results of HKR 102 100 °C powder samples

HKR 102 powder - T100	Lynx (**7**)	NHP (**8**)
TREF weight fraction (%)	7.10	8.64
HT-SEC M_w (g/mol)	84819	145909
HT-SEC PDI	4.44	2.84
^{13}C NMR mmmm (%)	95.20	95.70

From the results in Tables 6.3-6.6, we can see a summary of some basic analyses that were done on the samples, including fraction weight percentage, the weight average molar mass and dispersity calculated

from SEC, as well as the percentage isotacticity calculated from ^{13}C NMR. First, we observe that the isotacticity of the 90 °C samples differ between the HKQ 205 and HKR 102 grades. For the HKQ 205 grade, the Lynx catalysed sample has higher isotacticity, while the NHP catalysed sample has higher isotacticity for the HKR 102 grade. The same trend is observed for the 100 °C samples, however, the differences in isotacticity are much less significant.
The weight average molar mass (M_w) is significantly higher for the NHP catalysed samples in all cases, while the dispersity values show some interesting results. This holds true for the 100 °C samples, however, we observe that the NHP catalysed sample, which has higher molar mass, has a higher dispersity in the 90 °C samples. We previously noticed this trend when discussing the molar mass properties of all the fractions in Chapter 5. The NHP catalysed fractions also constitutes a larger weight percentage of the entire sample compared to the same temperature Lynx catalysed fractions of the same form, indicating that a larger amount of the dissolved NHP catalysed samples will crystallize in solution at these temperatures.

From these initial results some significant conclusions can be mentioned. The polymers that are compared here are all fractions of a bulk polymer samples, which was fractionated according to crystallizability. We see, however, that even though these samples that elute at the same temperature (and thus have similar crystallizabilities), they have different properties with respect to isotacticity and molar mass. This is a clear indication that the samples have different chemical compositions and is solely due to the effect that the catalyst has on the samples.

6.2.2 DSC

The DSC thermograms of the 8 powder samples investigated can be seen in Figure 6.1, while some selected results from DSC analysis have been summarized in Tables 6.7-6.10.

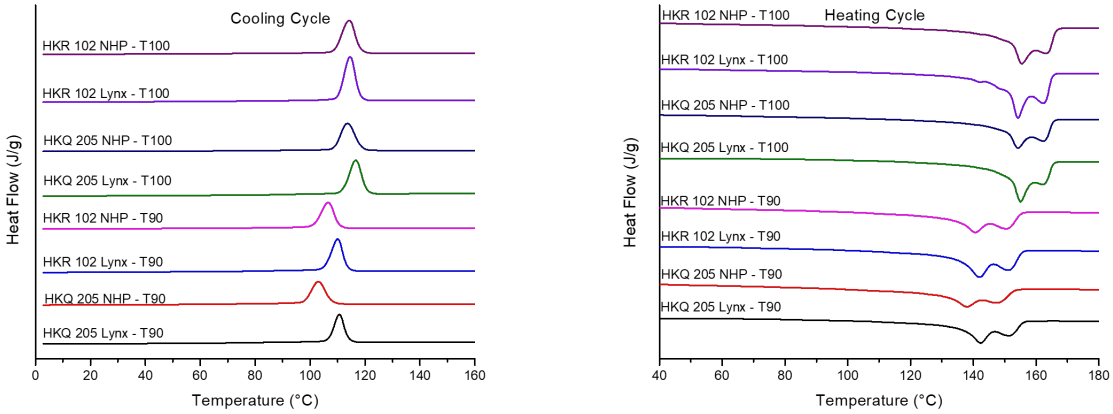

Figure 6.1: DSC cooling (left) and heating (right) curves of 8 powder fractions investigated

The eight samples investigated here were chosen partly due to them all having a double melting event as can be seen in Figure 6.1. It was discussed in Chapter 4 that these events occur due to molecular segregation within the sample, [1] and it was thus thought to be of significance to investigate the relative sizes of each of these peaks. Simply by observing the melting endotherms we can see that not a lot of variation occurs for the 90 °C fractions, however, the 100 °C fractions show some more significant differences. We see for these specific samples, that the size of the NHP catalysed 100 °C fraction peaks are more equal in size, while the lower temperature peak of the Lynx catalysed 100 °C fractions is larger compared to the higher temperature peak. We can thus clearly see that the Lynx and NHP catalysts produce polymer samples with different thermal properties simply from looking at the melting endotherms of the 100 °C fractions of the HKQ 205 and HKR 102 grades.

Table 6.7: DSC results of HKQ 205 90 °C powder samples

HKQ 205 powder - T90	Lynx (**1**)	NHP (**2**)
Crystallinity (%)	27.09	23.96
Crystallization temp (°C)	110.66	103.06
Melting temp (°C)	142.38	138.06
	151.82	148.20

Table 6.8: DSC results of HKR 102 90 °C powder samples

HKR 102 powder - T90	Lynx (**3**)	NHP (**4**)
Crystallinity (%)	34.15	28.31
Crystallization temp (°C)	110.07	106.60
Melting temp (°C)	142.15	140.68
	151.59	150.85

Table 6.9: DSC results of HKQ 205 100 °C powder samples

HKQ 205 powder - T100	Lynx (**1**)	NHP (**2**)
Crystallinity (%)	38.78	32.63
Crystallization temp (°C)	116.63	113.61
Melting temp (°C)	155.01	154.29
	162.70	162.58

Table 6.10: DSC results of HKR 102 100 °C powder samples

HKR 102 powder - T100	Lynx (**3**)	NHP (**4**)
Crystallinity (%)	45.27	39.08
Crystallization temp (°C)	114.57	114.22
Melting temp (°C)	154.25	155.45
	162.60	163.53

We can see from these results that the Lynx catalysed samples have higher percentage crystallinity compared to the NHP catalysed samples. We can also observe that the crystallization temperature (T_c) and melting temperature (T_m) of both peaks in the melting endotherms are generally higher for the Lynx catalysed samples, except in the case of the HKR 102 100 °C samples, where the values are fairly similar. These higher T_c and T_m values indicate that the Lynx catalysed samples generally crystallize stronger than the NHP catalysed samples. [2] We will further investigate these samples by looking at the results of some other analytical techniques.

6.2.3 HT-SEC

The HT-SEC curves of the 8 powder samples investigated can be seen in Figure 6.2 with some key results previously summarized in Tables 6.3-6.6. These results will be discussed shortly as they have been summarized previously in Section 6.2.1.

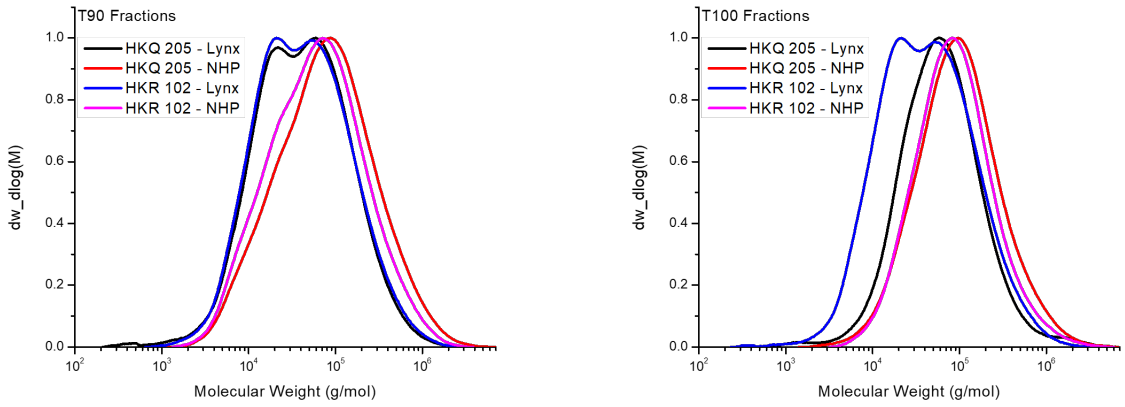

Figure 6.2: HT-SEC chromatograms of the 90 °C fractions (left) and 100 °C fractions (right)

From these results we can see that there are some noticeable differences between the samples investigated. Firstly, we see that the Lynx catalysed 90 °C fractions have a bimodal molar mass distribution while the NHP catalysed samples have a broad unimodal distribution. In fact, the NHP catalysed samples have a higher dispersity than the Lynx catalysed samples even though the Lynx catalysed samples seem to have a broad distribution. The NHP catalyst samples have a significantly higher molar mass compared to the Lynx catalysed samples.
For the 100 °C fractions we find that the Lynx catalysed HKR 102 grade sample is the only sample with a bimodal distribution, and subsequently has a higher dispersity as the other samples have a fairly narrow unimodal distribution. The NHP catalysed samples have a lower dispersity for these samples and also, as with the 90 °C fractions, a significantly higher molar mass. It is thus clear to see that the Lynx and NHP catalysts lead to samples with different molar mass properties.

6.2.4 FTIR

ATR-FTIR analysis was done in order to investigate the relationship between the stereodefect distribution and the conformational behaviour of the samples, the latter of which is determined from FTIR measurements. For this analysis, regularity band intensities from both samples were compared to each other, using the normalized values of the Lynx catalysed samples as the reference value. The intensity of each of the regularity bands relates to the relative amount of all length of helical sequences present within the sample. This is then also directly related to the conformational order degree of the sample. [2–4] The differences in conformational order observed for these samples can be attributed to the different molecular structural regularities of the sample, as the thermal history of the samples are the same. The distribution of stereodefects is determined by evaluating the intensity of the regularity bands reported on the FTIR graphs. If we assume that the same amount of stereodefects are present within the samples, then the sample which has a more uniform distribution of stereodefects will have lower intensity of all length of helical sequences. [2]
It is possible to determine the relative amount of stereodefects present within a sample from ^{13}C NMR by looking at the percentage isotacticity present within that sample, however, those values can't be used to discuss FTIR results, as NMR is done in the solution state while FTIR analysis is done in the solid state.

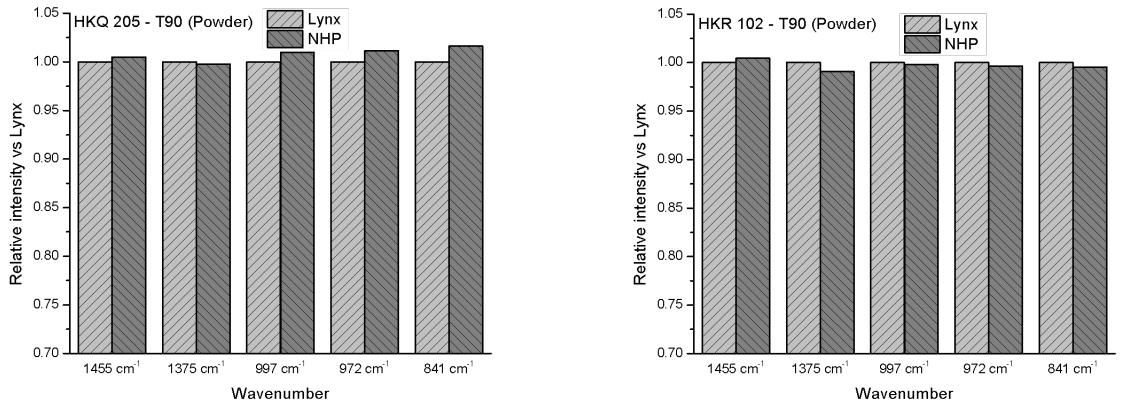

Figure 6.3: Comparison of FTIR peak intensities of the 90 °C HKQ 205 (left) and HKR 102 (right) fractions

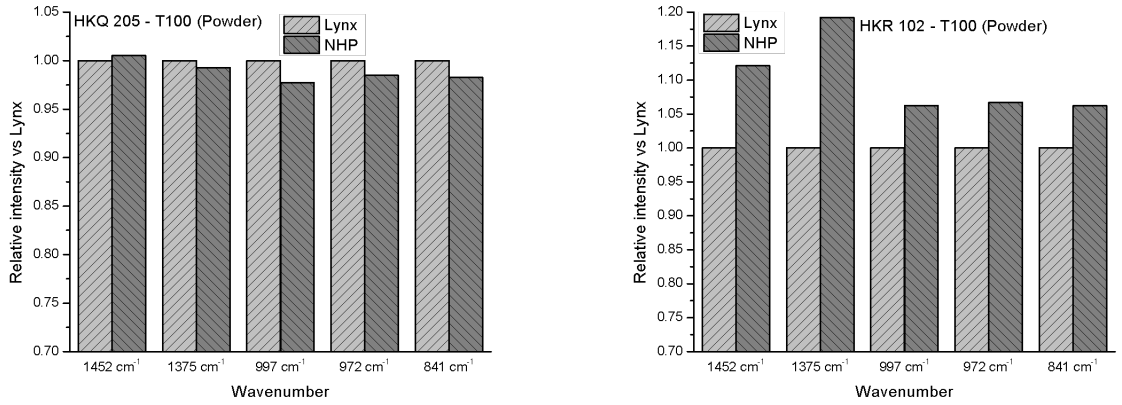

Figure 6.4: Comparison of FTIR peak intensities of the 100 °C HKQ 205 (left) and HKR 102 (right) fractions

Table 6.11: Comparison of FTIR results of NHP catalysed powder samples relative to Lynx catalysed samples

Samples		Overall Intensity	Content of helical sequence	Distribution of stereodefects
1 vs **2**	HKQ 205 T90 NHP	Higher	Higher	Less uniform
3 vs **4**	HKR 102 T90 NHP	Lower	Lower	More uniform
5 vs **6**	HKQ 205 T100 NHP	Lower	Lower	More uniform
7 vs **8**	HKR 102 T90 NHP	Higher	Higher	Less uniform

The results obtained from the FTIR graphs in Figures 6.3-6.4, were summarized in Table 6.11. We know that regularity bands at 1220, 840, 998 and 973 cm^{-1} have helical structures with a decreasing degree of order and have minimum n values (critical helix length) of 14, 12, 10 and 5 monomer units respectively. [3,4] We could thus calculate the relative intensity of helical structures of these orders between the Lynx and

NHP catalysed samples. We see from Table 6.11 that the intensities and subsequent properties related to the intensities, differ between temperature fractions of the same polymer grade, and also between different grades of the same temperature fraction. From these results it is clear that there is no definitive trend for these samples using FTIR, and no conclusion can be made regarding the effect that the catalyst has on the helical lengths of these samples.

6.2.5 WAXD

Wide angle X-ray diffraction analysis was done on the samples in order to observe the crystal structure present within the samples. The diffractograms obtained can be seen in Figures 6.5-6.6, from which some calculations could be made regarding crystal properties of the samples. The crystallite size (L) of each face was calculated from the individual peaks using the Debye-Scherrer Equation: $L = \frac{0.9\lambda}{\beta cos\theta}$ and the crystal spacing (d) of each peak was determined using Bragg's Law: $n\lambda = 2dsin\theta$. [3] The d-spacing values give us the distance between similar crystal faces within the sample. The results of these calculated values and some other values can be seen summarized in the Annexure on Page 145.

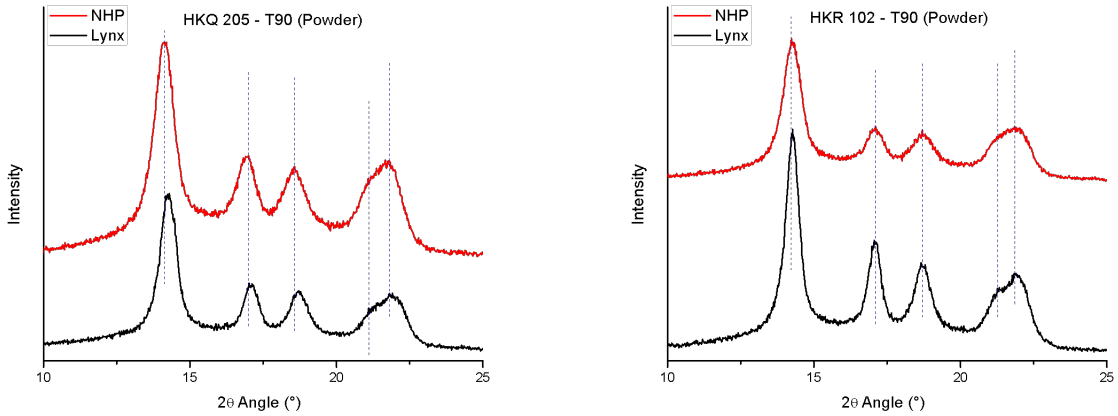

Figure 6.5: XRD diffractograms of the 90 °C HKQ 205 (left) and HKR 102 (right) fractions

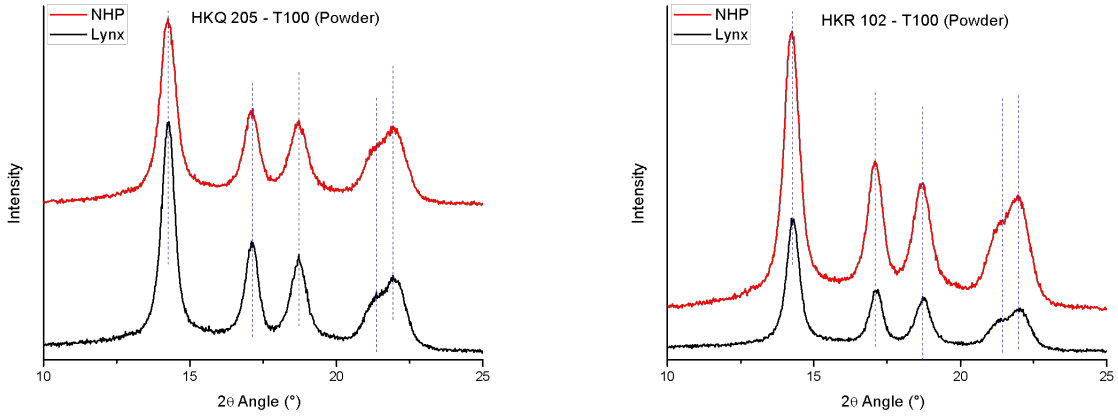

Figure 6.6: XRD diffractograms of the 100 °C HKQ 205 (left) and HKR 102 (right) fractions

From the XRD data tabulated in Section 8.5 and by visually investigating the figures above it is clear to see that the peaks of all the compared samples occur at roughly the same 2θ angles. This isn't unexpected and from this result we can conclude that all the samples analysed have an -monoclinic crystal structure due to the presence of peaks at 2 angles of about 14.3, 17.1, 18.5, 21.2 and 21.9 ° corresponding to the α(110), α(040), α(130), α(111) and α(-131) peaks respectively. [3,5] There are some slight variations in the calculated crystallite size *L* of each crystal face, however, these differences are not significant. The crystal spacing d were identical when taking two decimal figures into account and is also not significant. It can also be seen that the peaks of the 100 °C samples are much narrower than that of the 90 °C samples, which relates to the higher crystallinity of the 100 °C samples.

6.2.6 SSA

The final thermal analysis that was done on the samples is successive self-nucleation and annealing (SSA), and this method is used to thermally fractionate a specific area of interest, which in this case was the entire melting range of each sample as seen from DSC. Nucleation steps were programmed at eleven temperatures, starting from 170 °C ending at 130 °C with increments of 4 °C. [6] For the 90 °C samples the final melting endotherm of the SSA curve was fitted into seven individual peaks, while that of the 100 °C samples was fitted into nine individual peaks. The three highest temperature peaks, which will further on be denoted as peak 1 (highest temperature) and peaks 2 and 3 (next highest temperatures), will be discussed with regards to isotacticity , as these peaks relate to the highly isotactic thick lamellae (peak 1), and medium isotactic medium thickness lamellae (peaks 2 and 3) present within the sample. [2] The melting temperature of each peak, the percentage integral of the area under the curve and the lamellar thickness of each crystal is summarized and can be seen summarized in Section 8.5 on Page 145. The lamellar thickness (L) for each melting peak was calculated using the Thomson-Gibbs equation: [2] $T_m = T_m'^0(1 - \frac{2\sigma}{\Delta_0 L})$

The final melting endotherms of the 90 °C samples have been shown in Figures 6.7 (left) & 6.8 (left). These endotherms were deconvoluted in order to obtain qualitative information on the relative percentage areas for both samples, after which these percentage areas were plotted and can be seen in Figures 6.7 (right) & 6.8 (right). An example of how the final melting endotherms of the 90 °C samples were deconvoluted can be seen in Figure 6.9.

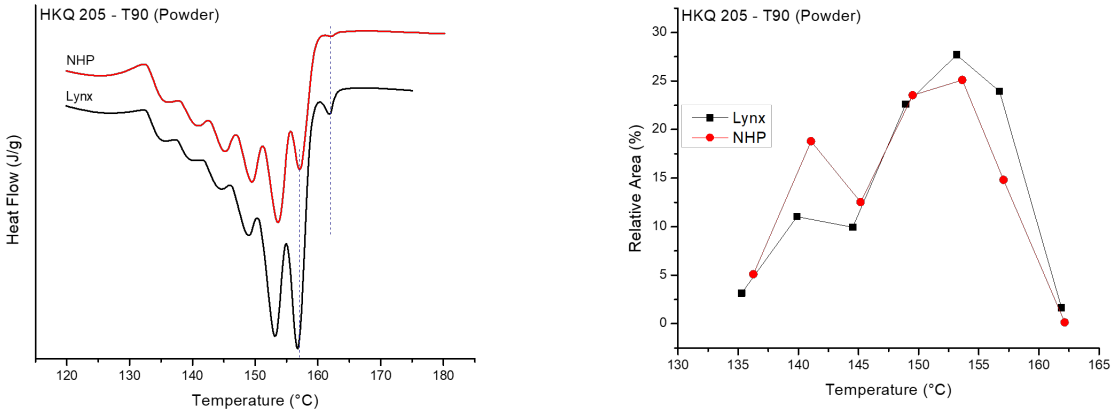

Figure 6.7: Final melting endotherm (left) and area comparison (right) of 90 °C HKQ 205 fractions

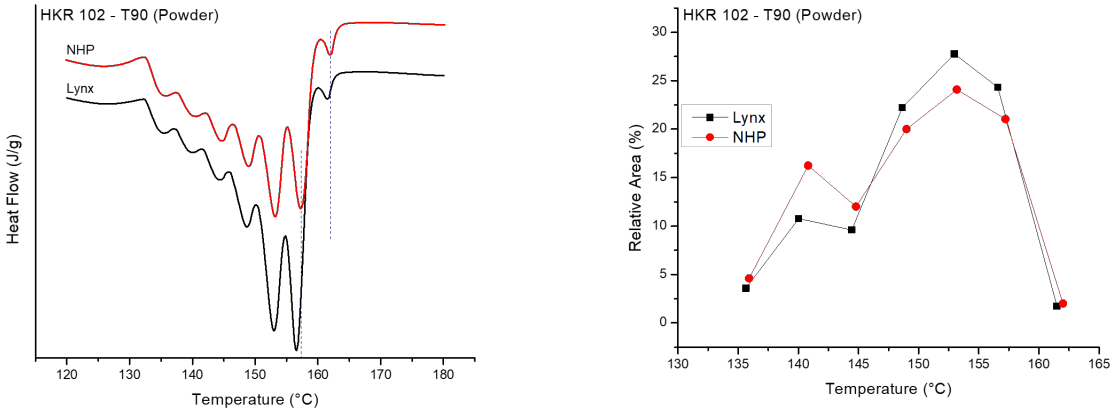

Figure 6.8: Final melting endotherm (left) and area comparison (right) of 90 °C HKR 102 fractions

(**1** & **2**). We can see from Figure 6.7 (left) that both samples have similar curves, however, the position and size of the peaks differ relatively to each other. We see from Figure 6.7 (right) that the Lynx catalysed sample has larger areas for the three highest temperature peaks, and thus we can say that there are more highly isotactic and medium isotactic areas in the Lynx catalysed sample.

We can also investigate the lamellar thickness for each crystal found in samples **1** and **2** by looking at the values found in Section 8.6. The lamellar thickness of the NHP catalysed sample is consistently slightly higher than that of the Lynx catalysed sample. This is confirmed by observing that the melting temperature for each peak is slightly higher for the NHP catalysed sample. We conclude for samples **1** and **2** that the Lynx catalysed sample has more areas of highly isotactic and medium isotactic material, however, the NHP catalysed sample has thicker lamellae.

(**3** & **4**). We again see from Figure 6.8 (left) that the peaks in the final melting endotherm of samples **3** and **4** look fairly similar. As we saw for samples **1** and **2**, we find from Figure 6.8 (right) that the Lynx catalysed sample has larger areas for the 2nd and 3d highest temperature peaks, however, we now have a similar value for the highly isotactic highest temperature peak.

When looking at the lamellar thickness values for samples **3** and **4** in Section 8.6, we see as we did for samples **1** and **2** that the NHP catalysed samples have higher values. The values are closer to each other than what we observed for samples **1** and **2**, which is confirmed by looking at the melting temperatures for each peak on Figure 6.8. We conclude that the Lynx catalysed sample has more areas of medium isotactic material, and similar amounts of highly isotactic material compared to the NHP catalysed sample. The NHP catalysed sample again has thicker lamellae compared to the Lynx catalysed sample.

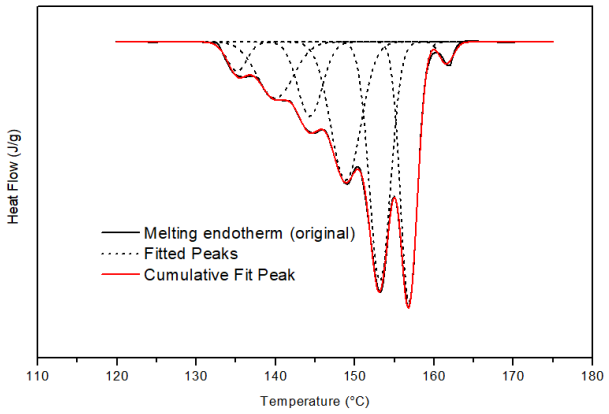

Figure 6.9: Example of deconvolution of final melting endotherm (90°C)

The final melting endotherms of the 100 °C samples have been shown in Figures 6.10 & 6.11 (left). These endotherms were deconvoluted in order to obtain quantitative information on the relative percentage areas for both samples, after which these percentage areas were plotted and can be seen in Figures 6.10 & 6.11 (right). An example of how the final melting endotherms of the 100 °C fractions were deconvoluted can be seen in Figure 6.12.

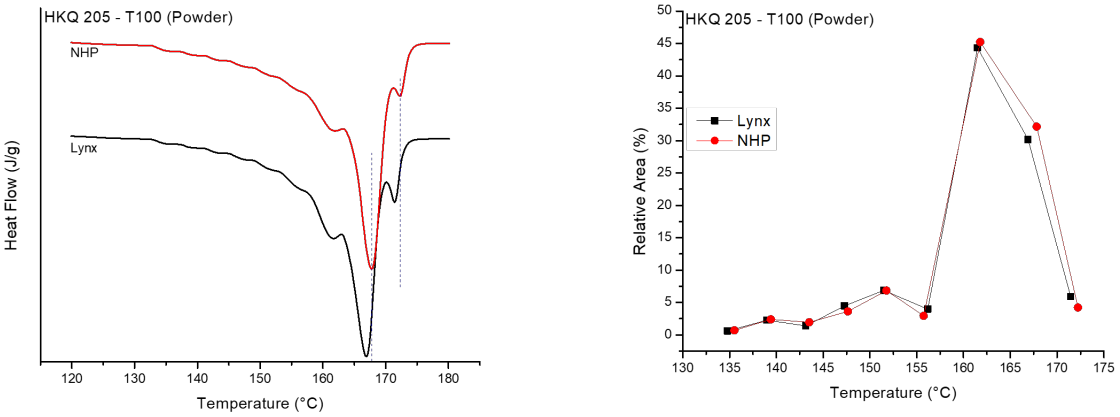

Figure 6.10: Final melting endotherm (left) and area comparison (right) of 100 °C HKQ 205 fractions

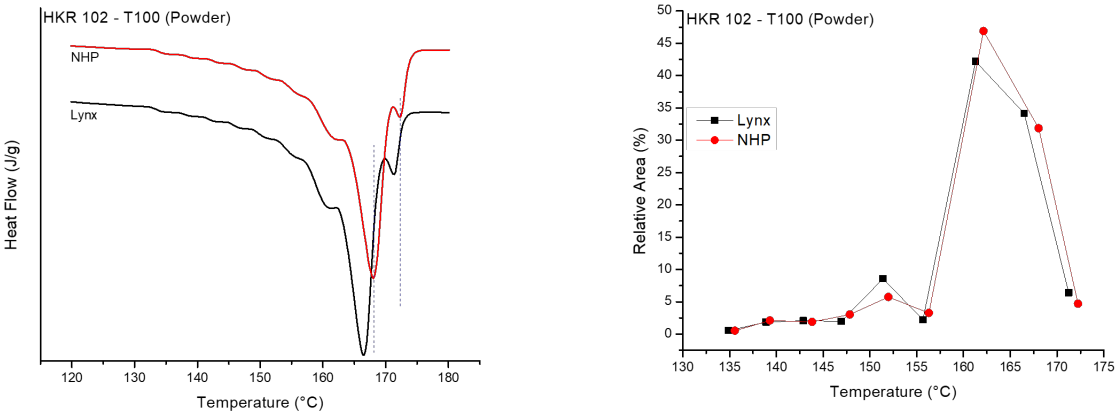

Figure 6.11: Final melting endotherm (left) and area comparison (right) of 100 °C HKR 102 fractions

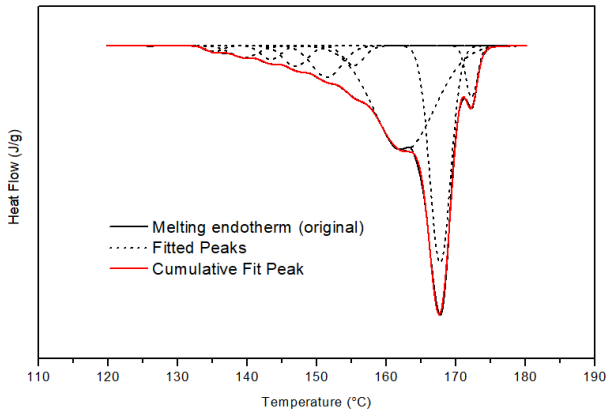

Figure 6.12: Example of deconvolution of final melting endotherm (100°) C)

(**5** & **6**). The first thing that we clearly observe from Figure 6.10 (left) is that the positions of the two highest temperature peaks of the NHP catalysed sample are clearly higher than those of the Lynx catalysed sample. The sizes of the peaks seem to have similar trends. The percentage areas from Figure 6.10 (right) follow a different trend to what was seen with the 90 °C samples (samples **1**-**4**). We observe that the percentage areas are closer together, and the majority of material is present in the three highest temperature peaks. We observe that the NHP catalysed sample has a slightly larger area for peak 2 (medium isotactic material), while the Lynx catalysed sample has a slightly larger area for peak 1 (highly isotactic material).
We observe similar trends for the lamellar thickness of samples **5** and **6** compared to samples **1** through **4**, in the sense that the NHP catalysed samples generally have a larger lamellar thickness. We conclude that the Lynx catalysed sample has more highly isotactic material, the NHP catalysed sample has more medium isotactic material, with the NHP catalysed sample having thicker lamellae for all ranges of isotactic material.

(**7** & **8**). We observe from Figure 6.11 (left) that the melting temperatures of the two highest temperature peaks are higher for the NHP catalysed sample. The peaks themselves seem to have similar trends when simply looking at the shape of the curves. We see a similar trend in the percentage areas from Figure 6.11 (right) to what was observed with samples **5** and **6**, in that the values for the first six peaks are fairly similar. Differences occur at the three highest temperature peaks, where we see that there is a larger area of medium isotactic material from peak 3 for the NHP catalysed sample, while the Lynx catalysed sample has larger areas for both peaks 1 and 2.
We again observe, as for all other comparisons in this study that the NHP catalysed sample has larger lamellar thickness values throughout. We do, however, have the most significant differences in lamellar thickness for all the samples investigated in this study. Peaks 1 and 2 of the NHP catalysed samples have lamellar thickness values of about 1 nm more than the Lynx catalysed samples, while the largest differences from the previous samples for peaks 1 and 2 were at most 0.85 nm. If considering that both peaks 2 and 3 contribute to medium isotactic material, we can conclude that the NHP catalysed sample has more medium isotactic material, while the Lynx catalysed sample has more highly isotactic material, with the NHP catalysed sample having considerably thicker lamellar than that of the Lynx catalysed sample.

6.2.7 HT-^{13}C NMR spectroscopy

We will interpret the results from HT - ^{13}C NMR by investigating the presence of pentads in the methyl region of the obtained NMR spectra. There are ten possible pentads that can occur in the methyl region of the NMR spectra. [7] Of these ten pentads, one (mmmm) directly relates to the isotacticity of the sample, three (mmmr, mmrr, mrrm) are expected to occur due to catalyst errors and corrections, and six other pentads (rmmr, mmrm, rmrm, rmrr, mrrr, rrrr) will lead to the formation of atactic material if present. The manner in

which the peaks were assigned to pentads can be seen in Figure 6.13. [8] The pentads won't necessarily all be present in each NMR spectrum. This can be explained by taking into consideration that the samples being analysed are 90 and 100 °C TREF fractions. These higher temperature fractions inherently have fairly good crystallizability, and we can deduct that there won't be an abundance of stereodefects present within the samples. The non mmmm pentads will thus appear small on the spectrum due to the large presence of the mmmm peak. The percentage pentads for all samples were summarized in Section 8.7 on Page 151.

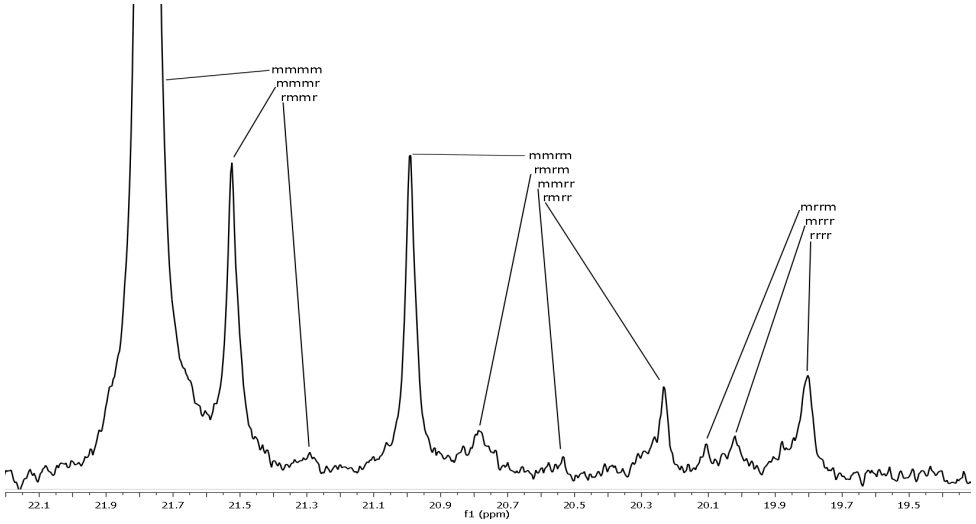

Figure 6.13: Assignment of pentads to NMR spectrum [8]

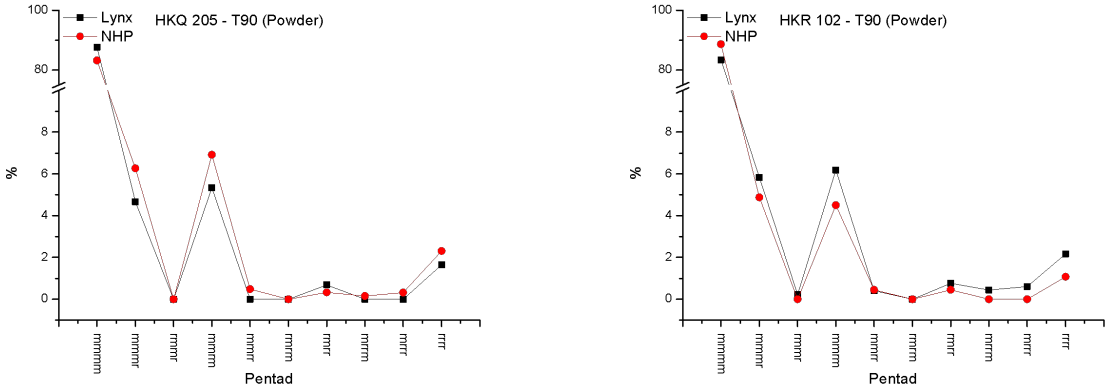

Figure 6.14: Percentage of pentads present on NMR spectra for HKQ 205 (left) and HKR 102 (right) 90 °C fractions

(**1** & **2**). From the pentad distributions in Section 8.7 and Figure 6.14 (left), we can see that the Lynx catalysed sample has higher istotacticity, lower values for the expected pentads, and generally lower values for the atactic pentads. All this information indicates that there are fewer stereo errors present in the Lynx catalysed sample overall, and importantly less atactic material. We would thus cautiously expect that the

Lynx catalysed sample (sample **1**) would have a higher percentage crystallinity when measured by DSC, which is what is observed experimentally. This argument can't be used as a definitive explanation for the differences in crystallinities, as the samples are in different physical states during analysis with DSC (solid state) and NMR (solution state).

(**3** & **4**). From the pentad distributions in Section 8.7 and Figure 6.14 (right), we can see that the Lynx catalysed sample has lower isotacticity, higher values for the expected pentads, and higher values for the atactic pentads. This is quite interesting as from these results we would expect that the NHP catalysed sample (sample 4) would have a higher percentage crystallinity, which is not what is found experimentally. This is a good example of why crystallinity shouldn't be predicted from the solution NMR results, as this result directly contradicts the prediction we would make.

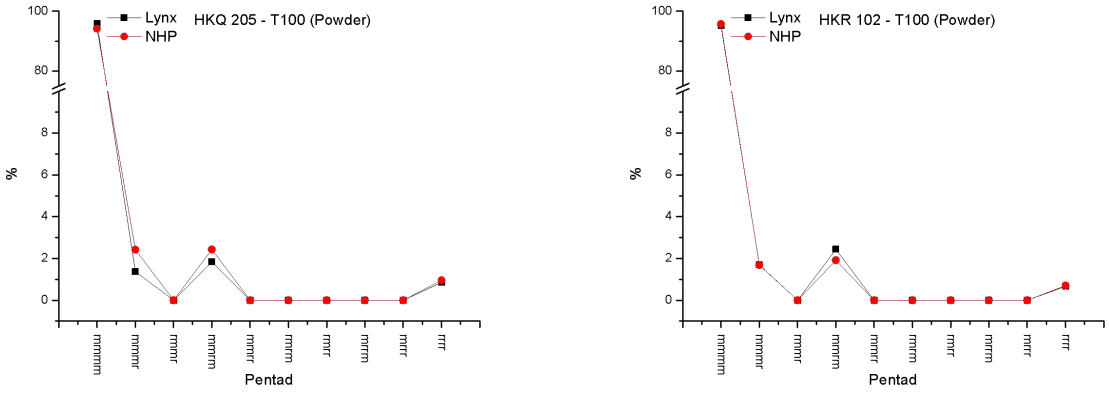

Figure 6.15: Percentage of pentads present on NMR spectra for HKQ 205 (left) and HKR 102 (right) 100 °C fractions

(**5** & **6**). From the pentad distributions in Section 8.7 and Figure 6.15 (left), we can see that the Lynx catalysed sample has higher isotacticity, lower values for the expected pentads, and lower values for the atactic pentads. All this information indicates that there are fewer stereo errors present in the Lynx catalysed sample overall, and importantly less atactic material. We would thus expect that the Lynx catalysed sample (sample **5**) would have a higher percentage crystallinity, which is what is observed experimentally.

(**7** & **8**). From the pentad distributions in Section 8.7 and Figure 6.15 (right), we can see that the two samples have very similar isotacticity, however, the NHP catalysed samples has slightly higher isotacticity, and a slightly lower presence of atactic pentads. There is also very little fine structure to work with as most of the pentads have zero presence in the spectrum. The differences that are observed are thus insignificant and no further deductions will be made.

6.2.8 Solid-state NMR spectroscopy

Solid-state nuclear magnetic resonance spectroscopy (solid-state NMR) was used in order to gain information regarding chain conformations in the solid state. [9] The solid-state techniques will focus on selectively observing both crystalline and amorphous regions of the polymers, to gain a better understanding of the dynamics associated with the molecules in the solid state. The first solid-state NMR experiment conducted was cross-polarization magic angle spinning (CPMAS), which is sensitive to the proton density and mobility of components within the sample. [9] CPMAS experiments were conducted on the 90 and 100 °C fractions of the powder samples of the HKQ 205 and HKR 102 grades, the results of which can be seen in Figures 6.16-6.17.

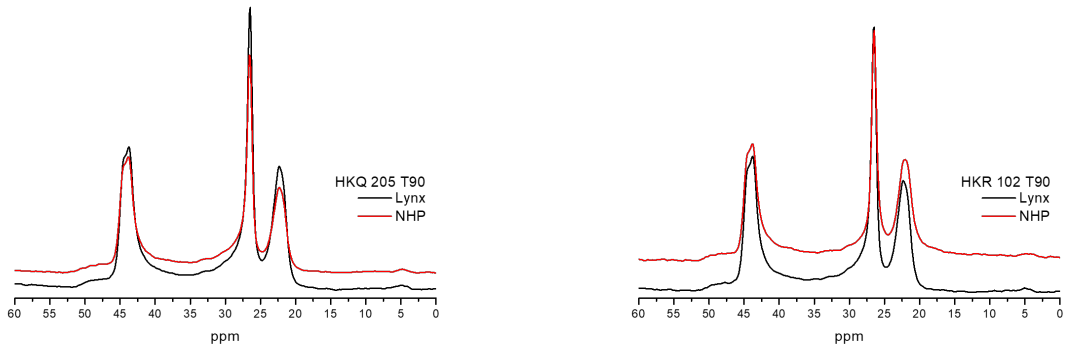

Figure 6.16: CPMAS results of HKQ 205 (left) and HKR 102 (rght) 90 °C fractions

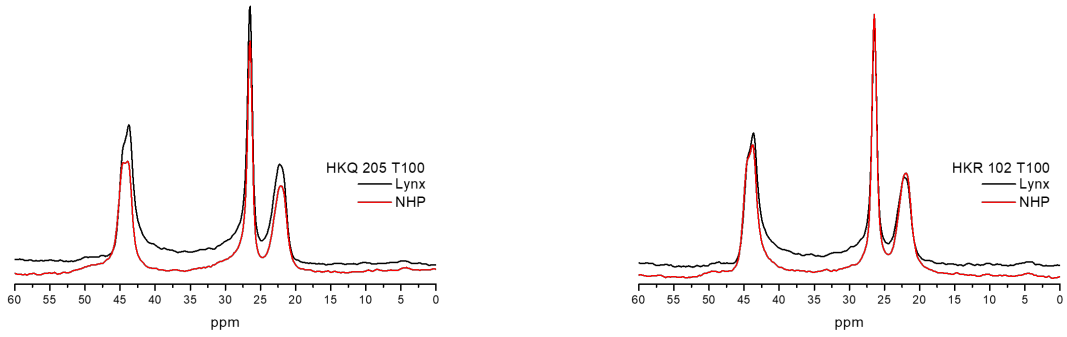

Figure 6.17: CPMAS results of HKQ 205 (left) and HKR 102 (rght) 100 °C fractions

The appearance of the peaks has been discussed previously when the solid-state NMR results of the bulk samples were discussed in Chapter 4. In the fractions we can see a much more pronounced splitting occurring in the methylene peak of the samples, especially for the NHP catalysed 100 °C fraction of the

HKQ 205 grade, compared to what we observed for the bulk samples. From literature we would expect the methylene peak to split as the methylene carbons exist in different environments, due to the 3_1 helix structure of the α allomorph of isotactic polypropylene. [10] These two peaks are expected to occur at 44.7 and 43.8 ppm respectively, representative of the ordered α phase. From a pure crystalline form, these two peaks should exist in a 2:1 ratio, however, might differ due to the presence of atactic sequences. [9] The α allomorph of isotactic polypropylene should be the single contributor to the methylene peak in order for us to have reliable data from the deconvolution of the methylene peak. [9] The XRD results from Section 6.2.5 shows that our samples do indeed exist as purely the α form. An example of how the methylene peak was deconvoluted was shown when the solid-state NMR results of the bulk samples were discussed in Chapter 4. The data obtained from the deconvolution of the methylene peaks, together with other relevant data from the CPMAS experiments can be seen in Table 6.12. Throughout the processing of the methylene peaks we used a Lorentz fit to deconvolute the methylene peak.

Table 6.12: Summarised CPMAS results of powder fractions

Sample	Chemical shift (ppm)			CH_2 Peak	
	CH_3	CH	CH_2	% Area	Ratio
HKQ 205 Lynx T90	22.33	26.50	44.43	27.50	2.64
			43.79	72.50	
HKQ 205 NHP T90	22.33	26.53	44.49	29.14	2.43
			43.88	70.86	
HKR 102 Lynx T90	22.33	26.51	44.50	27.93	2.58
			43.79	72.07	
HKR 102 NHP T90	22.08	26.48	44.50	26.43	2.78
			43.83	73.57	
HKQ 205 Lynx T100	22.28	26.51	44.54	28.67	2.49
			43.79	71.33	
HKQ 205 NHP T100	22.10	26.50	44.57	49.94	1.00
			43.94	50.06	
HKR 102 Lynx T100	22.16	26.44	44.43	26.60	2.76
			43.70	73.40	
HKR 102 NHP T100	21.94	26.46	44.52	35.03	1.58
			43.83	64.97	

For the deconvolutions of the fractions we see values for the split methylene peak much closer to what we would expect from literature, which is 44.7 and 43.8 ppm respectively. The ratios of these peaks, however, are nowhere near 2:1. It is observed that most of the ratios are somewhere around 2.5:1 except the 100 °C

NHP catalysed samples which are below 2:1. We can see that a good split exists for the NHP catalysed 100 °C fraction of the HKQ 205 grade, and we also observe that its ratio of peaks is 1:1.

We can conduct another experiment in solid-state NMR, which allows us to selectively visualise areas in our samples with higher mobility, which is called interruptive decoupling or dipolar dephasing. These experiments will further be referred to as IDREF experiments. These IDREF experiments make use of dipolar carbon-proton interactions, of which there is a faster decay in strongly coupled regions. These strongly coupled regions typically occur in areas of lower mobility, and thus we can observe the areas of higher mobility which have weaker dipolar interactions and slower decay times. The IDREF spectra obtained for the 90 and 100 °C fractions of the powder HKQ 205 and HKR 102 grades can be seen in Figures 6.18-6.19.

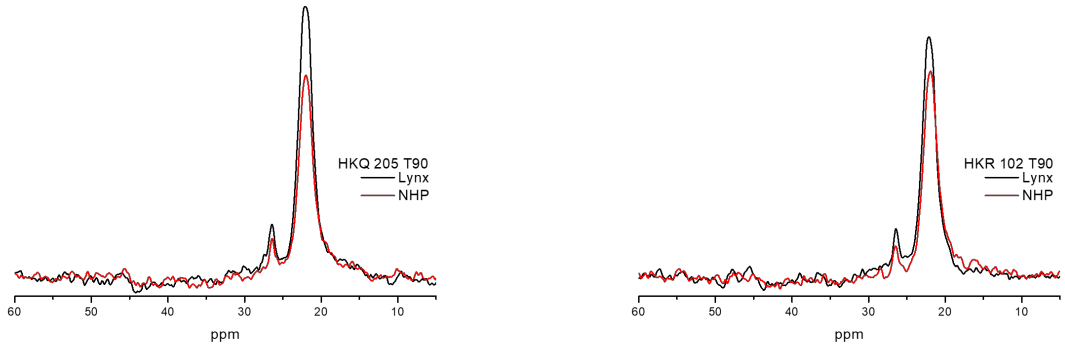

Figure 6.18: IDREF results of HKQ 205 (left) and HKR 102 (rght) 90 °C fractions

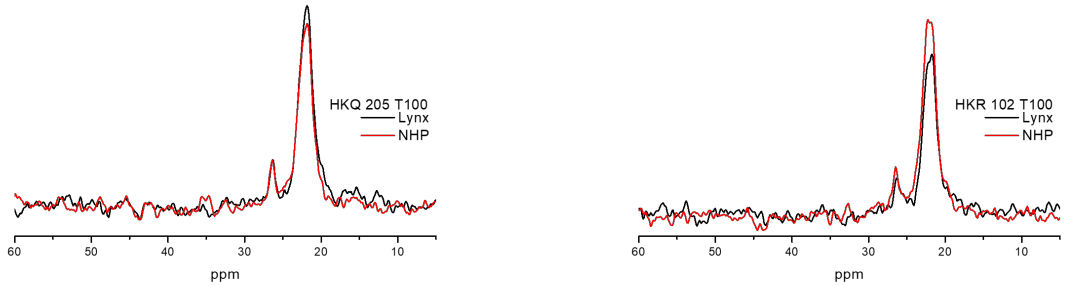

Figure 6.19: IDREF results of HKQ 205 (left) and HKR 102 (rght) 100 °C fractions

First, we can observe that the methylene peak isn't present at all on the IDREF spectra, and the methine

peak nearly completely disappeared. This is to be expected as the methylene and methine carbons form part of the polypropylene backbone and are expected to have low mobility. The methyl carbons are observed as a very pronounced peak, which is also expected due to it not being part of the backbone and will thus have inherent mobility. The most exciting result here is the presence of the methine peak which appears in the IDREF spectra. As it is part of the backbone of the polymer, we typically won't expect the methine peak to have mobility, but it seems they do experience some movement. These peaks in the IDREF spectra are enlarged, however, and for reference an overlay between a CPMAS and IDREF spectra of the same sample has been shown in Figure 6.20 to show the relative amounts of these groups present. From there we can see that the IDREF peaks are very small in comparison to the CPMAS peaks, which is indicative of the small amount of mobile components present within the sample. From Figure 6.20 we can see that there is in actuality a very low amount of mobile methine carbons present within the sample, which is more in line with what we would expect from carbons that form part of the backbone of the polymer.

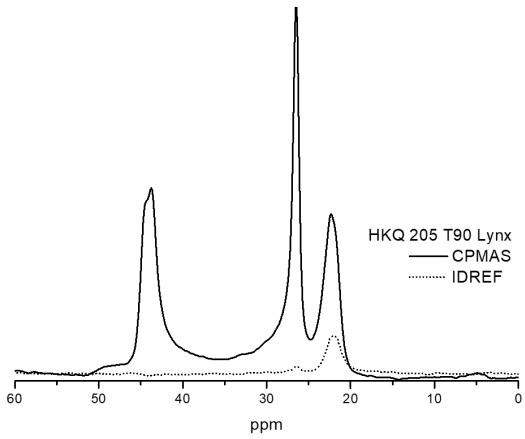

Figure 6.20: Comparison between CPMAS and IDREF spectra

6.3 Pellets

6.3.1 Background

Table 6.13: General results of HKQ 205 90 °C pellet samples

HKQ 205 powder - T90	Lynx (**1**)	NHP (**2**)
TREF weight fraction (%)	4.16	4.32
HT-SEC M_w (g/mol)	123887	128554
HT-SEC PDI	5.11	4.56
^{13}C NMR mmmm (%)	81.62	83.81

Table 6.14: General results of HKR 102 90 °C pellet samples

HKR 102 powder - T90	Lynx (**3**)	NHP (**4**)
TREF weight fraction (%)	3.25	4.44
HT-SEC M_w (g/mol)	88010	143313
HT-SEC PDI	5.07	5.03
^{13}C NMR mmmm (%)	80.89	82.17

Table 6.15: General results of HKQ 205 100 °C pellet samples

HKQ 205 powder - T100	Lynx (**5**)	NHP (**6**)
TREF weight fraction (%)	6.51	7.14
HT-SEC M_w (g/mol)	119472	134571
HT-SEC PDI	3.37	2.99
^{13}C NMR mmmm (%)	94.10	96.00

Table 6.16: General results of HKR 102 100 °C pellet samples

HKR 102 powder - T100	Lynx (**7**)	NHP (**8**)
TREF weight fraction (%)	5.77	7.28
HT-SEC M_w (g/mol)	103061	137638
HT-SEC PDI	2.92	2.91
^{13}C NMR mmmm (%)	94.64	95.25

From the results in Tables 6.13-6.16, we can see a summary of some basic analyses that were done on the samples, including the weight percentage calculated from TREF, the weight average molar mass and dispersity calculated from SEC, as well as the percentage isotacticity calculated from ^{13}C NMR. Firstly, we can see that the isotacticity of the NHP catalysed samples are consistently slightly higher than that of the Lynx catalysed samples. These differences are relatively small and are never significantly more than 2 %. The weight average molar mass (M_w) is significantly higher for the NHP catalysed samples in all cases except for the HKQ 205 90 °C samples, where a similar molar mass is observed. The dispersity of the NHP catalysed samples are lower for the HKQ 205 grade, as would be expected due to the NHP catalysed samples having higher molar mass. The dispersities for the HKR 102 grade are essentially identical, a strange result considering the vast difference in molecular weights of the NHP and Lynx catalysed samples. The NHP catalysed sample also makes up a larger weight percentage of the entire sample in all cases as determined from TREF elution, indicating that a larger amount of the dissolved NHP catalysed samples will crystallize in solution at these temperatures.

As we saw with the powder samples, we can draw some similar initial conclusions from these results. The polymers that are compared here are all fractions of a bulk polymer samples, which was fractionated according to crystallizability. We see, however, that even though these samples that elute at the same temperature (and thus have similar crystallizabilities), they have different properties with respect to isotacticity and molar mass. This is a clear indication that the samples have different chemical compositions and is solely due to the effect that the catalyst has on the samples.

6.3.2 DSC

The DSC thermograms of the 8 pellet samples investigated can be seen in Figure 6.21, while some selected results from DSC analysis have been summarized in Tables 6.17-6.20.

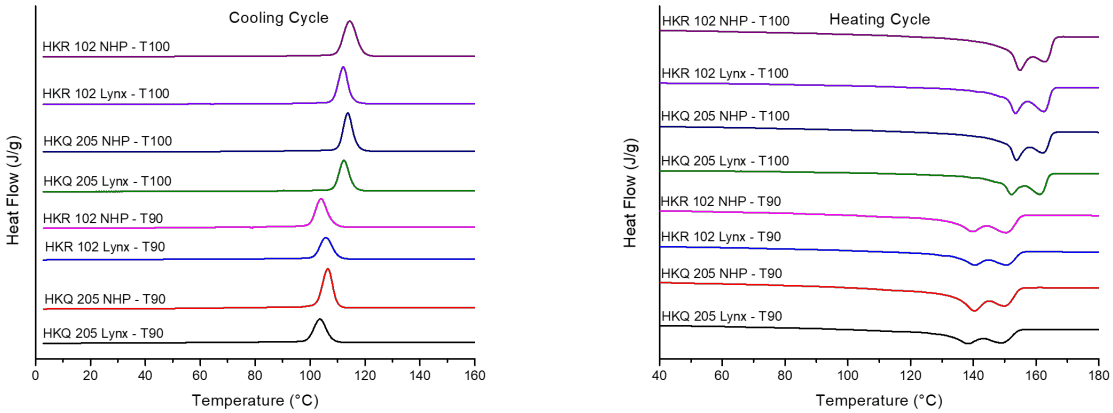

Figure 6.21: DSC cooling (left) and heating (right) curves of 8 pellet fractions investigated

The eight samples investigated here were chosen partly due to them all having a double melting event as can be seen in Figure 6.21 (right). It was discussed in Chapter 4 that these events occur due to molecular segregation within the sample, [1] and it was thus thought to be of significance to investigate the relative sizes of each of these peaks. These double melting endotherms, however, don't follow the same trend that was observed for the powder samples discussed earlier in Section 6.2.2. Here we see that the Lynx catalysed 100 °C fractions have peaks that are more similar in size, while the NHP catalysed 100 °C fractions have a small difference in peak size. The 90 °C fractions have, as for the powder samples, similar sizes throughout these investigated samples. We can thus clearly see that the Lynx and NHP catalysts produce polymer samples with different thermal properties simply from looking at the melting endotherms of the 100 °C fractions of the HKQ 205 and HKR 102 grades.

Table 6.17: DSC results of HKQ 205 90 °C pellet samples

HKQ 205 pellet - T90	Lynx (**1**)	NHP (**2**)
Crystallinity (%)	25.01	36.15
Crystallization temp (°C)	103.52	106.49
Melting temp (°C)	138.54	1140.44
	149.61	150.37

Table 6.18: DSC results of HKR 102 90 °C pellet samples

HKR 102 pellet - T90	Lynx (**3**)	NHP (**4**)
Crystallinity (%)	23.83	29.75
Crystallization temp (°C)	105.78	103.98
Melting temp (°C)	140.48	139.49
	150.91	150.45

Table 6.19: DSC results of HKQ 205 100 °C pellet samples

HKQ 205 pellet - T100	Lynx (**1**)	NHP (**2**)
Crystallinity (%)	29.40	34.62
Crystallization temp (°C)	112.30	113.76
Melting temp (°C)	152.16	153.76
	161.60	162.50

Table 6.20: DSC results of HKR 102 100 °C pellet samples

HKR 102 pellet - T100	Lynx (**3**)	NHP (**4**)
Crystallinity (%)	33.92	41.96
Crystallization temp (°C)	112.09	114.44
Melting temp (°C)	153.27	154.84
	162.44	163.09

We can see from these results that the NHP catalysed samples have higher percentage crystallinity compared to the Lynx catalysed samples. We can also observe that the crystallization temperature (T_c) and melting temperature (T_m) of both peaks in the melting endotherm are generally higher for the NHP catalysed samples, except in the case of the HKR 102 90 °C samples, where the values are fairly similar. These higher T_c and T_m values indicate that the NHP catalysed samples generally crystallize stronger than the Lynx catalysed samples. [2] We will further investigate these samples by looking at the results of some other analytical techniques.

6.3.3 HT-SEC

The HT-SEC curves of the 8 pellet samples investigated can be seen in Figure 6.22 with some key results previously summarized in Tables 6.13-6.16. These results will be discussed shortly as they have been summarized previously in Section 6.3.1.

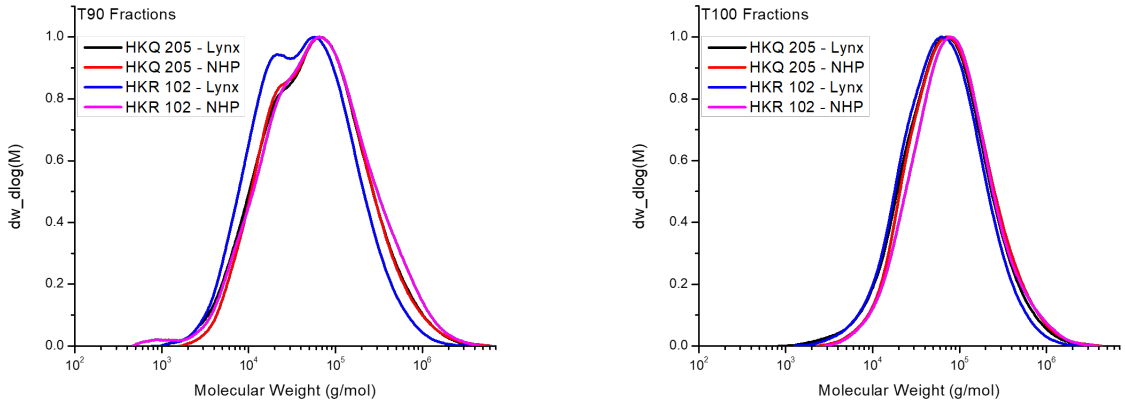

Figure 6.22: HT-SEC chromatograms of the 90 °C fractions (left) and 100 °C fractions (right)

These results are more similar than what we observed for the powder samples discussed in Section 6.2. We see that all the 90 °C fractions have a bimodal distribution. For the HKQ 205 grade the NHP catalysed sample has lower dispersity, while the HKR 102 grade samples have similar dispersities. The NHP catalysed sample generally has higher molar mass. For the 100 °C fractions we see very similar curves in terms of broadness and molar mass. The NHP catalysed sample has a narrower dispersity for the HKQ 205 grade, however, and the HKR 102 grade dispersities are again similar. The NHP catalysed samples have slightly higher molar mass. The differences between samples using different catalysts are less clear visually for the pellets, however, the tabulated values still show a clear difference as for the powder samples.

6.3.4 FTIR

The reason for the use of FTIR and the manner in which the results will be explained has been discussed previously in Section 6.2.4 on Page 82. We will thus use this section only to observe and discuss the results obtained from this analysis technique.

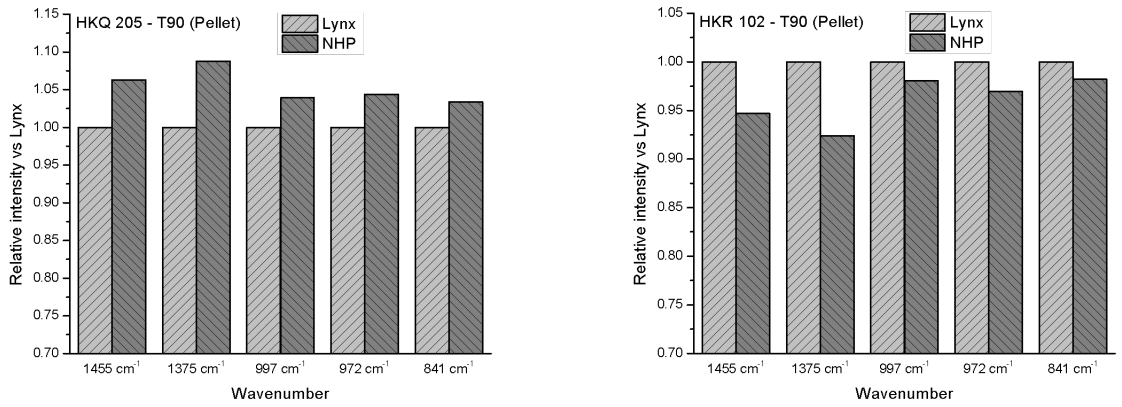

Figure 6.23: Comparison of FTIR peak intensities of the 90 °C HKQ 205 (left) and HKR 102 (right) fractions

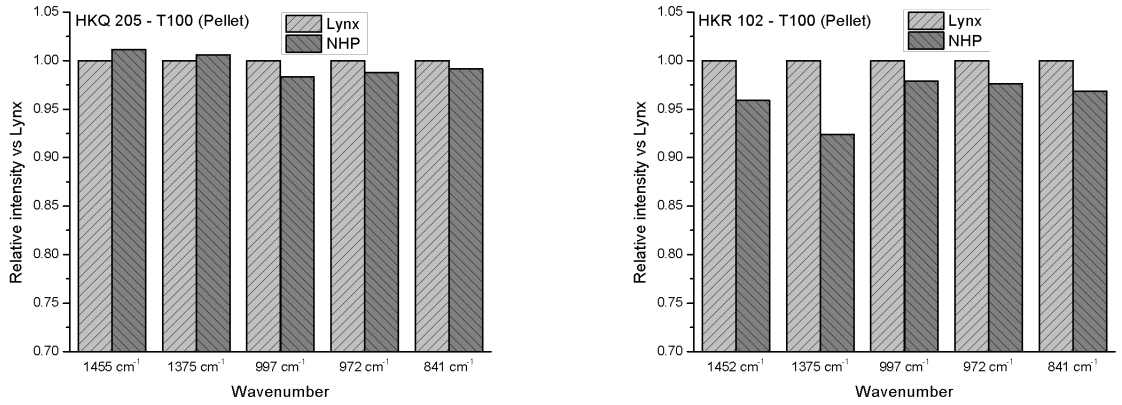

Figure 6.24: Comparison of FTIR peak intensities of the 100 °C HKQ 205 (left) and HKR 102 (right) fractions

Table 6.21: Comparison of FTIR results of NHP catalysed pellet samples relative to Lynx catalysed samples

Samples		Overall Intensity	Content of helical sequence	Distribution of stereodefects
1 vs **2**	HKQ 205 T90 NHP	Higher	Higher	Less uniform
3 vs **4**	HKR 102 T90 NHP	Lower	Lower	More uniform
5 vs **6**	HKQ 205 T100 NHP	Similar	Similar	Similar
7 vs **8**	HKR 102 T90 NHP	Lower	Lower	More uniform

The results obtained from the FTIR graphs in Figures 6.23-6.24, were summarized in Table 6.21. We know that regularity bands at 1220, 840, 998 and 973 cm^{-1} have helical structures with a decreasing degree of order and have minimum n values (critical helix length) of 14, 12, 10 and 5 monomer units respectively. We could thus calculate the relative intensity of helical structures of these orders between the Lynx and NHP

catalysed samples. [3,4] We see from Table 6.21 that the intensities and subsequent properties related to the intensities, differ between temperature fractions of the same polymer grade, and also between different grades of the same temperature fraction. The sole consistent result is that the intensity of the NHP catalysed sample regularity bands are lower for the HKR 102 grade compared to the Lynx catalysed samples. There are no clear conclusions that can be drawn from these results, and thus no information is obtained regarding the effect that the catalyst has on the helical lengths of these samples.

6.3.5 WAXD

Some background on WAXD and the manner in which the results will be explained have been discussed previously in Section 6.2.5 on Page 84. This section will thus be used only for the observation and discussion of the actual results obtained from this analysis technique.

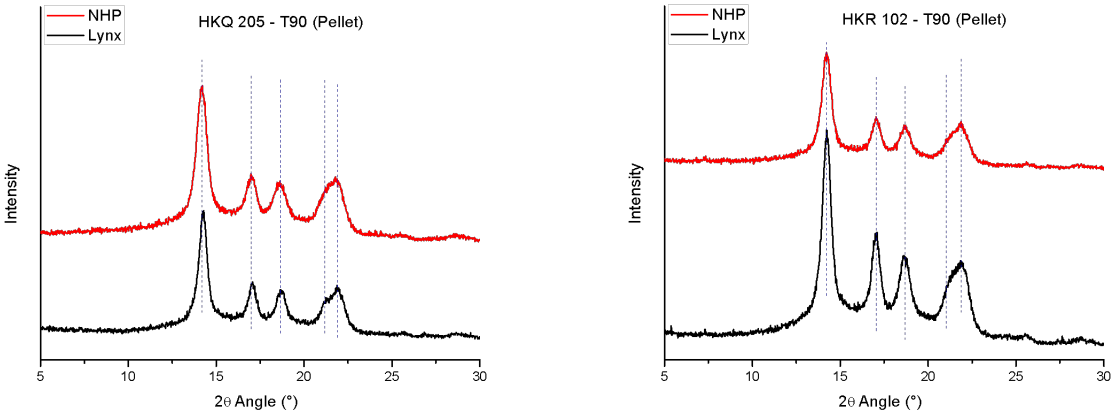

Figure 6.25: XRD diffractograms of the 90 °C HKQ 205 (left) and HKR 102 (right) fractions

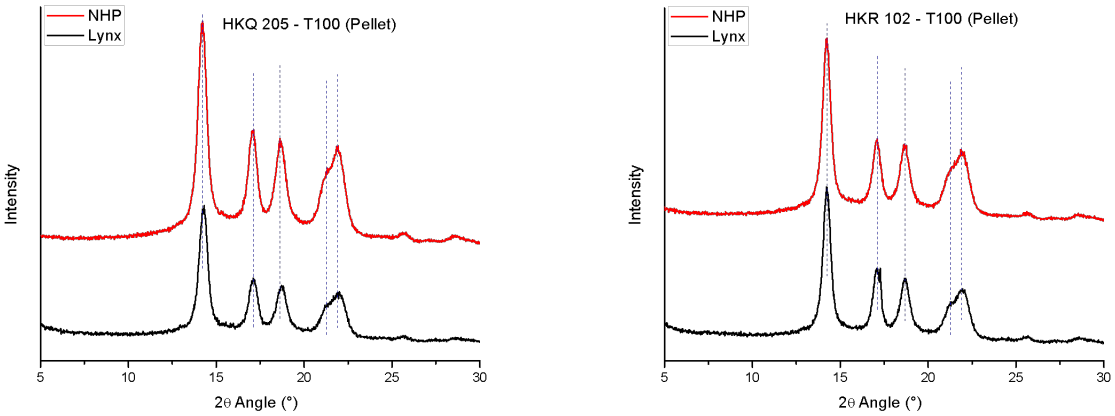

Figure 6.26: XRD diffractograms of the 100 °C HKQ 205 (left) and HKR 102 (right) fractions

From the XRD data tabulated in Section 8.5 and by visually investigating Figures 6.25 & 6.26 it is clear to see that the peaks of all the compared samples occur at roughly the same 2α angles. This isn't unexpected and from this result we can conclude that all the samples analysed have an α-monoclinic crystal structure due to the presence of peaks at 2α angles of about 14.3, 17.1, 18.5, 21.2 and 21.9 ° corresponding to the α(110), α(040), α(130), α(111) and α(-131) peaks respectively. [3,5] There are some slight variations in the calculated crystallite size L of each crystal face, however, these differences are not significant. The crystal spacing d were identical when looking only at two decimal figures and is also not significant. It can also be seen that the peaks of the 100 °C samples are much narrower than that of the 90 °C samples, which relates to the higher crystallinity of the 100 °C samples.

6.3.6 SSA

Some background on SSA and the manner in which the results will be explained have been discussed previously in Section 6.2.6 on Page 86. This section will thus be used only for the observation and discussion of the actual results obtained from the successive self-nucleation and annealing experiments.

The final melting endotherms of the 90 °C samples have been shown in Figures 6.27 & 6.28 (left). These endotherms were deconvoluted in order to obtain qualitative information on the relative percentage areas for both samples, after which these percentage areas were plotted and can be seen in Figures 6.27 & 6.28 (right). An example of how the final melting endotherms of the 90 °C samples were deconvoluted was shown previously and can be seen in Figure 6.9 on Page 88.

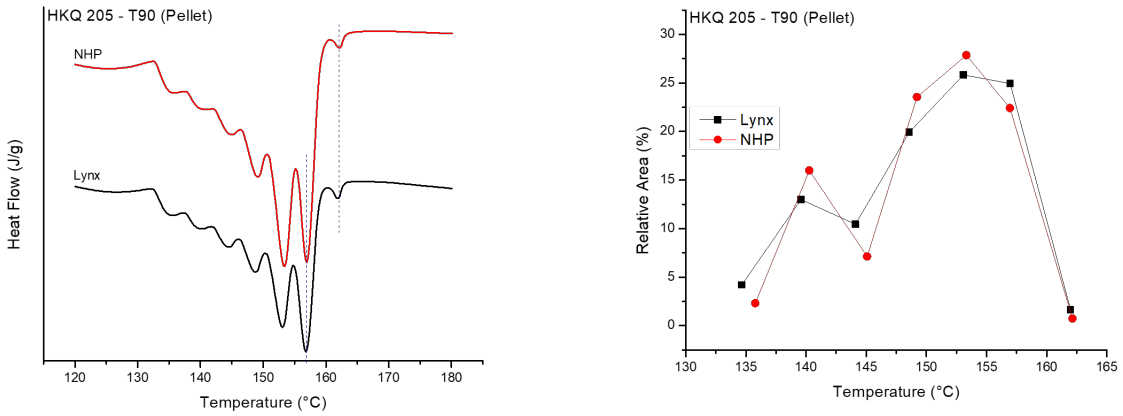

Figure 6.27: Final melting endotherm (left) and area comparison (right) of 90 °C HKQ 205 fractions

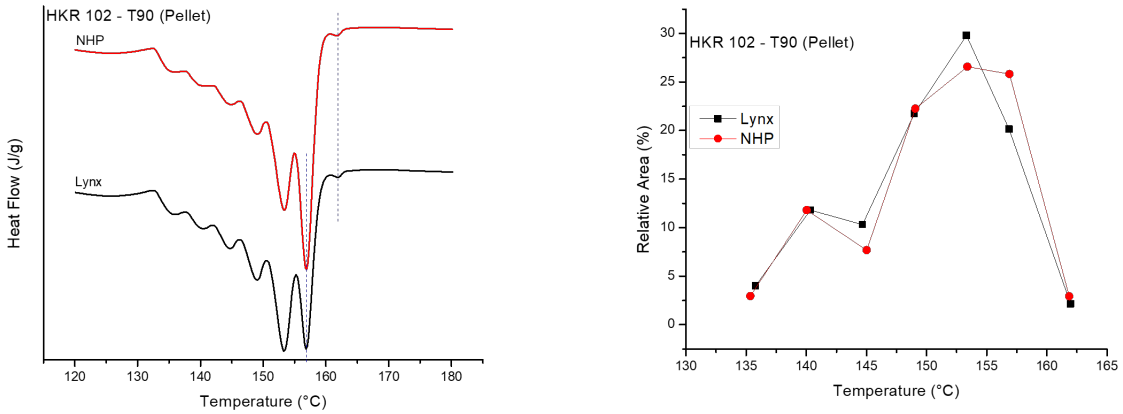

Figure 6.28: Final melting endotherm (left) and area comparison (right) of 90 °C HKR 102 fractions

(**1** & **2**). We can see from Figure 6.27 (left) that both samples have similar curves, however, the position and size of the peaks differ slightly relative to each other. We see from Figure 6.27 (right) that the relative percentages for the Lynx and NHP catalysed samples are all similar, however, the NHP catalysed sample has a slightly lower percentage area for peak 1 and thus has less highly isotactic material. If peaks 2 and 3 are added together it can be concluded that samples **1** and **2** have a similar amount of medium isotacticity. When investigating the lamellar thickness of samples **1** and **2** in Section 8.6, it can be seen that the lamellar thickness of the NHP catalysed sample (**2**), is consistently slightly higher than the Lynx catalysed sample (sample **1**). This is confirmed when observing that the melting temperature for each peak of sample **2** is slightly higher than the corresponding peaks in sample **1**. We can thus conclude that sample **2** has slightly less highly isotactic areas, similar medium isotactic areas, but the lamellar thickness of those areas are greater, albeit slightly, for the NHP catalysed samples compared to the Lynx catalysed sample.

(**3** & **4**). We again see from Figure 6.28 (left) that the relative sizes of peaks 1 and 2 are similar for the two samples, however we see that the peak which would be peak 3, is different relative to peak 2 for the two samples. We see from Figure 6.28 (right) that the areas of peaks 2 and 3 are again similar for both samples and there is thus a similar amount of medium isotactic material within each sample. The areas for peak 1 are also similar and indicate that the two samples have similar amounts of highly isotactic material.
When we look at the lamellar thickness of the samples found in Section 8.6, we observe that the lamellar thickness of the samples are very similar, with no clear differences between the values. This is confirmed by observing that the melting temperature of the same peaks for both samples very similar.

The final melting endotherms of the 100 °C samples have been shown in Figures 6.29 & 6.30 (left). These endotherms were deconvoluted in order to obtain quantitative information on the relative percentage areas for both samples, after which these percentage areas were plotted and can be seen in Figures 6.29 & 6.30 (right). An example of how the final melting endotherms of the 100 °C samples were deconvoluted was shown previously and can be seen in Figure 6.12 on Page 89.

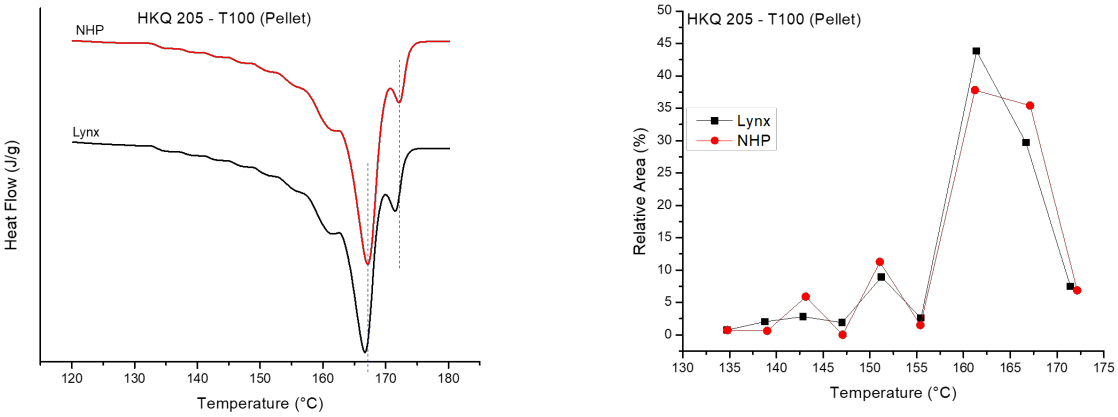

Figure 6.29: Final melting endotherm (left) and area comparison (right) of 100 °C HKQ 205 fractions

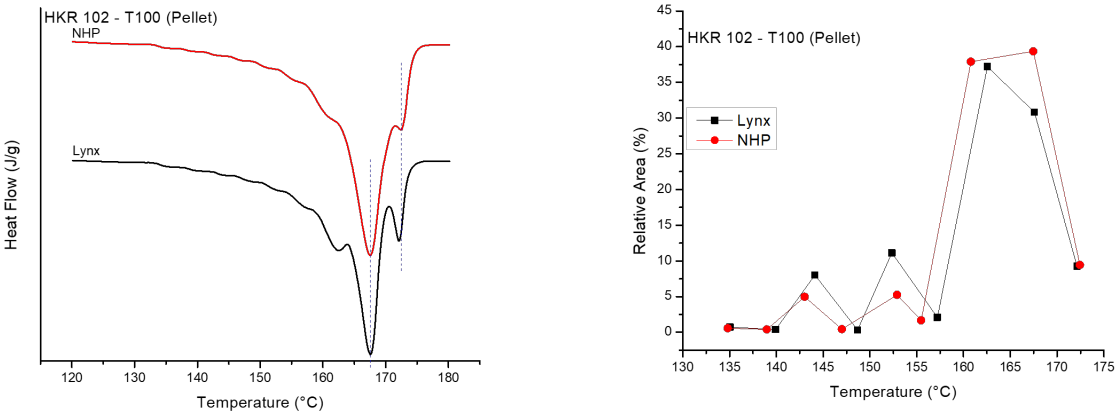

Figure 6.30: Final melting endotherm (left) and area comparison (right) of 100 °C HKR 102 fractions

(**5** & **6**). We can see from Figure 6.29 (left) that the relative sizes of peaks 1 and 2 of the Lynx and NHP catalysed samples are fairly similar. Investigating the relative percentage areas from Figure 6.29 (right) for both samples **5** and **6** we see a different trend than what was observed for samples 1 and 2. We do see that the six lowest temperature peaks have very similar percentage areas. We also see that the two samples have essentially the same area for peak 1, however, peak 2 of the NHP catalysed sample is much larger than the Lynx catalysed sample. For the HKQ 205 90 °C samples (**1** and **2**), we observed that the NHP catalysed sample had a slightly smaller peak 2 area. Adding the areas for peaks 2 and 3 again shows us that the samples have similar amounts of medium isotactic material present.

When investigating the lamellar thickness of samples **5** and **6** found in Section 8.6, we see that the lamellar thickness of the 7 lowest temperature peaks are very similar for both samples **5** and **6**, however, the NHP catalysed samples have thicker lamellar for peaks 1 and 2. This is confirmed when observing that the melting temperature for peaks 1 and 2 is higher for sample **6** than for sample **5**. We can thus conclude that

sample **5** and **6** have similar percentages of high isotactic and medium isotactic material, with the NHP catalysed sample having slightly thicker lamellae in the highly and medium isotactic areas of the sample.

(**7** & **8**). From Figure 6.30 (left) it seems as if peak 1 of the Lynx catalysed sample is much larger relative to peak 2 than the relative sizes of peaks 1 and 2 of the NHP catalysed sample. This isn't exactly the case, however, as the deconvoluted curves show that samples **7** and **8** have very similar percentage areas for peak 1. Peak 2 of the NHP catalysed sample is in fact much larger relative to peak 2 of the Lynx catalysed sample, which gives rise to the observed anomaly. From this information we can say that the NHP catalysed sample has more medium isotactic material, and similar high isotactic material compared to the Lynx catalysed sample. We can now look at the lamellar thickness of samples **7** and **8**, the values of which are given in Section 8.6. It is observed that generally the Lynx catalysed sample has thicker lamellae, however, importantly peak 1 of the NHP catalysed sample has a larger lamellar thickness than that of the Lynx catalysed sample. These results can also be observed by investigating the melting points of each peak of the final melting endotherm. We thus make the conclusion that samples 7 and 8 have similar amounts of highly isotactic material, with sample **8** having slightly thicker lamellae in the highly isotactic regions.

6.3.7 HT-^{13}C NMR

Some background on NMR and the manner in which the results will be explained have been discussed previously in Section 6.2.7 on Page 90. This section will thus be used only for the observation and discussion of the actual results obtained from NMR spectroscopy.

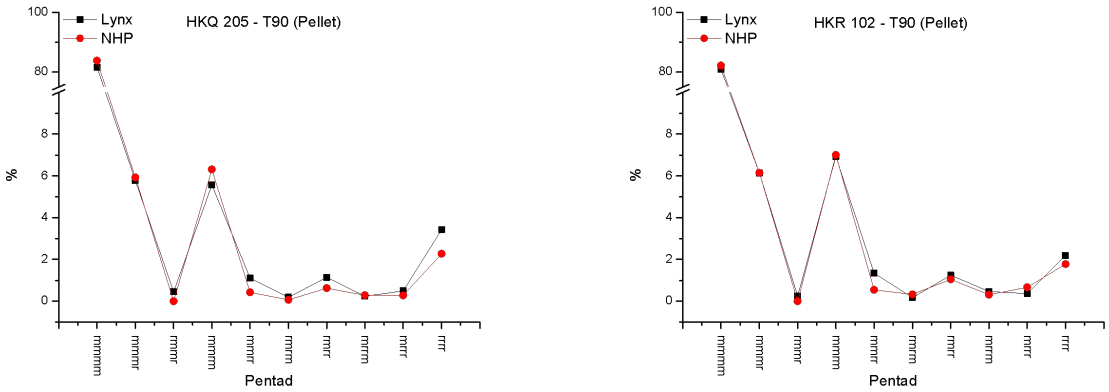

Figure 6.31: Percentage of pentads present on NMR spectra for HKQ 205 (left) and HKR 102 (right) 90 °C fractions

(**1** & **2**). From the pentad distributions in Section 8.7 and Figure 6.31 (left), we can see that the NHP

catalysed sample has higher istotacticity, similar values for the expected pentads, and generally lower values for the atactic pentads. All this information indicates that there are fewer stereo errors present in the NHP catalysed sample overall and importantly, less atactic material. We would thus cautiously expect that the NHP catalysed sample (sample **2**) would have a higher percentage crystallinity, which is what we observed experimentally. This argument cant be used as a definitive explanation for the differences in crystallinities, as the samples are in different physical states during analysis with DSC (solid state) and NMR (solution state).

(**3** & **4**). From the pentad distributions in Section 8.7 and Figure 6.31 (right), we can see that the NHP catalysed sample has higher istotacticity, similar values for the expected pentads, and generally lower values for the atactic pentads. All this information indicates that there are fewer stereo errors present in the NHP catalysed sample overall and importantly, less atactic material. We could thus again predict that the NHP catalysed sample (sample **4**) would have a higher percentage crystallinity, which is what was found experimentally.

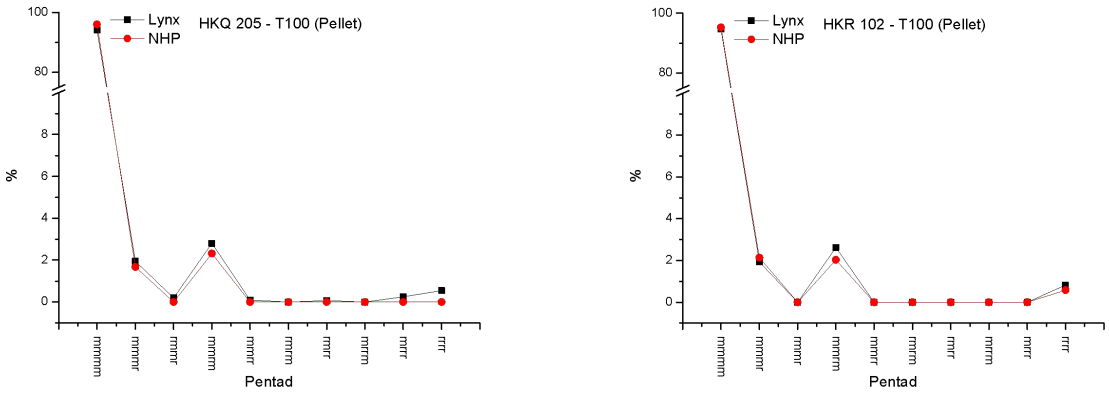

Figure 6.32: Percentage of pentads present on NMR spectra for HKQ 205 (left) and HKR 102 (right) 100 °C fractions

(**5** & **6**). From the pentad distributions in Section 8.7 and Figure 6.32, we can see that the NHP catalysed sample has higher istotacticity, lower values for the expected pentads, and lower values for the atactic pentads. All this information indicates that there are fewer stereo errors present in the NHP catalysed sample overall and importantly, less atactic material. We would thus expect that the NHP catalysed sample (sample **6**) would have a higher percentage crystallinity, which is what was found experimentally.

(**7** & **8**). From the pentad distributions in Section 8.7 and Figure 6.32, we can see that the two samples have similar isotacticity, with the NHP catalysed sample having higher values for the expected pentads, and

lower values for the atactic pentads. There is not enough fine structure on the spectrum to investigate these samples thoroughly, as most of the pentads have zero presence in the spectrum. The differences that are observed are thus insignificant and no further deductions will be made.

The 100 °C fractions have much less fine material in their respective spectra, and caution should be exercised when relaying amounts of pentads present. Throughout these results several predictions were made regarding the crystallinities of the samples simply based on the presence of stereodefects within the samples. This should be done with caution, as it has been mentioned before that a direct correlation can't be drawn based simply on these results, as crystallinity is measured by DSC in the solid state while NMR analysis is conducted in the solution state.

6.4 Summary

The samples that were compared directly in this study were identical except for the catalyst used during polymerization, allowing us to investigate the effect that the catalyst (Lynx vs NHP) has on the fundamental properties of our isotactic polypropylene samples. The thermal histories of the samples are identical, as they were all fractionated using TREF, and like temperature fractions were compared to each other. These samples could then be defined as having similar crystallizabilities due to the fractionation mechanism of the TREF technique, however, we see that these samples have noticeably different properties despite their similar crystallizability. Using the full analytical toolbox that was at our disposal, we could determine that there are clear differences in the polymer samples catalysed with two different catalysts, as was discussed throughout this chapter.

6.5 References

1. Zhu, X. & Yan, D. In situ FTIR spectroscopy study on the crystallization process of isotactic polypropylene in isotactic polypropylene/polyethylene-glycol blends. *Macromol. Chem. Phys* **202**, 11091113 (2001).

2. Kang, J., Yang, F., Wu, T., Li, H., Liu, D., Cao, Y. & Xiang, M. Investigation of the Stereodefect Distribution and Conformational Behavior of Isotactic Polypropylene Polymerized with Different ZieglerNatta Catalysts. *Polym. Polym. Compos.* **12** 30763083 (2012).

3. Kang, J., Chen, J., Cao, Y. & Li, H. Effects of ultrasound on the conformation and crystallization behavior of isotactic polypropylene and -isotactic polypropylene. *Polymer (Guildf)*. **51**, 249256 (2010).

4. Zhu, X., Yan, D. & Fang, Y. In Situ FTIR Spectroscopic Study of the Conformational Change of Isotactic Polypropylene during the Crystallization Process. *J. Phys. Chem. B* **105**, 1246112463 (2001).

5. Somani, R. H., Yang, L. & Hsiao, B.S. Shear-induced precursor structures in isotactic polypropylene melt by in-situ rheo-SAXS and rheo-WAXD studies. *Macromolecules* **35**, 90969104 (2002).

6. Muller, a J., Hernandez, Z. H., Arnal, M. L. & Sanchez, J. J. A novel technique to study molecular segregation during crystallization. *Polym. Bull.* **472**, 465472 (1997).

7. Randall, J. C. & Petroleum, P. Distribution of Monomer Configurations in Polypropylene as Determined with 13C NMR. *J. Polym. Sci.* **12**, 703712 (1974).

8. Inoue, Y., Nishioka, A. & Chujo, R. Carbon-13 Nuclear Magnetic Resonance Spectroscopy of Polypropylene. *Die Makromol. Chemie* **152**, 1526 (1972).

9. Botha, L. The effect of in-process ethylene incorporation on the evolution of particle morphology and molecular characteristics of commercial heterophasic ethylene propylene copolymers (HEPCs). (Stellenbosch University, 2014). doi:10.1016/j.eurpolymj.2013.04.020

10. Comotti, A., Simonutti, R., Bracco, S., Castellani, L. & Sozzani, P. Simultaneous crystallization of isotactic and syndiotactic sequences of polypropylene. *Macromolecules* **34**, 48794885 (2001).

Chapter 7

Conclusions

This chapter will summarize the observations made from Chapters 4 through 6 and conclude the entire project. Some further recommendations for this study, as well as some suggestions for future work based on this project is mentioned.

7.1 Summary

The main goal of this project was to investigate a set of isotactic polypropylene samples, which will be used as a baseline in the future for further projects. These polypropylene samples were made with two different catalysts, and these catalysts were compared throughout the study with regards to the effect on the end properties of the polymer samples. This problem statement is the basis against which the conclusions reached in this project will be made.

7.2 Conclusions

The study was divided into three parts. These were, first, the fractionation, analysis and characterization of the bulk polymer samples; second, the analysis and characterization of the fractionated polymer samples; and finally, the detailed analysis and characterization of identified key areas. Each of these three parts were investigated at length and completed.

The TREF fractionation of the bulk polymer samples revealed some important basic information. It showed us that while all of the 20 bulk samples investigated have a similar trend in their crystallizabilities, they still have noticeable differences between samples of different form as well as between samples of different catalysts. It was found that the large majority of polymer crystallizes at high temperatures (110 and 140 °C), and it is in this region that the differences between the samples were mostly observed. Further analyses were done on these bulk samples using techniques such as CRYSTAF, FTIR, DSC, HT-SEC and solid-state NMR. CRYSTAF specifically gave some insightful results as it was observed that the smaller crystallization events surrounding the main crystallization event in solution varied as the form of the polymer and catalyst used were varied. An attempt was made at setting up a protocol for quick analysis by FTIR to relay basic spectra back to more detailed insights, however, was unsuccessful. DSC and HT-SEC both showed results that seemed if they were similar, however, upon further investigation it was found that some important differences were present. The DSC melting endotherms showed some significant differences, in that the powder samples displayed a double melting event. The relative sizes of these two melting events were then investigated, and it was found that the catalyst used may influence these melting events. HT-SEC clearly showed that the NHP catalysed samples had a higher molar mass relative to the Lynx catalyst samples. It was also observed from HT-SEC that the dispersities of the samples never differed significantly across all grades of all samples. Finally, solid-state NMR analysis of the bulk powder samples of the HKQ 205 and HKR 102 grades showed enough proof for us to continue with solid-state NMR of the fractionated samples to gain further insights into the effect that the catalyst has on the molecular properties of the

polymer samples.

The 20 bulk samples were fractionated into seven fractions each using TREF, which led to a total of 140 fractions. Due to the large number of these fractions it was impossible to do comprehensive analysis on all of them. It was thus clear that only basic analysis could be done on these fractions, which included FTIR, DSC, HT-SEC and SEM. The FTIR results showed no noteworthy results, and thus were not included in the main body of the thesis. The DSC and HT-SEC results, however, gave some more noteworthy results which could be investigated. From DSC it was found that across all of the bulk samples, the 90 and 100 °C fractions showed double melting endotherms. This was noteworthy because it was found that the powdered bulk samples showed these double melting endotherms, however, in the fractions these double melting events were present for both the as-is reactor powder as well as the extruded pellet samples. The relative sizes of these two melting peaks were then investigated as they were for the original bulk samples, and it was found that the catalyst used during polymerization may influence the relative size of each of the peaks. This was insightful because these two melting peaks are present due to molecular segregation within the fraction which leads to the crystallization of different size crystals during the cooling cycle during analysis. We could then determine that the catalyst used during polymerization may influence the amounts of these segments within a polymer sample. HT-SEC results generally showed a similar trend in all samples. In each case the samples would move from a low molar mass, high dispersity fraction (30 °C amorphous fraction) to the high molar mass, low dispersity fractions (110 and 140 °C fractions). These trends never changed, however, some specific fractions showed some variations. Finally, the SEM results of the powder samples showed that samples catalysed by the Lynx and NHP catalysts have definite differences in structural morphologies. It was observed that the Lynx catalysed powder sample surfaces has a less smooth surface, albeit more consistent, as individual polypropylene particles packed together to form a 'bumpy' surface. The NHP catalysed samples had a smoother surface overall, however, had individual polypropylene particles that were scattered on the surface of the polymer. Both Lynx and NHP catalysed samples showed the presence of micro- and macro pores within the samples.

For the third part of the project, we investigated a small set of specific fractions in great detail, to allow us to set up a final conclusion from the study and pave the way for future work. It was decided to continue further with only sixteen fractions, due to practical reasons, and these fractions consisted of eight powder and eight pellet samples. The powder samples have enjoyed attention throughout the study due to it being the purest form of the polymer as it comes from production. The pelletized form is mixed with stabilizers and pelletized, and thus processing may affect the final properties of these polymer samples. Each set of eight samples consisted of the 90 and 100 °C fractions of both Lynx and NHP catalysed samples of the HKQ 205 and HKR 102 grades. These samples were analysed not only by DSC, HT-SEC and FTIR, but also by XRD,

SSA, solution- and solid-state ^{13}C NMR.

Throughout both the powder and the pellet samples it was found that the NHP catalysed samples made up a larger weight fraction of the entire sample determined by TREF, compared to the Lynx catalysed samples. FTIR was used to determine the content of helical sequences, however, no significant results could be deduced from the FTIR spectra as the results varied greatly between samples. The double melting endotherms were investigated from the DSC thermograms and it was found that the catalyst used during production has some effect on the relative contents of molar masses within the 90 and 100 °C fractions. This was concluded following investigation of the relative peak sizes of the double melting event within the endotherm. From HT-SEC we concluded that the NHP catalysed samples generally had higher molar mass, while dispersity varied between powder and pellet samples, meaning no set trend could be identified. XRD analysis confirmed that all the samples investigated consisted purely of the α allomorph of isotactic polypropylene, as no presence of any β or γ material was found within the diffractograms. This was irrespective of the catalyst used during production. This was important for the solid-state NMR discussions of the powder samples. Crystallite size and d-spacing were calculated from the diffractograms, however, were found to be insignificant as little to no differences were observed. SSA analysis showed that the 90 °C fractions nucleated into seven different crystal sizes during analysis, while the 100 °C fractions nucleated into nine different crystal sizes. Given that both the 90 and 100 °C fractions were analysed using the same temperature profile, we can deduce that TREF fractionation does indeed differentiate between crystallizabilities, which in turn is dependent on varying molar masses, dispersities and stereodefects presence and distribution thereof. It was further found from SSA that the NHP catalysed samples consistently have slightly thicker lamellae compared to the Lynx catalysed samples. The presence of highly isotactic and medium isotactic areas was discussed within the thesis, however, no set trend was observed between the Lynx and NHP catalysed samples. Solution ^{13}C NMR of the powder samples didn't show consistent results related to the isotacticity of the sample, as values varied between samples of different grade and catalyst. For the pellet samples, however, it was found that the NHP catalysed samples generally had a slightly higher isotacticity compared to the Lynx catalysed samples. Solid-state NMR was done only on the powder samples and showed some splitting of the methylene peak, indicative of the 3_1 helix structure of the α allomorph of isotactic polypropylene. The presence of mobile methine components within the samples were also observed, which is significant due to the methine carbons being part of the backbone of the polymer and are thus not generally thought of to have mobility. No significant or consistent differences were observed between samples catalysed with the Lynx and NHP catalysts.

7.3 Recommendations and future work

This approach could be expanded to other grades of polymers; in addition this study could be used to evaluate catalyst or system changes on specific grades of polymers produced. There are several other analytical techniques that could potentially be employed to expand on this study. This could include a BET analysis which will allow for the quantification of the porosity within the reactor powder samples; HT-HPLC which may give further information on the amounts of iso- syndio- and atactic components within the polypropylene sample, as well as possible information regarding fine polymers that occur during the production of polypropylene; extended NMR studies, both in the solution and solid-state to obtain information from the other grades of polymers investigated as well.

Future work may include TREF fractionation of smaller increments, or possibly the combination of same fractions from multiple TREF experiments on the same grade of polymer. This will allow for the investigation of other specific fractions, or to get further information on some of the lower temperature fractions. As this was a baseline study of isotactic polypropylene samples for future work, it could be speculated as to what this future work might entail. This could include testing these polymers by copolymerization with ethylene to form heterophasic ethylene propylene copolymers (HEPCs), to see what the effect of the catalyst used during polypropylene polymerization has on the final HEPC properties. Furthermore, a topic of study could be to investigate the effect of polymerization technology on the fundamental properties of isotactic polypropylene, as only the effect of the catalyst was investigated during this study.

Chapter 8

Annexure

Within this annexure is a set of results summarized in both graphical and tabular form. These graphs and tables are added here due to them not fitting within the main body of the thesis, however, still form a fundamental part of the results. These results included graphs and/or tables of TREF, CRYSTAF, DSC, HT-SEC, XRD, SSA and NMR results. Complete sets of graphs or tables that have been added within the thesis have not been added to the annexure.

8.1 TREF

8.1.1 HKQ 205 Fractograms

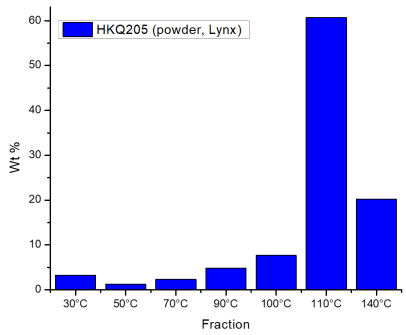

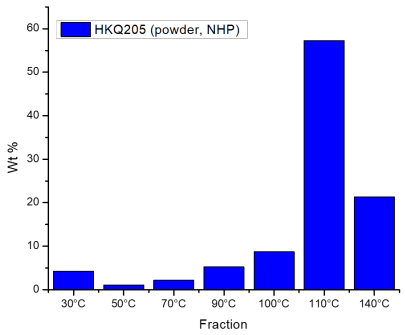

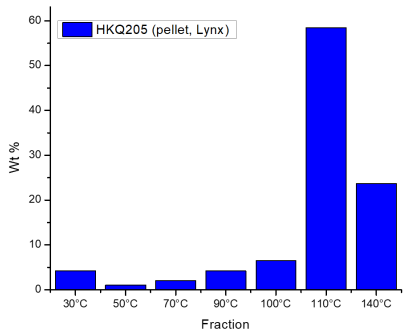

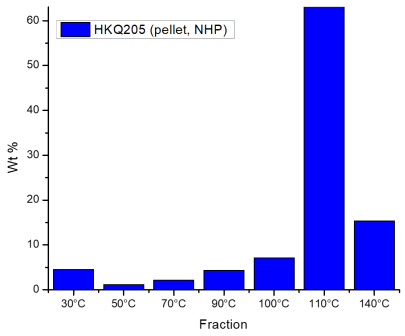

8.1.2 HKR 102 Fractograms

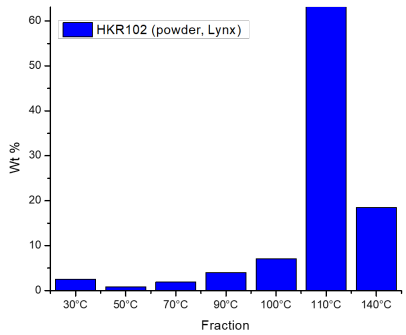

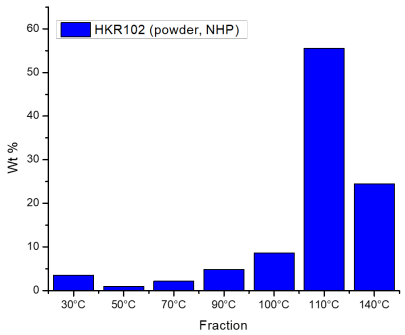

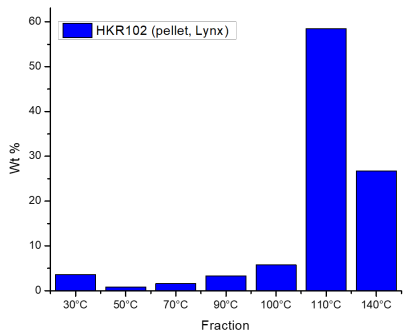

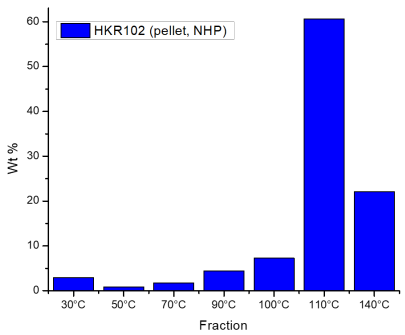

8.1.3 HMR 127 Fractograms

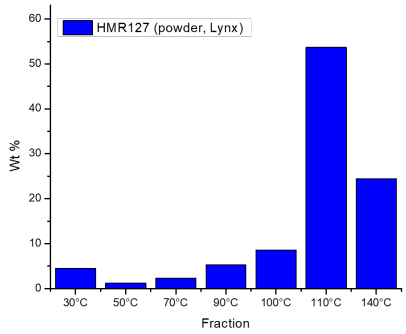

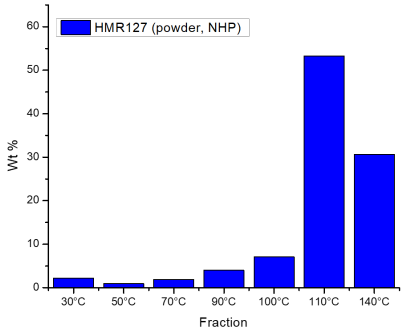

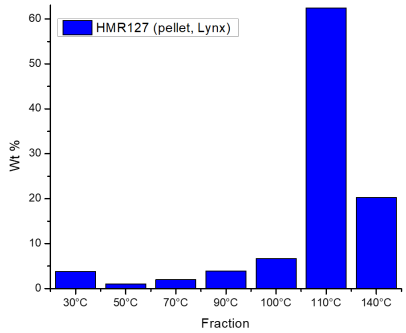

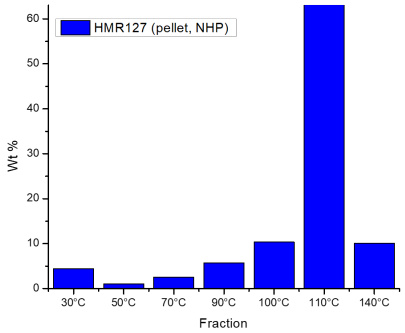

8.1.4 HNR 100 Fractograms

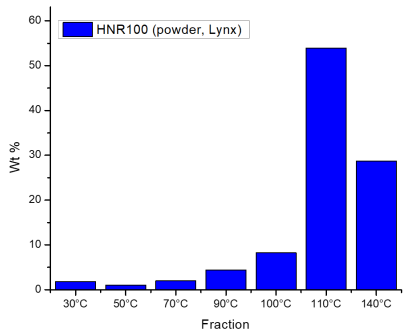

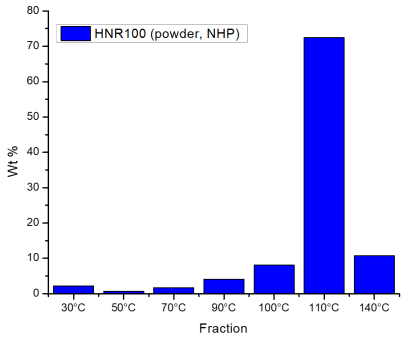

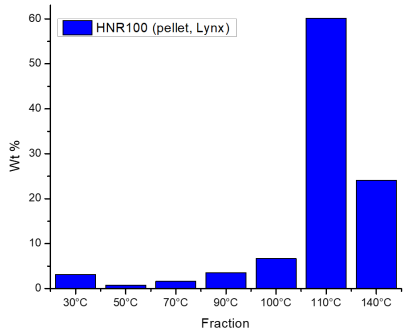

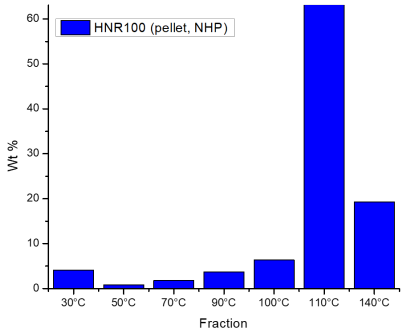

8.1.5 HNR 101 Fractograms

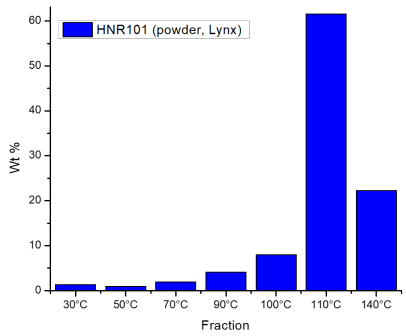

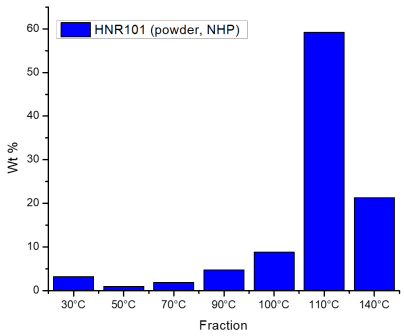

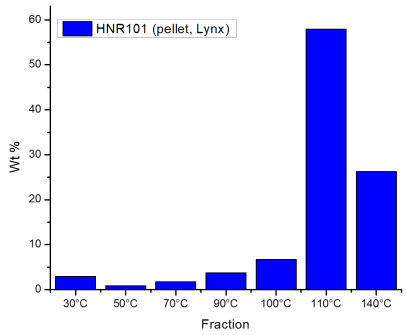

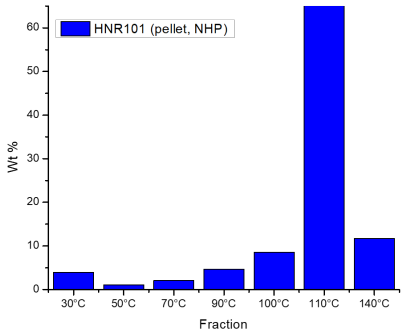

8.1.6 Grade comparisons

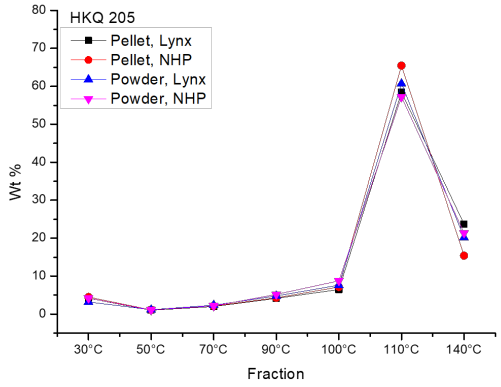

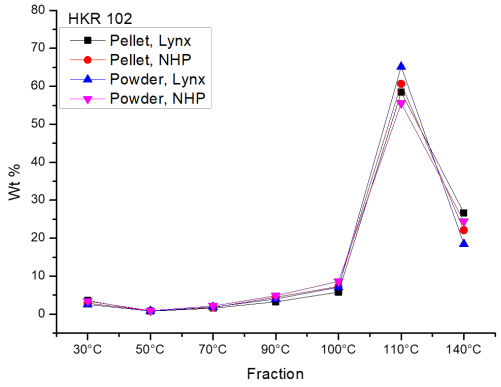

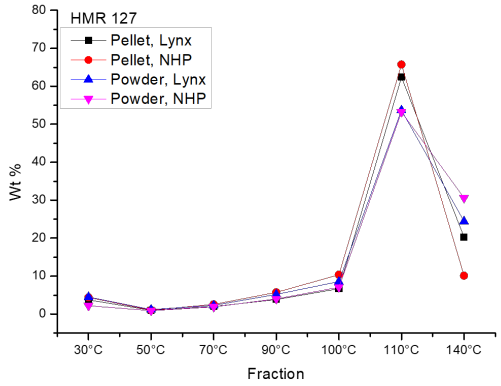

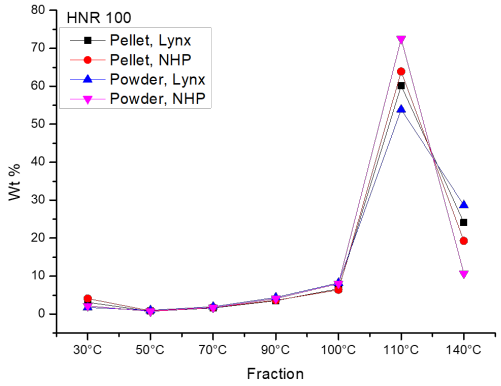

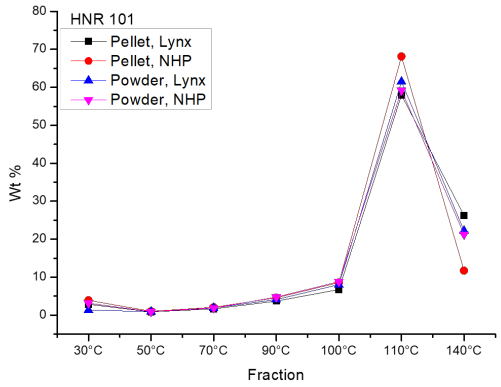

8.2 CRYSTAF

8.2.1 HKQ 205 Bulk samples

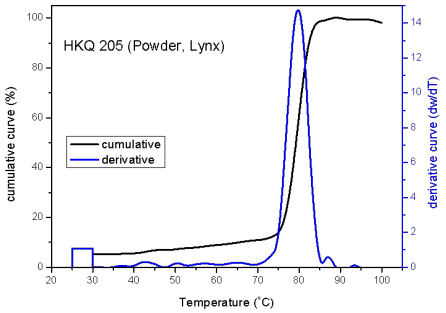

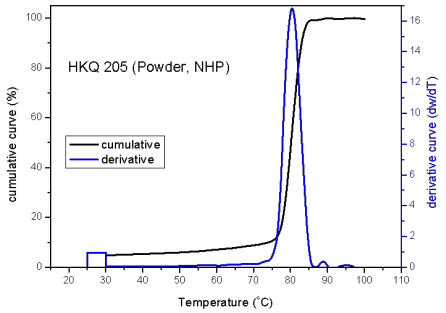

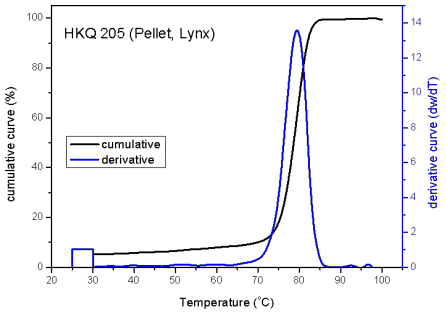

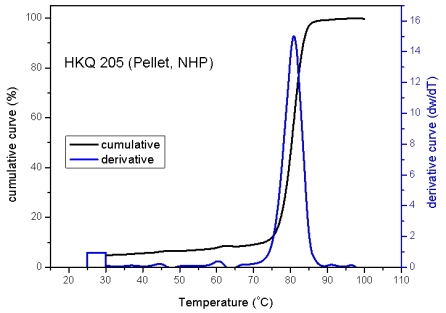

8.2.2 HKR 102 Bulk samples

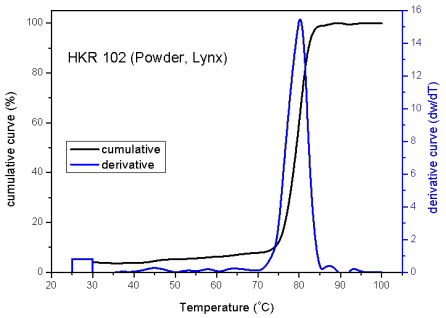

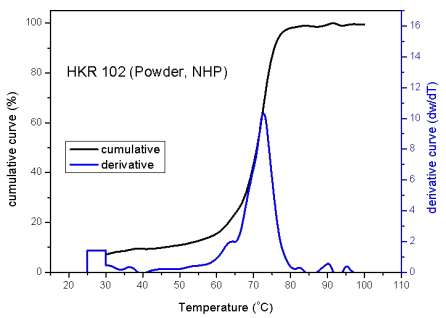

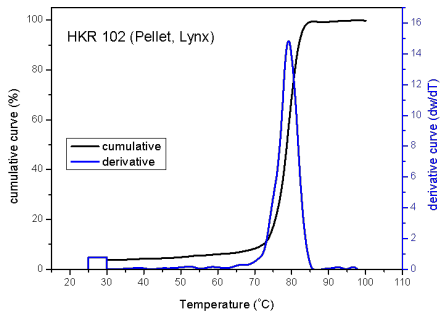

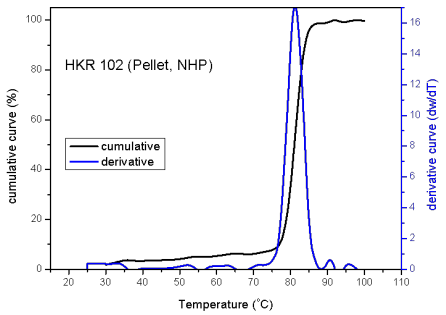

8.2.3 HMR 127 Bulk samples

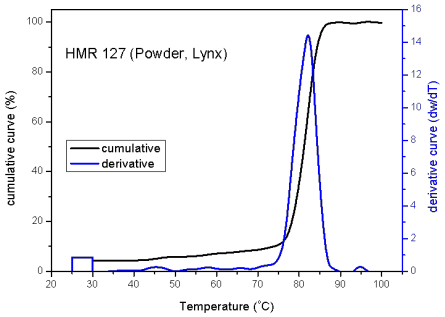

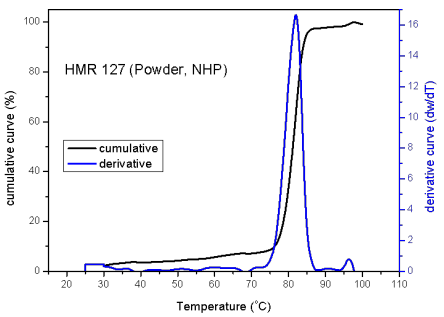

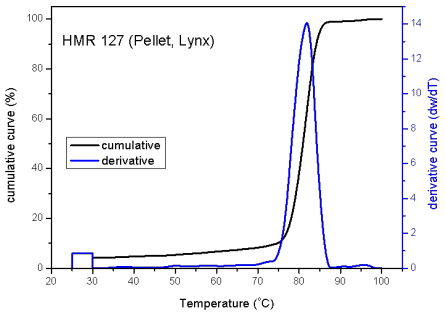

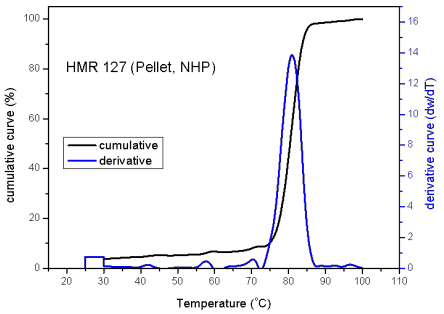

8.2.4 HNR 100 Bulk samples

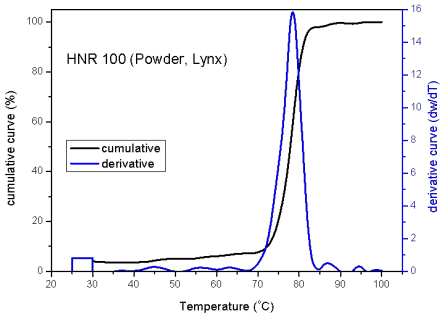

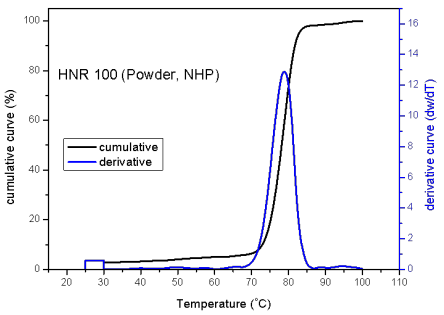

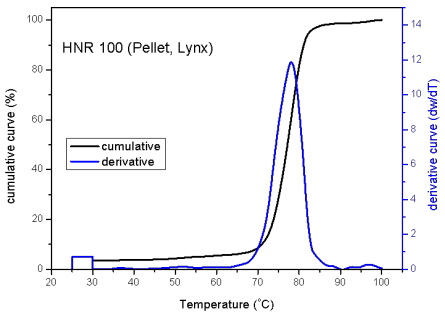

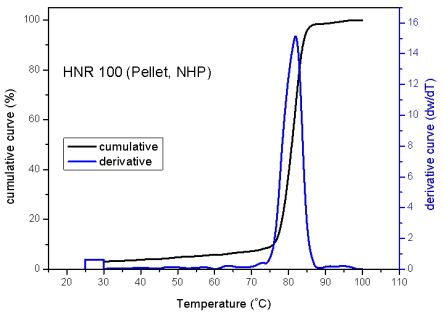

8.2.5 HNR 101 Bulk samples

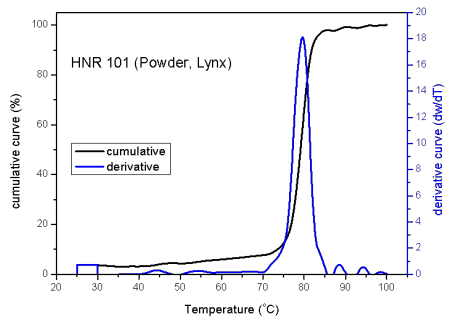

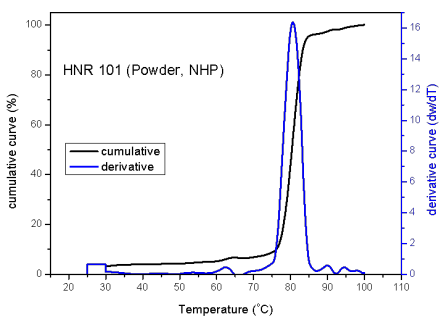

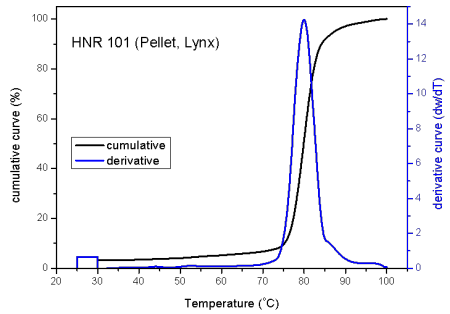

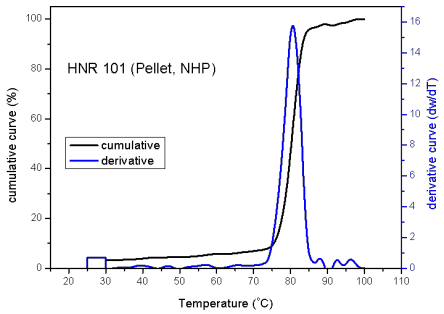

8.3 DSC

8.3.1 Bulk samples: Graphs

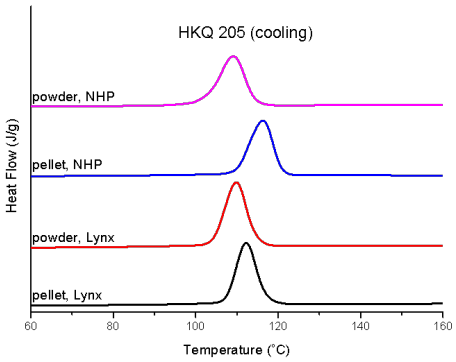

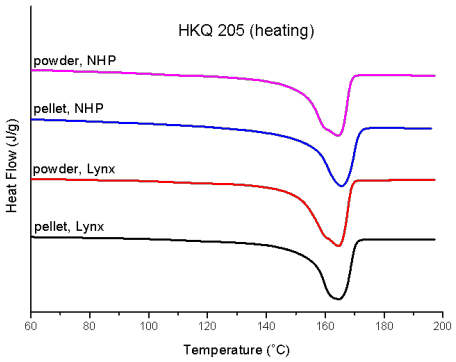

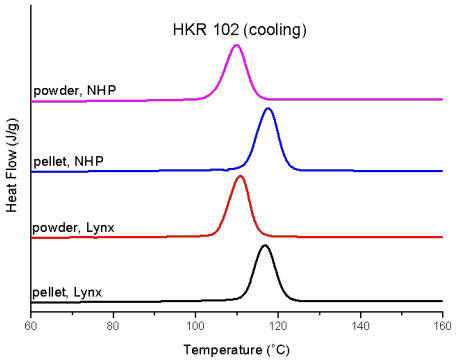

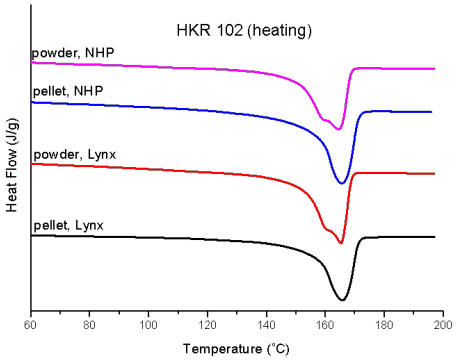

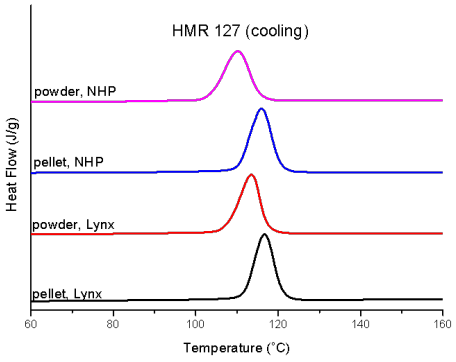

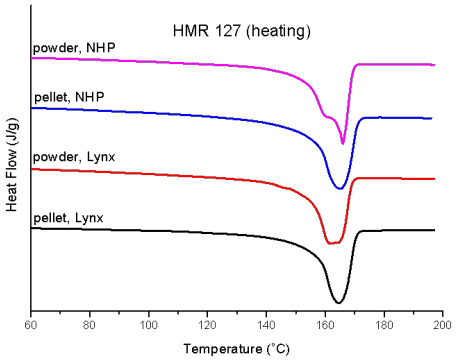

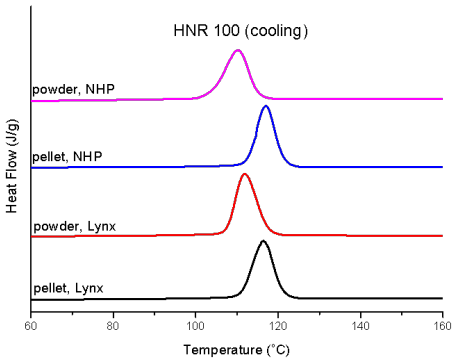

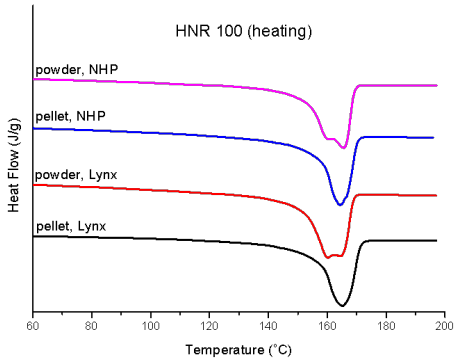

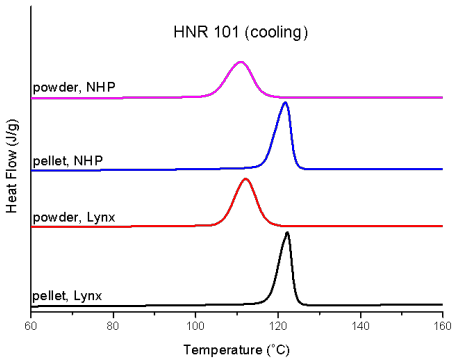

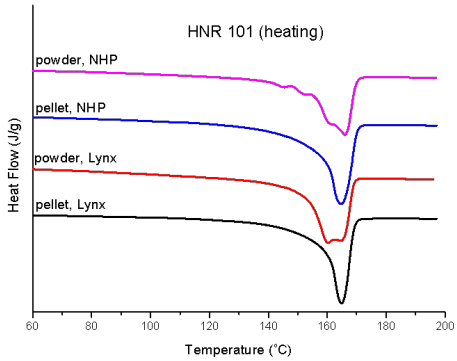

8.3.2 Fractionated samples: Graphs

8.3.2.1 HKQ 205: Fractionated samples

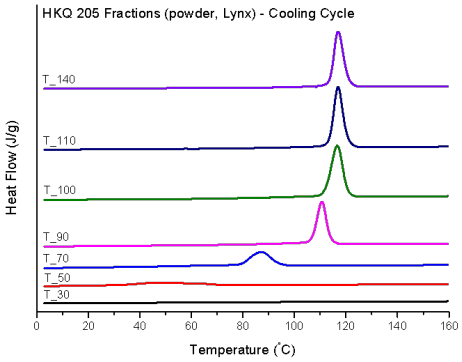

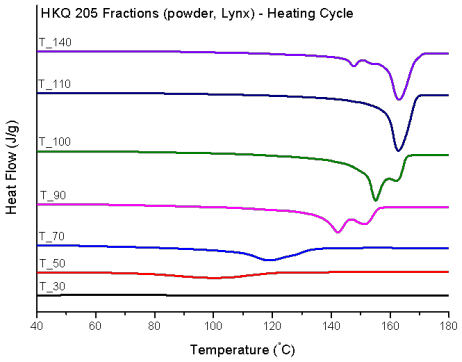

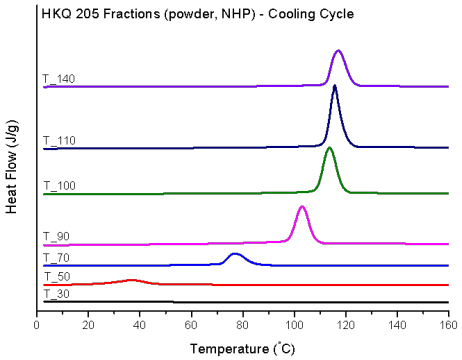

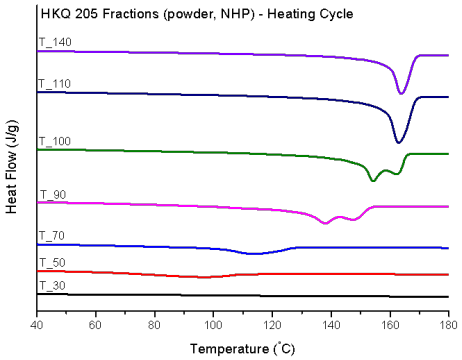

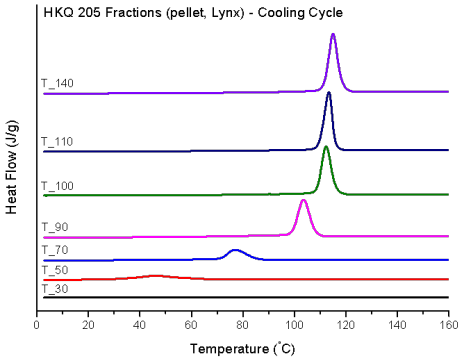

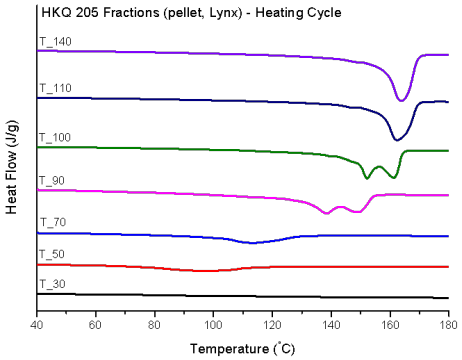

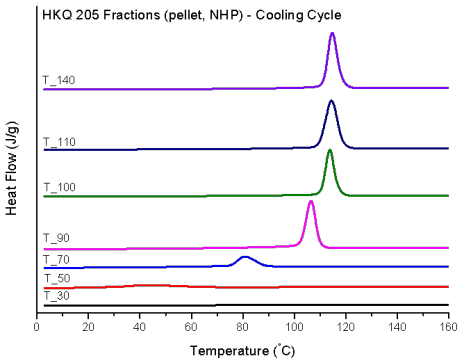

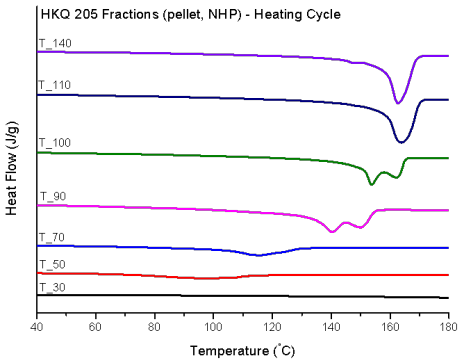

8.3.2.2 HKR 102: Fractionated samples

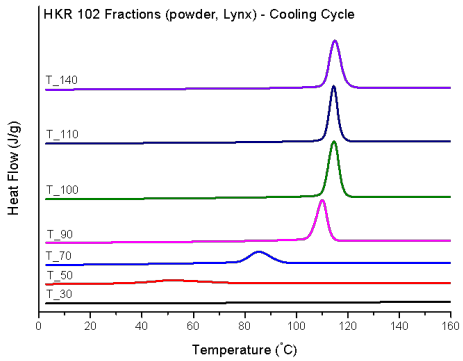

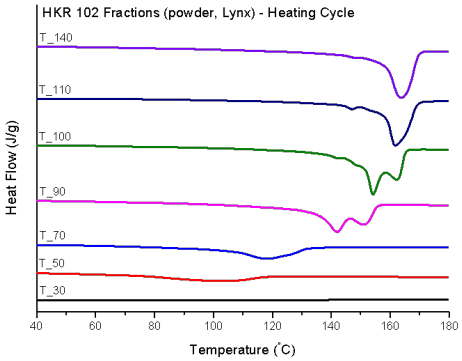

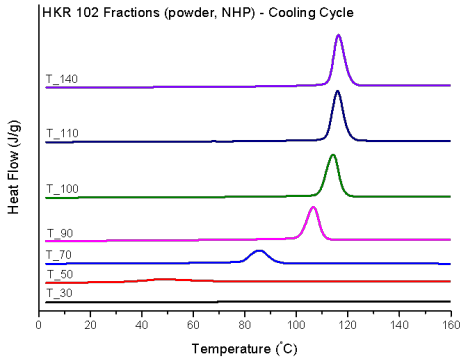

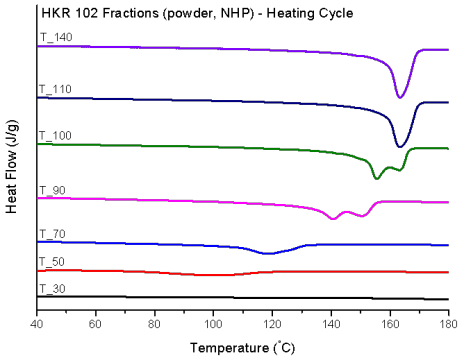

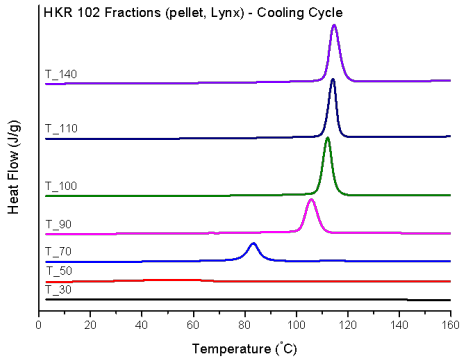

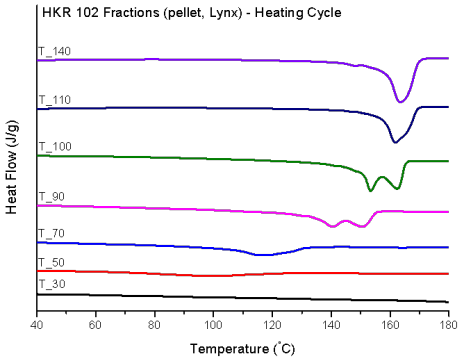

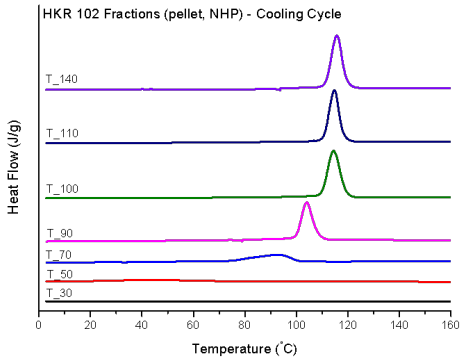

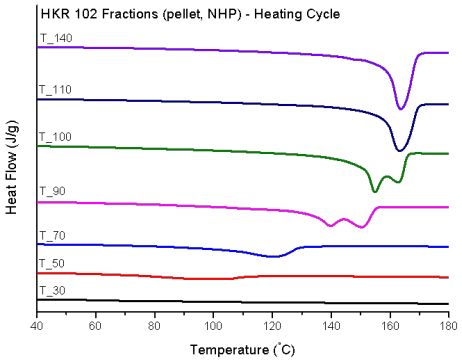

8.3.2.3 HMR 127: Fractionated samples

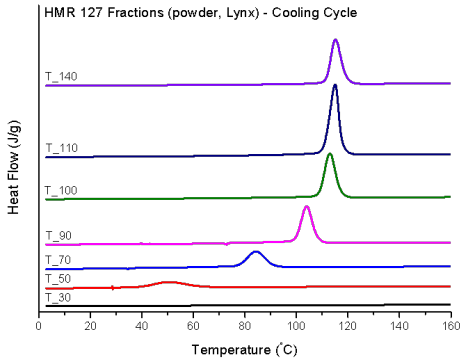

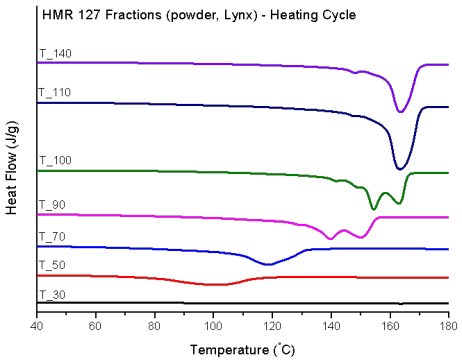

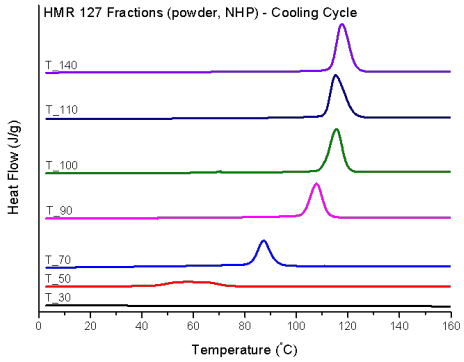

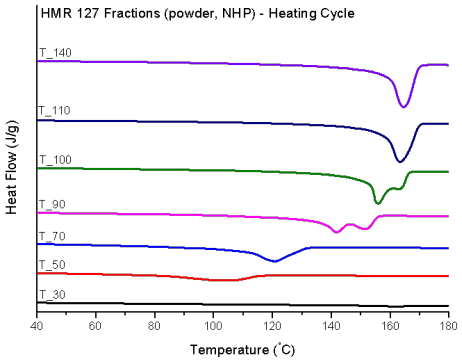

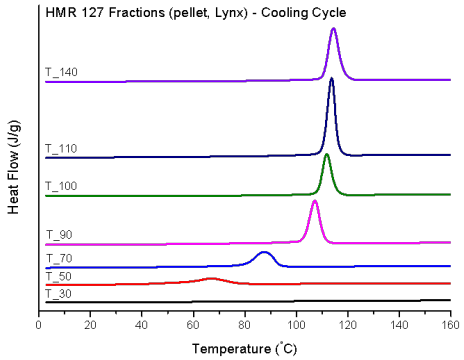

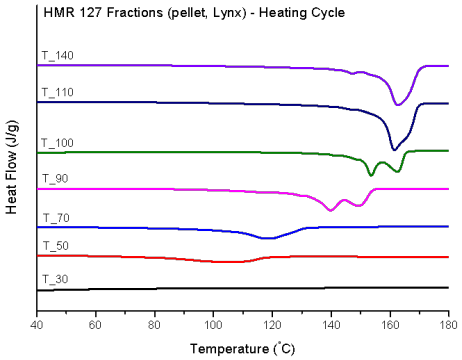

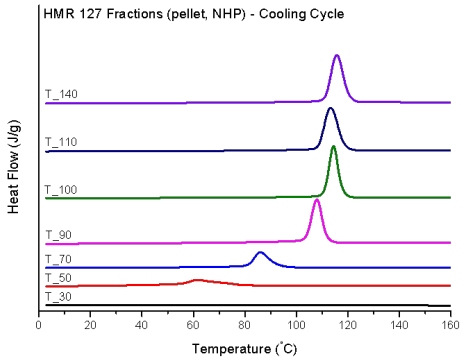

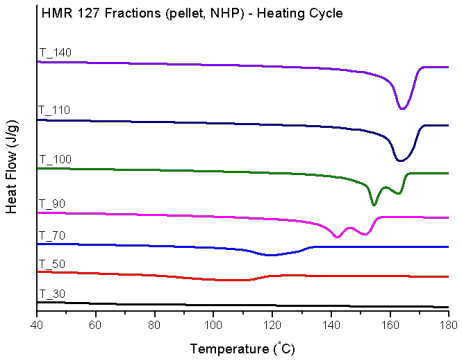

8.3.2.4 HNR 100: Fractionated samples

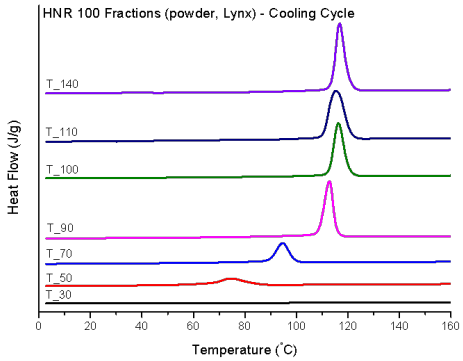

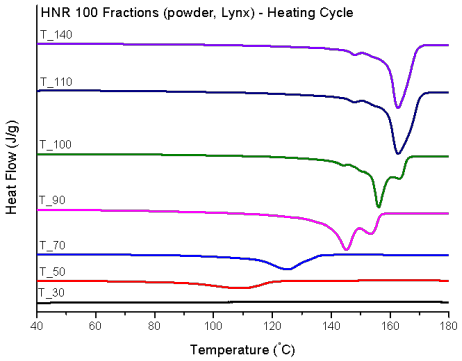

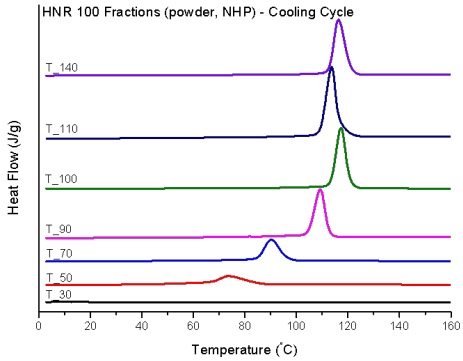

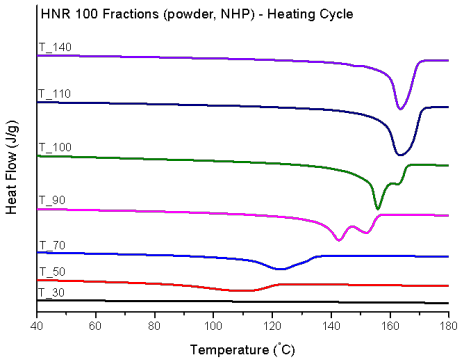

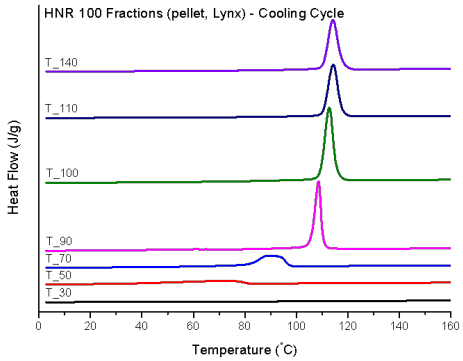

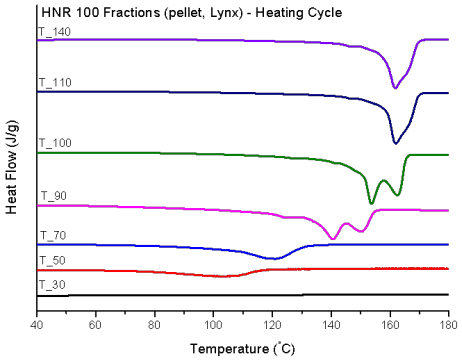

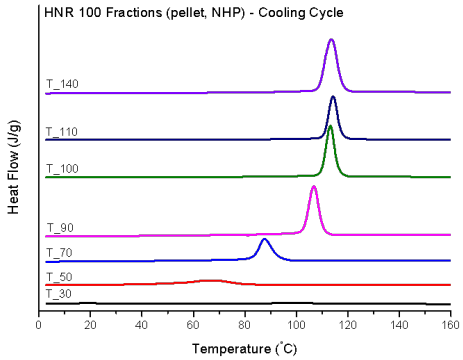

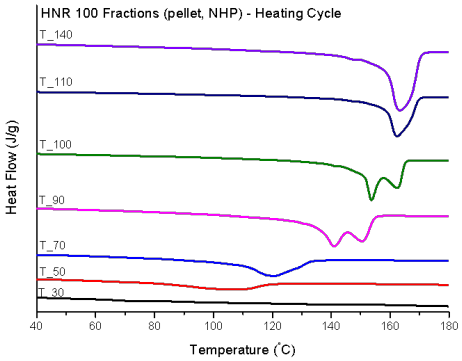

8.3.2.5 HNR 101: Fractionated samples

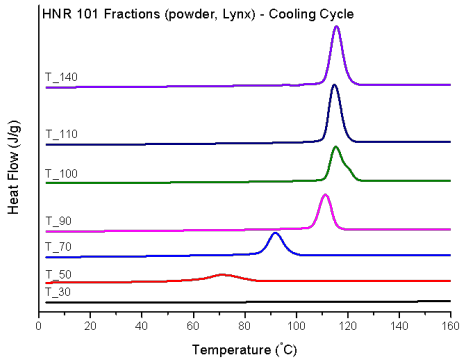

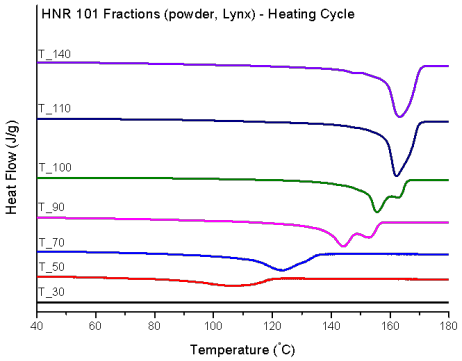

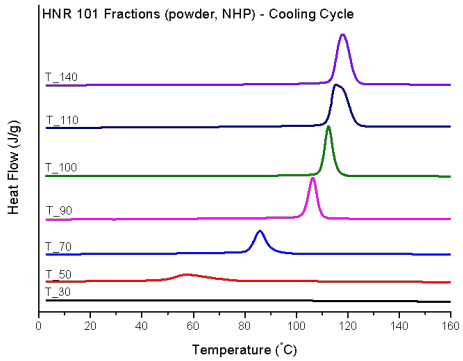

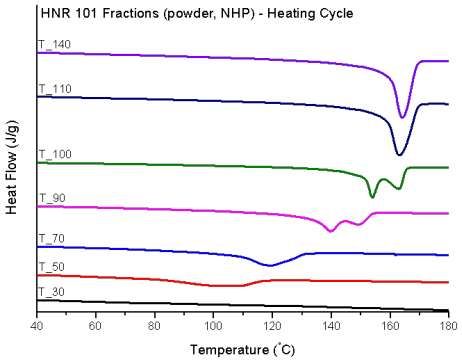

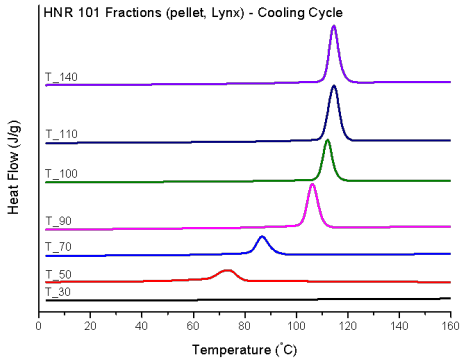

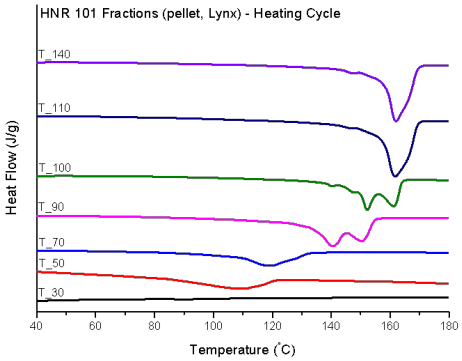

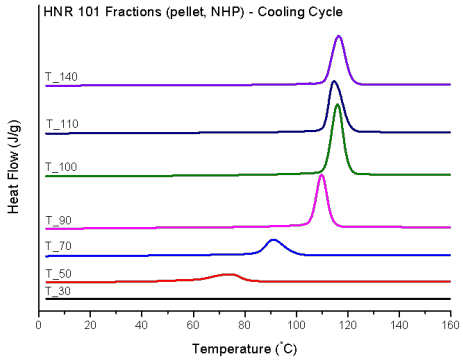

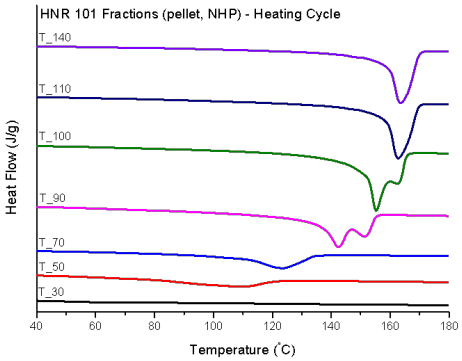

8.3.3 Bulk samples: Tabulated values

Table 8.1: DSC results: Bulk samples

	Sample	Crystallization Temp (°C)	Melting Temp (°C)	% Crystalline	Melt Enthalpy (J/g)
HKQ 205	Powder, Lynx	109.86	164.29	38.52	79.74
	Powder, NHP	109.16	164.00	35.51	73.51
	Pellet, Lynx	112.23	164.80	34.84	72.12
	Pellet, NHP	116.29	165.45	34.01	70.40
HKR 102	Powder, Lynx	110.84	160.33/165.40	38.02	78.70
	Powder, NHP	109.87	158.94/164.52	35.99	74.50
	Pellet, Lynx	116.80	165.82	33.79	69.95
	Pellet, NHP	117.55	165.75	39.63	82.03
HMR 127	Powder, Lynx	113.46	161.28/164.64	37.47	77.56
	Powder, NHP	110.24	159.98/165.99	38.45	79.59
	Pellet, Lynx	116.64	164.35	38.09	78.85
	Pellet, NHP	115.97	165.10	40.57	83.98
HNR 100	Powder, Lynx	111.94	159.78/165.01	39.09	80.92
	Powder, NHP	110.29	159.90/165.62	36.60	75.76
	Pellet, Lynx	116.44	165.27	35.75	74.00
	Pellet, NHP	117.04	164.40	34.27	70.94
HNR 101	Powder, Lynx	112.12	160.34/165.21	39.34	81.43
	Powder, NHP	110.87	160.43/165.94	33.01	68.33
	Pellet, Lynx	122.25	164.92	36.63	75.82
	Pellet, NHP	121.78	164.87	40.31	83.44

8.3.4 Fractionated samples: Tabulated values

Table 8.2: DSC results: HKQ 205 Fractionated samples

Sample		Crystallization Temp (°C)	Melting Temp (°C)	% Crystalline	Melt Enthalpy (J/g)
HKQ 205 Powder, Lynx	T30	-	-	-	-
	T50	47.40	100.29	13.39	27.72
	T70	87.10	119.19	19.12	39.58
	T90	110.66	142.38 & 151.82	27.09	56.08
	T100	116.63	155.01 & 162.70	38.78	80.28
	T110	116.98	162.77	35.62	73.72
	T140	116.95	147.69/153.73/162.90	31.64	65.49
HKQ 205 Powder, NHP	T30	36.39	-	-	-
	T50	36.40	95.99	12.68	26.26
	T70	76.97	114.06	13.05	27.00
	T90	103.06	138.06/148.20	23.96	49.60
	T100	113.61	154.29/162.58	32.63	67.55
	T110	115.60	162.96	34.89	72.22
	T140	117.13	163.83	26.76	55.40
HKQ 205 Pellet, Lynx	T30	-	-	-	-
	T50	45.57	96.66	11.68	24.18
	T70	76.99	113.65	13.00	26.91
	T90	103.52	138.54/149.61	25.01	51.77
	T100	112.30	152.16/161.60	29.40	60.86
	T110	113.35	162.36	30.34	62.80
	T140	115.01	164.06	33.70	69.76
HKQ 205 Pellet, NHP	T30	-	-	-	-
	T50	42.45	97.20	14.27	29.55
	T70	80.77	115.62	16.77	34.72
	T90	106.49	140.44/150.37	36.15	74.83
	T100	113.76	153.76/162.50	34.62	71.66
	T110	114.35	163.94	45.47	94.11
	T140	114.69	162.72	43.56	90.18

Table 8.3: DSC results: HKR 102 Fractionated samples

Sample		Crystallization Temp (°C)	Melting Temp (°C)	% Crystalline	Melt Enthalpy (J/g)
HKR 102 Powder, Lynx	T30	-	-	-	-
	T50	50.75	101.11	15.91	32.94
	T70	85.61	118.66	20.87	43.20
	T90	110.07	142.15/151.59	34.15	70.68
	T100	114.57	154.25/162.60	45.27	93.71
	T110	114.46	146.92/161.84	35.09	72.64
	T140	114.96	163.9	37.69	78.02
HKR 102 Powder, NHP	T30	-	-	-	-
	T50	47.38	100.00	12.33	25.51
	T70	85.72	119.06	18.11	37.49
	T90	106.60	140.68/150.85	28.31	58.60
	T100	114.22	155.45/163.53	39.08	80.90
	T110	115.97	163.33	40.06	82.93
	T140	116.28	163.36	39.46	81.68
HKR 102 Pellet, Lynx	T30	-	-	-	-
	T50	54.66/108.82	98.29/164.12	10.14/0.389	20.99
	T70	83.29/115.95	117.62	16.96	35.11
	T90	105.78	140.48/150.91	23.83	49.33
	T100	112.09	153.27/162.44	33.92	70.22
	T110	114.17	161.72	28.92	59.87
	T140	114.60	163.50	35.30	73.07
HKR 102 Pellet, NHP	T30	-	-	-	-
	T50	41.63	98.35	12.04	24.93
	T70	92.64	120.94	19.51	40.39
	T90	103.98	139.49/150.45	29.75	61.58
	T100	114.44	154.84/163.09	41.96	86.85
	T110	114.73	163.25	38.10	78.87
	T140	115.72	163.73	41.40	85.70

Table 8.4: DSC results: HMR 127 Fractionated samples

Sample		Crystallization Temp (°C)	Melting Temp (°C)	% Crystalline	Melt Enthalpy (J/g)
HMR 127 Powder, Lynx	T30	-	-	-	-
	T50	50.00	100.38	17.46	36.14
	T70	84.28	118.96	23.53	48.70
	T90	103.98	128.78/139.80/150.58	29.20	60.44
	T100	113.01	141.46/148.53/154.51/163.27	36.59	75.74
	T110	114.99	147.58/163.54	48.14	99.65
	T140	115.16	147.77/163.48	33.82	70.00
HMR 127 Powder, NHP	T30	-	-	-	-
	T50	58.03	103.94	15.94	32.99
	T70	87.23	120.83	25.31	52.39
	T90	107.83	141.82/151.68	26.87	55.63
	T100	115.51	155.96/163.48	37.16	76.93
	T110	115.26	163.45	37.83	78.30
	T140	117.61	164.59	37.55	77.73
HMR 127 Pellet, Lynx	T30	-	-	-	-
	T50	66.18	105.41	14.16	29.31
	T70	87.41	119.30	19.30	39.96
	T90	107.16	139.76/149.85	27.21	56.33
	T100	111.81	153.48/162.83	24.83	51.39
	T110	113.67	161.46	39.45	81.66
	T140	114.36	162.67	33.87	70.12
HMR 127 Pellet, NHP	T30	-	-	-	-
	T50	61.26	104.90	19.81	41.00
	T70	86.13	119.91	19.50	40.37
	T90	107.94	142.10/151.99	32.64	67.56
	T100	114.42	154.55/163.09	35.89	74.29
	T110	113.21	163.65	38.77	80.25
	T140	115.70	164.15	39.25	81.25

Table 8.5: DSC results: HNR 100 Fractionated samples

Sample		Crystallization Temp (°C)	Melting Temp (°C)	% Crystalline	Melt Enthalpy (J/g)
HNR 100 Powder, Lynx	T30	-	-	-	-
	T50	74.14	109.59	13.74	28.44
	T70	94.64	125.43	18.38	38.05
	T90	112.76	145.13/153.84	35.63	73.75
	T100	116.29	143.75/156.11/163.45	36.77	76.12
	T110	115.39	147.47/162.74	43.00	89.01
	T140	116.75	147.82/162.65	39.37	81.49
HNR 100 Powder, NHP	T30	-	-	-	-
	T50	73.84	109.91	21.09	43.66
	T70	90.24	123.11	24.66	51.05
	T90	109.25	142.60/152.28	34.96	72.36
	T100	117.32	155.85/163.11	42.46	87.90
	T110	113.68	163.67	49.36	102.20
	T140	116.27	163.53	39.10	80.94
HNR 100 Pellet, Lynx	T30	-	-	-	-
	T50	71.98	104.72	13.14	27.19
	T70	88.94	120.84	19.27	39.90
	T90	108.56	140.48/150.65	29.38	60.81
	T100	112.71	153.64/162.77	40.36	83.55
	T110	114.26	161.92	30.67	63.49
	T140	114.17	161.78	30.59	63.32
HNR 100 Pellet, NHP	T30	-	-	-	-
	T50	65.92	105.58	15.52	32.14
	T70	87.63	120.29	21.96	45.46
	T90	106.71	140.97/150.86	31.20	64.57
	T100	113.19	153.72/162.65	29.72	61.52
	T110	114.21	162.34	24.09	49.87
	T140	113.57	163.34	39.75	82.29

Table 8.6: DSC results: HNR 101 Fractionated samples

Sample		Crystallization Temp (°C)	Melting Temp (°C)	% Crystalline	Melt Enthalpy (J/g)
HNR 101 Powder, Lynx	T30	-	-	-	-
	T50	70.78	106.31	18.04	37.35
	T70	91.90	123.24	27.01	55.91
	T90	111.3	144.08/153.17	29.31	60.67
	T100	115.31	155.63/163.09	31.26	64.71
	T110	114.70	162.16	41.91	86.75
	T140	115.56	163.38	42.65	88.28
HNR 101 Powder, NHP	T30	-	-	-	-
	T50	57.03	103.83	18.45	38.18
	T70	85.88	119.21	21.70	44.91
	T90	106.37	139.81/149.73	22.94	47.49
	T100	112.45	153.98/162.96	27.09	56.08
	T110	115.32	163.25	38.77	80.26
	T140	117.96	164.19	37.74	78.12
HNR 101 Pellet, Lynx	T30	-	-	-	-
	T50	73.54	108.80	20.46	42.35
	T70	86.72	119.56	17.76	36.75
	T90	106.25	140.67/150.79	29.18	60.41
	T100	112.07	152.29/161.44	25.58	52.94
	T110	114.55	161.72	36.77	76.12
	T140	114.51	162.00	34.27	70.95
HNR 101 Pellet, NHP	T30	-	-	-	-
	T50	74.35	108.83	20.34	42.09
	T70	91.08	123.34	21.96	45.45
	T90	109.78	142.46/151.76	38.48	79.65
	T100	115.96	155.30/162.89	53.90	111.60
	T110	114.62	162.71	41.46	85.83
	T140	116.45	163.55	38.82	80.35

8.4 HT-SEC

8.4.1 Bulk Samples: Graphs

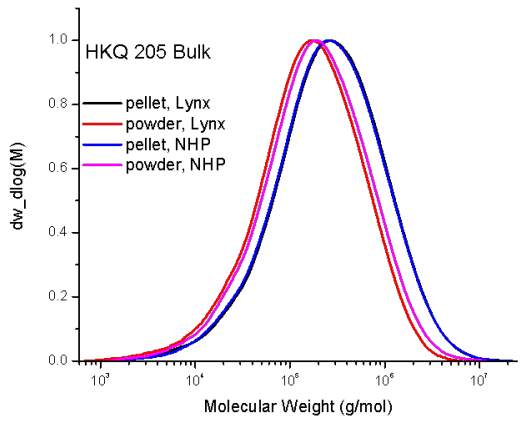

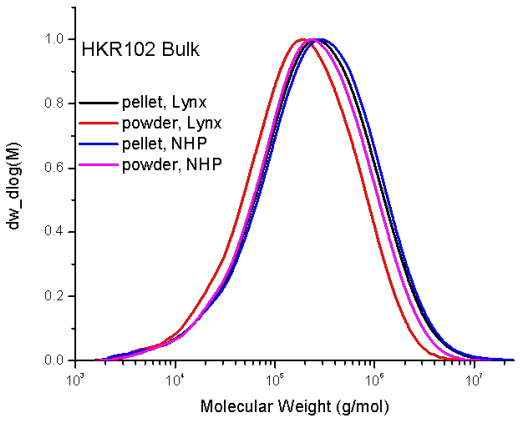

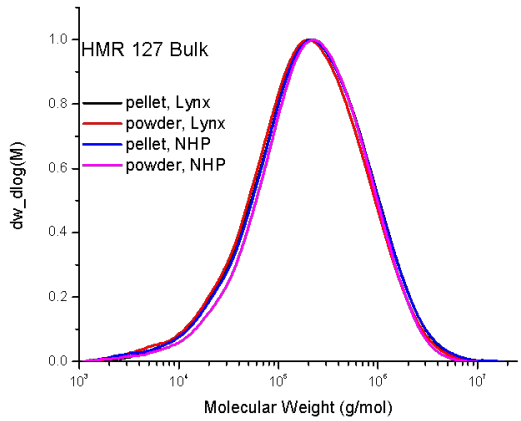

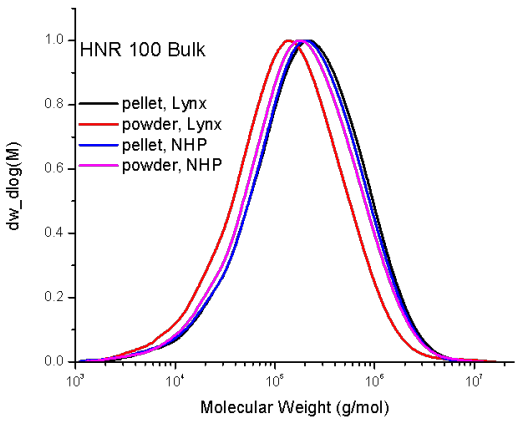

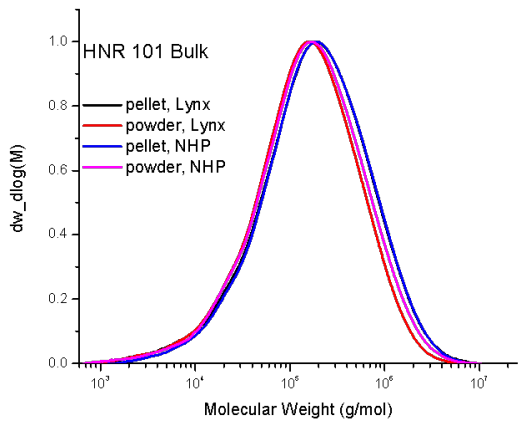

8.4.2 Fractionated Samples: Graphs

8.4.2.1 HKQ 205: Fractionated samples

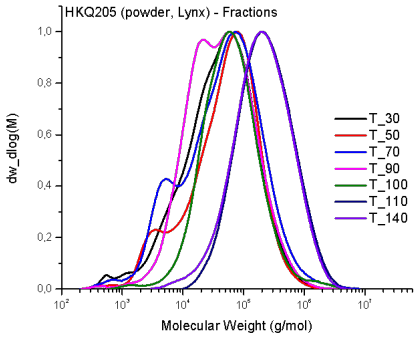

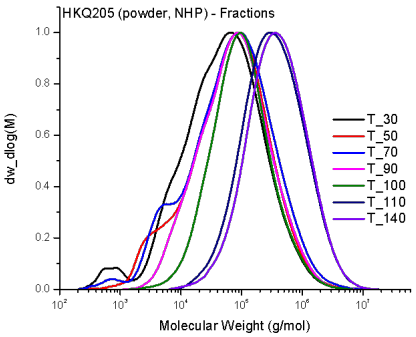

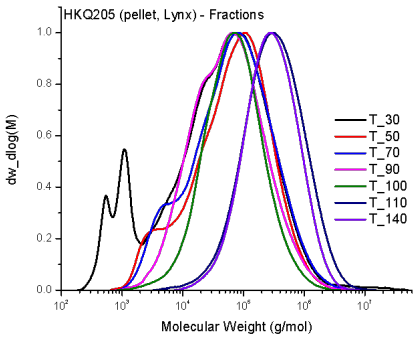

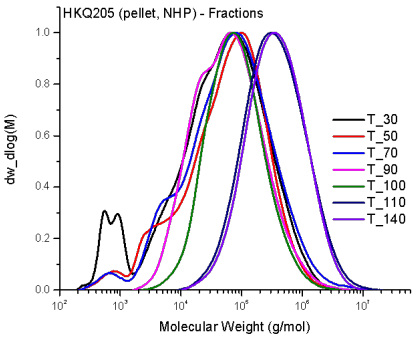

8.4.2.2 HKR 102: Fractionated samples

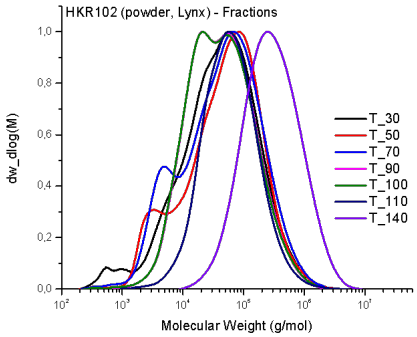

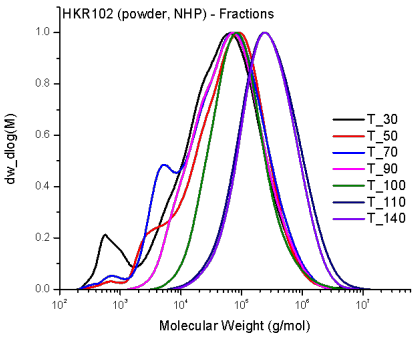

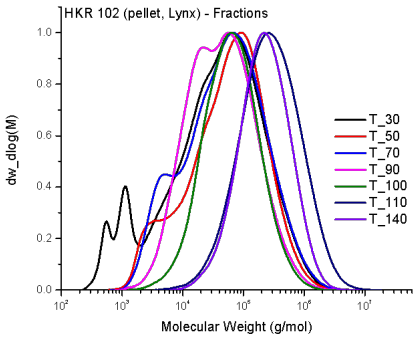

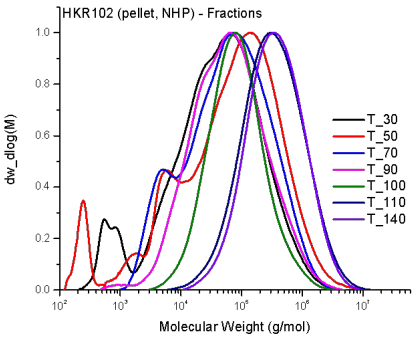

8.4.2.3 HMR 127: Fractionated samples

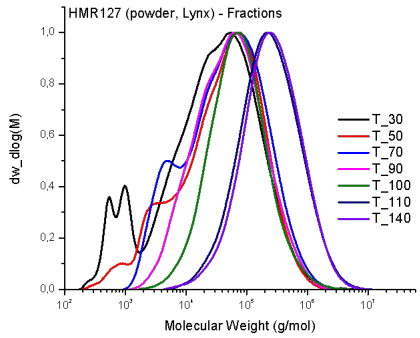

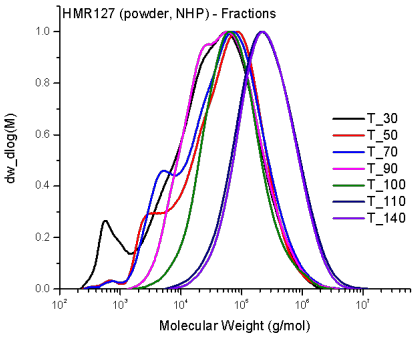

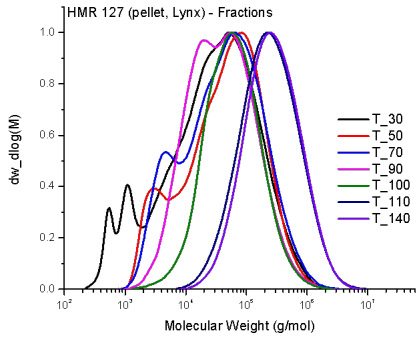

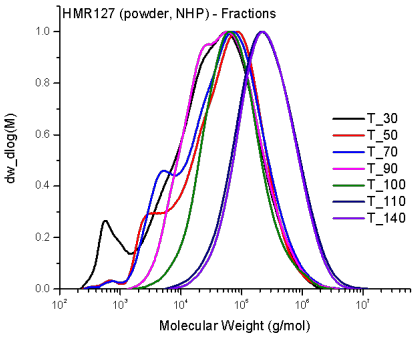

8.4.2.4 HNR 100: Fractionated samples

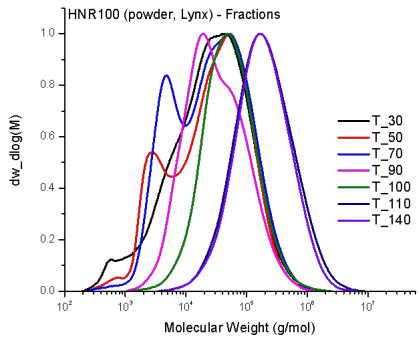

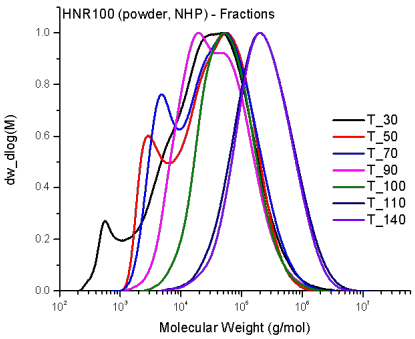

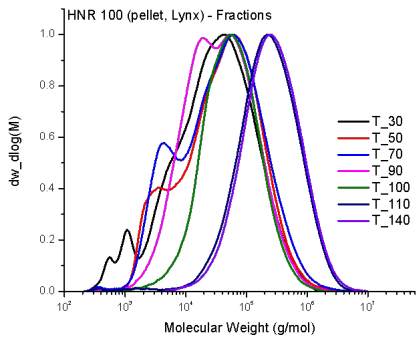

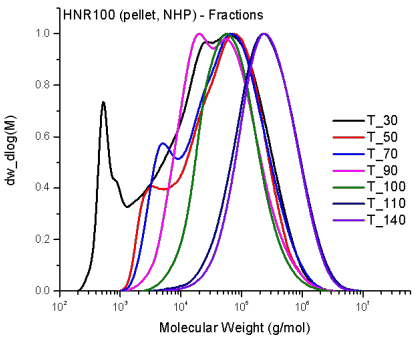

8.4.2.5 HNR 101: Fractionated samples

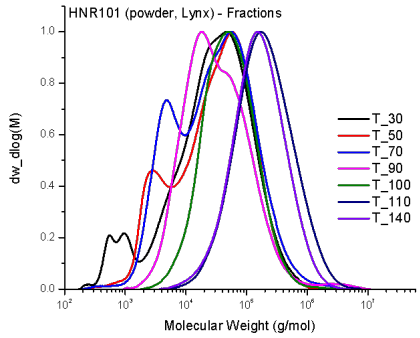

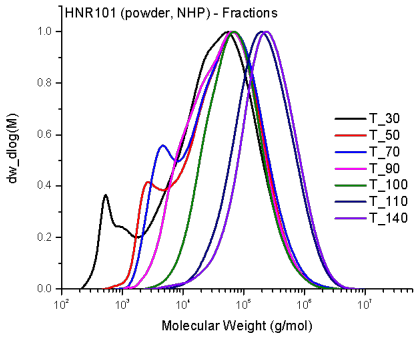

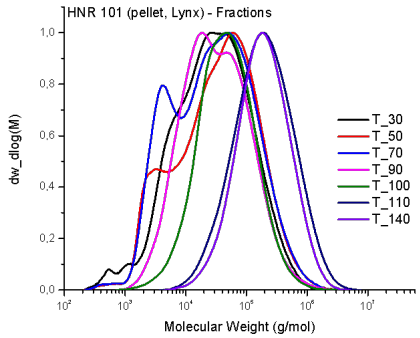

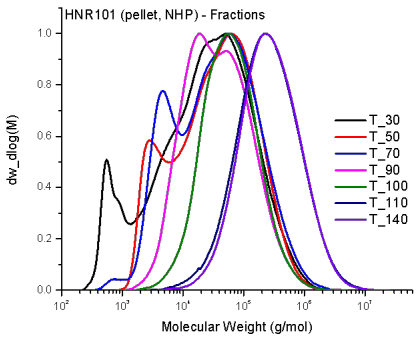

8.4.3 Bulk samples: Tabulated values

Table 8.7: HT-SEC results: Bulk samples

	Sample	M_n [a]	M_w [b]	M_z [c]	PDI [d]
HKQ 205	Powder, Lynx	58056	298116	850163	5.13
	Powder, NHP	69473	355829	1172527	5.12
	Pellet, Lynx	91440	516902	1771901	5.65
	Pellet, NHP	92361	512639	1790059	5.55
HKR 102	Powder, Lynx	69877	329733	990190	4.72
	Powder, NHP	86300	432469	1313715	5.01
	Pellet, Lynx	87191	507135	1945306	5.82
	Pellet, NHP	86178	547423	2255325	6.35
HMR 127	Powder, Lynx	67202	380260	1262735	5.66
	Powder, NHP	79090	390346	1085460	4.94
	Pellet, Lynx	77488	414788	1390600	5.35
	Pellet, NHP	70397	419518	1501439	5.96
HNR 100	Powder, Lynx	53430	257292	1163225	4.82
	Powder, NHP	69725	339510	1112411	4.87
	Pellet, Lynx	80999	383422	1156667	4.73
	Pellet, NHP	71353	359719	1032912	5.04
HNR 101	Powder, Lynx	52983	274665	805463	5.18
	Powder, NHP	53793	316147	1038829	5.88
	Pellet, Lynx	58435	358429	1182988	6.13
	Pellet, NHP	69947	362746	1137696	5.19

[a] - Number average molar mass

[b] - Weight average molar mass

[c] - Z-average molar mass

[d] - Dispersity value (M_w/M_n)

8.4.4 Fractionated samples: Tabulated values

Table 8.8: HT-SEC results: HKQ 205 + HKR 102 Fractionated samples

Sample		M_n [a]	M_w [b]	M_z [c]	PDI [d]	Sample		M_n [a]	M_w [b]	M_z [c]	PDI [d]
HKQ 205 Powder, Lynx	T30	12188	81950	273750	6.72	HKQ 205 Powder, NHP	T30	11592	123939	744891	10.69
	T50	14048	86849	237699	6.18		T50	17942	147501	672927	8.22
	T70	12576	111754	736406	8.89		T70	15528	171762	895379	11.06
	T90	17902	82242	296737	4.59		T90	33072	159040	614448	4.81
	T100	31233	110874	546445	3.55		T100	51498	172580	613969	3.35
	T110	130569	354261	849024	2.71		T110	165710	579439	1689115	3.45
	T140	98158	324231	776555	3.30		T140	190797	630313	1743015	3.30
HKQ 205 Pellet, Lynx	T30	4755	176214	5633286	37.06	HKQ 205 Pellet, NHP	T30	6025	123887	505108	20.56
	T50	18091	140828	507543	7.78		T50	11311	126223	466151	11.16
	T70	19482	155791	670665	8.00		T70	12642	175380	1272850	13.87
	T90	24245	123887	529188	5.11		T90	28200	128554	605676	4.56
	T100	35462	119472	370686	3.37		T100	44934	134571	440679	2.99
	T110	149523	526341	1412784	3.52		T110	178624	614004	1952471	3.44
	T140	161384	426851	945725	2.64		T140	193644	588056	1493864	3.07
HKR 102 Powder, Lynx	T30	10050	92005	365992	9.15	HKR 102 Powder, NHP	T30	6784	104404	521399	15.39
	T50	13764	102058	387792	7.41		T50	14677	117143	403452	7.98
	T70	13172	99810	364080	7.58		T70	11892	113833	439631	9.57
	T90	20742	84737	308213	4.09		T90	28038	121318	425980	4.33
	T100	19113	84819	329364	4.44		T100	51335	145909	508513	2.84
	T110	34238	100066	338167	2.92		T110	144696	471754	1350697	3.26
	T140	159473	463237	1168408	2.90		T140	149317	415291	998848	2.78
HKR 102 Pellet, Lynx	T30	5701	105930	481195	18.58	HKR 102 Pellet, NHP	T30	6300	112047	526208	17.79
	T50	16225	117017	420571	7.21		T50	3945	204473	1081946	51.83
	T70	15961	119833	482435	7.51		T70	17255	147284	560561	8.54
	T90	17345	88010	352563	5.07		T90	28490	143313	602885	5.03
	T100	35309	103061	277863	2.92		T100	47259	137638	425661	2.91
	T110	134058	467638	1335542	3.49		T110	159261	570914	1683560	3.58
	T140	131274	319980	679737	2.44		T140	191668	572290	1432209	2.99

[a] - Number average molar mass

[b] - Weight average molar mass

[c] - Z-average molar mass

[d] - Dispersity value (M_w/M_n)

Table 8.9: HT-SEC results: HMR 127 + HNR 100 Fractionated samples

Sample		M_n [a]	M_w [b]	M_z [c]	PDI [d]	Sample		M_n [a]	M_w [b]	M_z [c]	PDI [d]
HMR 127 Powder, Lynx	T30	4630	79672	413057	17.21	HMR 127 Powder, NHP	T30	5884	84548	333888	14.37
	T50	8715	89372	293734	10.26		T50	12906	105237	391362	8.15
	T70	14732	105524	391734	7.16		T70	13195	109485	462637	8.30
	T90	23702	103444	335313	4.36		T90	23585	104332	426806	4.42
	T100	39767	123123	408892	3.10		T100	38274	118492	385378	3.10
	T110	118603	406177	1159501	3.42		T110	124866	418476	1247294	3.35
	T140	129930	422515	1115925	3.25		T140	138679	401067	1008126	2.89
HMR 127 Pellet, Lynx	T30	5053	76902	325570	15.22	HMR 127 Pellet, NHP	T30	3461	78571	345206	22.70
	T50	13047	91966	302041	7.05		T50	13128	96201	342291	7.33
	T70	13923	97492	384625	7.00		T70	15184	109240	456896	7.19
	T90	18877	77250	284740	4.09		T90	22185	94053	376872	4.24
	T100	33243	96792	283272	2.91		T100	40118	107022	317276	2.67
	T110	126929	394926	1078415	3.11		T110	146099	433129	1148037	2.96
	T140	152612	420075	1030729	2.75		T140	165475	474444	1147585	2.87
HNR 100 Powder, Lynx	T30	7058	56266	206278	7.97	HNR 100 Powder, NHP	T30	5385	70122	368243	13.02
	T50	7960	54213	172108	6.81		T50	10623	65752	208778	6.19
	T70	9484	57000	202346	6.01		T70	12210	75839	295988	6.21
	T90	17065	55289	171080	3.24		T90	18658	69576	249364	3.73
	T100	31500	82472	229882	2.62		T100	35123	90841	253181	2.59
	T110	101927	323024	942066	3.17		T110	118671	377333	1049238	3.18
	T140	102652	290263	737191	2.83		T140	128397	363021	889363	2.83
HNR 100 Pellet, Lynx	T30	7253	70709	263717	9.75	HNR 100 Pellet, NHP	T30	3542	87754	394408	24.78
	T50	11712	86798	342406	7.41		T50	13945	99667	344065	7.15
	T70	11372	95945	454476	8.44		T70	15309	107931	410594	7.05
	T90	16507	76170	280339	4.61		T90	20973	90599	368388	4.32
	T100	29740	90933	248906	3.06		T100	37110	103958	311592	2.80
	T110	58494	375514	934007	6.42		T110	123711	409959	1091281	3.31
	T140	133565	418151	1081560	3.13		T140	147075	413312	988785	2.81

[a] - Number average molar mass

[b] - Weight average molar mass

[c] - Z-average molar mass

[d] - Dispersity value (M_w/M_n)

Table 8.10: HT-SEC results: HNR 101 Fractionated samples

	Sample	M_n [a]	M_w [b]	M_z [c]	PDI [d]		Sample	M_n [a]	M_w [b]	M_z [c]	PDI [d]
HNR 101 Powder, Lynx	T30	6003	60614	208321	10.10	HNR 101 Powder, NHP	T30	4668	76022	329059	16.29
	T50	9363	60626	183298	6.48		T50	12130	89017	325381	7.34
	T70	10098	72871	421934	7.22		T70	14172	96226	389688	6.79
	T90	17146	84424	1375232	4.92		T90	20811	92756	322879	4.46
	T100	31562	80704	241845	2.56		T100	39881	112595	339306	2.82
	T110	106916	320632	880036	3.00		T110	112199	332830	827663	2.97
	T140	90223	240623	562444	2.67		T140	125417	388518	921955	3.10
HNR 101 Pellet, Lynx	T30	8650	63008	225315	7.28	HNR 101 Pellet, NHP	T30	4177	69911	311146	16.74
	T50	9779	82239	365730	8.41		T50	11128	79249	273277	7.12
	T70	9078	72812	319753	8.02		T70	10778	88639	388915	8.22
	T90	15302	65638	291415	4.29		T90	18951	74612	296275	3.94
	T100	25417	79241	255337	3.12		T100	34861	98499	300338	2.83
	T110	97504	321858	862212	3.30		T110	118672	452733	1472294	3.81
	T140	107935	283361	637015	2.62		T140	140723	465657	1423291	3.31

[a] - Number average molar mass

[b] - Weight average molar mass

[c] - Z-average molar mass

[d] - Dispersity value (M_w/M_n)

8.5 XRD

Table 8.11: XRD results of powder samples

Sample					Peak and Classification				
#	Grade	Catalyst	Temp Fraction (°C)	Property	1 α(110)	2 α(040)	3 α(130)	4 α(111)	5 α(-131)
1	HKQ 205	Lynx	90	2θ angle (°)	14.30	17.00	18.71	21.11	21.94
				Crystallite size (nm)	2.06	2.63	2.20	2.04	1.61
				d-spacing (Å)	0.31	0.26	0.24	0.21	0.21
2	HKQ 205	NHP	90	2θ angle (°)	14.14	17.00	18.56	21.05	21.79
				Crystallite size (nm)	1.88	2.20	2.07	1.84	1.75
				d-spacing (Å)	0.32	0.26	0.24	0.21	0.21
3	HKR 102	Lynx	90	2θ angle (°)	14.26	17.07	18.65	21.27	21.91
				Crystallite size (nm)	2.47	2.93	2.37	2.06	1.89
				d-spacing (Å)	0.31	0.26	0.24	0.21	0.21
4	HKR 102	NHP	90	2θ angle (°)	14.24	17.13	18.74	21.24	21.85
				Crystallite size (nm)	1.98	2.45	2.08	1.70	1.98
				d-spacing (Å)	0.31	0.26	0.24	0.21	0.21
5	HKQ 205	Lynx	100	2θ angle (°)	14.26	17.13	18.71	21.36	21.94
				Crystallite size (nm)	2.51	2.76	2.40	1.96	1.93
				d-spacing (Å)	0.31	0.26	0.24	0.21	0.21
6	HKQ 205	NHP	100	2θ angle (°)	14.24	17.13	18.74	21.27	21.94
				Crystallite size (nm)	2.21	2.55	2.28	2.14	1.72
				d-spacing (Å)	0.31	0.26	0.24	0.21	0.21
7	HKR 102	Lynx	100	2θ angle (°)	14.24	17.19	18.71	21.39	22.03
				Crystallite size (nm)	2.57	2.89	2.48	2.02	2.00
				d-spacing (Å)	0.31	0.26	0.24	0.21	0.21
8	HKR 102	NHP	100	2θ angle (°)	14.26	17.07	18.71	21.42	21.97
				Crystallite size (nm)	2.23	2.51	2.29	2.14	1.85
				d-spacing (Å)	0.31	0.26	0.24	0.21	0.21

Table 8.12: XRD results of pellet samples

Sample					Peak and Classification				
#	Grade	Catalyst	Temp Fraction (°C)	Property	1 α(110)	2 α(040)	3 α(130)	4 α(111)	5 α(-131)
1	HKQ 205	Lynx	90	2θ angle (°)	14.30	17.07	18.65	21.24	21.88
				Crystallite size (nm)	2.40	2.79	2.44	2.48	1.79
				d-spacing (Å)	0.31	0.26	0.24	0.21	0.21
2	HKQ 205	NHP	90	2θ angle (°)	14.20	16.98	18.62	21.21	21.79
				Crystallite size (nm)	2.01	2.41	2.05	2.02	1.71
				d-spacing (Å)	0.31	0.26	0.24	0.21	0.21
3	HKR 102	Lynx	90	2θ angle (°)	14.18	17.07	18.62	21.18	21.82
				Crystallite size (nm)	2.42	2.65	2.40	1.81	2.02
				d-spacing (Å)	0.31	0.26	0.24	0.21	0.21
4	HKR 102	NHP	90	2θ angle (°)	14.20	17.04	18.68	21.21	21.88
				Crystallite size (nm)	2.34	2.61	2.28	2.05	1.85
				d-spacing (Å)	0.31	0.26	0.24	0.21	0.21
5	HKQ 205	Lynx	100	2θ angle (°)	14.33	17.10	18.71	21.15	22.00
				Crystallite size (nm)	2.36	2.72	2.25	1.88	1.84
				d-spacing (Å)	0.31	0.26	0.24	0.21	0.21
6	HKQ 205	NHP	100	2θ angle (°)	14.24	17.10	18.62	21.33	21.94
				Crystallite size (nm)	2.18	2.69	2.38	1.80	1.73
				d-spacing (Å)	0.31	0.26	0.24	0.21	0.21
7	HKR 102	Lynx	100	2θ angle (°)	14.24	17.07	18.71	21.27	22.00
				Crystallite size (nm)	2.65	2.83	2.47	2.14	1.83
				d-spacing (Å)	0.31	0.26	0.24	0.21	0.21
8	HKR 102	NHP	100	2θ angle (°)	14.24	17.10	18.62	21.39	21.85
				Crystallite size (nm)	2.48	2.78	2.44	2.18	1.77
				d-spacing (Å)	0.31	0.26	0.24	0.21	0.21

8.6 SSA

Table 8.13: SSA results of 90 °C powder samples

Sample					Peak and Classification						
#	Grade	Catalyst	Temp Fraction (°C)	Property	1	2	3	4	5	6	7
1	HKQ 205	Lynx	90	Melting temperature (°)	135.29	139.90	144.52	148.94	153.17	156.73	161.88
				Area integral (%)	3.14	11.04	9.93	22.62	27.68	23.93	1.66
				Lamellar thickness (nm)	4.81	5.28	5.86	6.54	7.36	8.23	9.93
2	HKQ 205	NHP	90	Melting temperature (°)	136.27	141.06	145.18	149.52	153.63	157.06	162.15
				Area integral (%)	5.10	18.79	12.53	23.53	25.10	14.81	0.15
				Lamellar thickness (nm)	4.90	5.42	5.95	6.64	7.47	8.32	10.04
3	HKR 102	Lynx	90	Melting temperature (°)	135.64	140.04	144.44	148.64	152.97	156.59	161.50
				Area integral (%)	3.58	10.77	9.61	22.21	27.77	24.32	1.74
				Lamellar thickness (nm)	4.84	5.30	5.85	6.49	7.32	8.20	9.78
4	HKR 102	NHP	90	Melting temperature (°)	135.92	140.82	144.80	149.00	153.19	157.23	162.00
				Area integral (%)	4.61	16.25	12.01	20.01	24.09	21.04	1.99
				Lamellar thickness (nm)	4.87	5.39	5.90	6.55	7.37	8.37	9.98

Table 8.14: SSA results of 100 °C powder samples

Sample					Peak and Classification								
#	Grade	Catalyst	Temp Fraction (°C)	Property	1	2	3	4	5	6	7	8	9
5	HKQ 205	Lynx	100	Melting temperature (°)	134.78	138.98	143.16	147.29	151.48	156.17	161.50	166.90	171.46
				Area integral (%)	0.60	2.27	1.38	4.49	6.88	3.97	44.34	30.17	5.90
				Lamellar thickness (nm)	4.76	5.18	5.68	6.27	7.01	8.08	9.78	12.43	16.11
6	HKQ 205	NHP	100	Melting temperature (°)	135.52	139.43	143.52	147.64	151.77	155.75	161.79	167.82	172.24
				Area integral (%)	0.70	2.39	1.95	3.61	6.83	2.92	45.22	32.15	4.22
				Lamellar thickness (nm)	4.83	5.23	5.72	6.32	7.07	7.97	9.90	13.03	16.97
7	HKR 102	Lynx	100	Melting temperature (°)	134.90	138.90	142.88	146.94	151.39	155.67	161.29	166.48	171.24
				Area integral (%)	0.54	1.87	2.06	1.98	8.57	2.23	42.22	34.15	6.39
				Lamellar thickness (nm)	4.77	5.17	5.64	6.21	6.99	7.95	9.70	12.17	15.89
8	HKR 102	NHP	100	Melting temperature (°)	135.57	139.32	143.83	147.86	151.98	156.31	162.14	168.04	172.24
				Area integral (%)	0.53	2.11	1.89	3.01	5.74	3.26	46.91	31.85	4.71
				Lamellar thickness (nm)	4.84	5.22	5.76	6.36	7.11	8.12	10.04	13.18	16.97

Table 8.15: SSA results of 90 °C pellet samples

Sample					Peak and Classification						
#	Grade	Catalyst	Temp Fraction (°C)	Property	1	2	3	4	5	6	7
1	HKQ 205	Lynx	90	Melting temperature (°)	134.65	139.58	144.10	148.58	153.08	156.96	161.98
				Area integral (%)	4.21	12.99	10.45	19.93	25.83	24.94	1.65
				Lamellar thickness (nm)	4.75	5.25	5.80	6.48	7.34	8.30	9.97
2	HKQ 205	NHP	90	Melting temperature (°)	135.78	140.26	145.08	149.21	153.33	156.95	162.14
				Area integral (%)	2.32	15.98	7.13	23.54	27.87	22.42	0.74
				Lamellar thickness (nm)	4.86	5.32	5.94	6.59	7.40	8.29	10.04
3	HKR 102	Lynx	90	Melting temperature (°)	135.79	140.34	144.67	148.98	153.31	156.86	161.97
				Area integral (%)	4.03	11.81	10.32	21.73	29.80	20.15	2.16
				Lamellar thickness (nm)	4.86	5.33	5.88	6.55	7.39	8.27	9.97
4	HKR 102	NHP	90	Melting temperature (°)	135.35	140.04	145.02	149.07	153.40	156.89	161.86
				Area integral (%)	2.96	11.80	7.68	22.25	26.57	25.81	2.93
				Lamellar thickness (nm)	4.82	5.30	5.93	6.56	7.41	8.28	9.92

Table 8.16: SSA results of 100 °C pellet samples

Sample					Peak and Classification								
#	Grade	Catalyst	Temp Fraction (°C)	Property	1	2	3	4	5	6	7	8	9
5	HKQ 205	Lynx	100	Melting temperature (°)	134.74	138.76	142.86	147.02	151.23	155.46	161.4	166.67	171.43
				Area integral (%)	0.76	2.04	2.82	1.87	8.93	2.60	43.82	29.69	7.47
				Lamellar thickness (nm)	4.76	5.16	5.64	6.23	6.96	7.90	9.74	12.29	16.08
6	HKQ 205	NHP	100	Melting temperature (°)	134.78	139.02	143.16	147.08	151.06	155.39	161.22	167.12	172.16
				Area integral (%)	0.71	0.61	5.87	-0.02	11.27	1.50	37.78	35.41	6.86
				Lamellar thickness (nm)	4.76	5.19	5.68	6.24	6.93	7.88	9.68	12.57	16.88
7	HKR 102	Lynx	100	Melting temperature (°)	135.06	139.92	144.12	148.68	152.34	157.21	162.54	167.57	172.13
				Area integral (%)	0.74	0.39	8.03	0.34	11.13	2.10	37.21	30.83	9.24
				Lamellar thickness (nm)	4.79	5.28	5.80	6.50	7.19	8.37	10.20	12.86	16.85
8	HKR 102	NHP	100	Melting temperature (°)	134.80	138.99	143.02	147.00	152.91	155.47	160.79	167.46	172.44
				Area integral (%)	0.57	0.41	4.97	0.44	5.26	1.67	37.89	39.35	9.44
				Lamellar thickness (nm)	4.76	5.18	5.66	6.22	7.31	7.90	9.52	12.79	17.21

8.7 NMR

8.7.1 Solution ^{13}C NMR

Table 8.17: HT - ^{13}C NMR pentad distributions of powder samples

Sample				mm			mr				rr		
#	Grade	Catalyst	Temp Fraction (°C)	mmmm	mmmr	rmmr	mmrm	rmrm	mmrr	rmrr	mrrm	mrrr	rrrr
1	HKQ 205	Lynx	90	87.66	4.67	0.00	5.33	0.00	0.00	0.68	0.00	0.00	1.65
2	HKQ 205	NHP	90	83.23	6.26	0.00	6.91	0.48	0.00	0.33	0.16	0.32	2.31
3	HKR 102	Lynx	90	83.38	5.83	0.22	6.19	0.40	0.00	0.76	0.44	0.61	2.16
4	HKR 102	NHP	90	88.64	4.88	0.00	4.50	0.45	0.00	0.45	0.00	0.00	1.08
5	HKQ 205	Lynx	100	95.95	1.37	0.00	1.84	0.00	0.00	0.00	0.00	0.00	0.85
6	HKQ 205	NHP	100	94.20	2.42	0.00	2.43	0.00	0.00	0.00	0.00	0.00	0.96
7	HKR 102	Lynx	100	95.20	1.69	0.00	2.44	0.00	0.00	0.00	0.00	0.00	0.67
8	HKR 102	NHP	100	95.70	1.68	0.00	1.92	0.00	0.00	0.00	0.00	0.00	0.70

Table 8.18: HT - ^{13}C NMR pentad distributions of pellet samples

Sample				mm			mr				rr		
#	Grade	Catalyst	Temp Fraction (°C)	mmmm	mmmr	rmmr	mmrm	rmrm	mmrr	rmrr	mrrm	mrrr	rrrr
1	HKQ 205	Lynx	90	81.62	5.77	0.45	5.57	1.10	0.19	1.14	0.24	0.49	3.43
2	HKQ 205	NHP	90	83.81	5.93	0.00	6.31	0.42	0.07	0.63	0.28	0.27	2.27
3	HKR 102	Lynx	90	80.89	6.14	0.25	6.94	1.34	0.17	1.25	0.47	0.36	2.20
4	HKR 102	NHP	90	82.17	6.14	0.00	7.00	0.55	0.33	1.05	0.31	0.67	1.78
5	HKQ 205	Lynx	100	94.10	1.94	0.20	2.80	0.10	0.00	0.07	0.00	0.25	0.54
6	HKQ 205	NHP	100	96.00	1.68	0.00	2.32	0.00	0.00	0.00	0.00	0.00	0.00
7	HKR 102	Lynx	100	94.64	1.92	0.00	2.62	0.00	0.00	0.00	0.00	0.00	0.82
8	HKR 102	NHP	100	95.25	2.14	0.00	2.03	0.00	0.00	0.00	0.00	0.00	0.58